FINE STRUCTURE OF THE SUBDUCTING OCEANIC PLATES BENEATH THE KANTO DISTRICT, CENTRAL JAPAN

(関東地方下に沈み込む海洋プレートの微細構造)

A Thesis in Geophysics

by

Shiro OHMI

Submitted in Partial Fulfillment

of the Requirements for

the Degree of Doctor of Science

in Tohoku University

1997

Acknowledgement

I am greatful to Prof. Akira Hasegawa for his stimulate discussion and continual encouragement. I also thank Prof. Masakazu Ohtake, Prof. Tomoo Hirasawa, and Prof. Hiroyuki Hamaguchi for their valuable suggestions. Dr. Jonathan M. Lees and Dr. Shoji Sekiguchi kindly provided me their computer program. I appreciate Dr. Yoshimitsu Okada for allowing me to use seismic data obtained by the National Research Institute for Earth Science and Disaster Prevention. Dr. Nobuo Hurukawa and Dr. Masajiro Imoto contributed helpful discussions especially on chapter 2. Useful discussions with Dr. Sadaki Hori and Dr. Toru Matsuzawa on chapter 3 are greatly appreciated. I also appreciate the critical review by Dr. Shigeki Horiuchi that improved the manuscript. Finally, I would like to thank Prof. Masataka Ando, Prof. Kazuro Hirahara, and Dr. Keiji Kasahara for their continual encouragements.

Abstract

A fine structure of the subducting Philippine Sea and Pacific plates beneath the Kanto district, central Japan, has been revealed from a high resolution seismic tomography analysis and a travel time analysis of conspicuous SP converted waves in conjunction with hypocenter distribution and focal mechanism studies.

First, a high resolution seismic tomography technique is applied to regional seismic data in the Kanto area to obtain slowness perturbations in the target area. The result of the inversion has generally small estimation errors, less than 2.4 % variation in all regions. Thin low velocity layers, which are considered to be subducted oceanic crusts, are detected at the top of both the Philippine Sea and the Pacific plates. Their thicknesses are 5 - 10 km for both plates and their velocities are about 12 % and 3 % lower than the surrounding mantle for the Philippine Sea and the Pacific plates, respectively. The low velocity layers are detectable down to a depth of $\sim$ 60 km for the Philippine Sea plate and $\sim$ 90 km for the Pacific plate. Relatively high velocity thick layers underlie the low velocity layers.

Low angle thrust fault type earthquakes occur in the low velocity layers found at the top of the Philippine Sea and the Pacific plates. The southwestern Ibaraki earthquake swarm is interpreted as interplate earthquakes between the Eurasia and the Philippine Sea plates. Similar fault type earthquakes, such as the swarm activity of Tsukuba - Chiba seismic belt and the southern Ibaraki earthquake of 1983, are considered to be interplate earthquakes between the Philippine Sea and the Pacific plate occurring in the low velocity layer on the top of the Pacific plate.

On the other hand, earthquakes interpreted as intraplate events from their focal mechanisms are located in the high velocity portions. The

Ibaraki-Chiba border earthquake of 1985 occurred in the high velocity portion of the Pacific plate, and the east off Chiba earthquake of 1987, which is an intra Philippine Sea plate event, occurred in the high velocity portion of the Philippine Sea plate.

The obtained result shows that there is a low velocity layer on the top of the Philippine Sea plate down to a depth of 65 - 70 km in some regions in the northwest Kanto area. This result does not support the previous studies that the gabbro-eclogite transition is expected in this depth range.

Low velocity bodies are detected in the mantle wedge portion beneath active volcanoes in the northwest Kanto area, which is probably associated with the deep structure of the volcanoes.

Second, a detailed structure of the Pacific plate was studied by the use of conspicuous SP converted waves that is generated near the upper boundary of the Pacific plate. The conversion interface is located above the upper seismic plane of the double seismic zone. It generally coincides with the result of previous studies of the upper boundary of the Pacific plate, with slight differences in the northern Kanto area. Comparison to the result of the three-dimensional tomographic inversion revealed that the conversion interface is located in the low velocity layer that attaches at the top of the Pacific plate.

Finally, taking into account the result of tomographic inversion and SP converted wave analysis, the relation among the low velocity layer at the top of the Pacific plate and the conversion interface are discussed in conjunction with hypocenter distribution and focal mechanisms.

In northern Kanto, most seaward area forms 'triple seismic zone'. In this area, the location of the conversion interface that generates SP waves coincides with that of the main thrust zone, and has a separation of about 10 km from the upper plane of the double seismic zone.

In the northern part of central Kanto, the separation between the conversion interface and the upper seismic plane is not clear. Low angle thrust fault type earthquakes occur at deeper depths than in the northern Kanto area. The conversion interface is located at the bottom of the area of earthquake clusters with low angle thrust faulting. In the southern part of central Kanto and southern Kanto, the separation between the upper seismic plane and the conversion interface is not clear again. The conversion interface is located at the the upper boundary of the earthquake cluster zone of thrust fault type events.

Since a converted wave is generated only at a velocity boundary, the conversion interface should be located either at the upper boundary or lower boundary of the low velocity layer. Previous studies conducted in the Tohoku district attributed the conversion interface to the upper boundary of the low velocity layer. On the other hand, in the Kanto district, the conversion interface seems to be located at the lower boundary of the low velocity layer in its central area.

The thermal condition around the subducting Pacific plate in the Kanto area may be different from that in Tohoku district, because of the existence of the subducting Philippine Sea plate above the Pacific plate. It is probable that both of the upper and lower boundaries of the crust that attaches on the top of the Pacific plate will act as conversion interfaces. Thus the conversion interface derived in this study is considered to correspond to the lower boundary of the subducted crust, which is the Moho discontinuity of the subducing Pacific plate beneath the central Kanto area. The spatial distribution of low-angle thrust fault type earthquakes indicates that these earthquakes occur in the whole portion of the crust in the subducting Pacific slab, between the Moho and the upper boundary of the Pacific plate.

Contents

Chapter 1

Introduction

1.1 Overview on Upper Mantle Structure Studies around Japan Islands

There are two types of convergent plate boundaries in the scheme of the plate tectonics: one is the subduction zone and the other is the continental collision zone. Currently more than 90 % of the world's convergent boundaries are subduction zones. Oceanic plates are created at mid-oceanic ridges and migrate laterally beneath oceans, with thickening and cooling with time. These plates finally subduct beneath other plates. The subducted portions of the rigid lithospheric plates are called slabs and they produce remarkable features that characterize island arc systems. They are trenchs, active volcanoes, inclined seismic zone which is called Wadati-Benioff zone, back arc basins, and laterally heterogeneous structures in the crust and upper mantle (e.g. Sugimura and Uyeda, 1973).

The Pacific plate (PAC plate) is moving westward, and consumes at several subduction zones in the western Pacific regions. They are Aleutian, Kuril, Japan, Izu-Bonin, New Hebrides, Tonga-Kermadec, and New Zealand regions. Because there are large number of shallow, intermediate, and deep earthquakes whose data are observed by seismic networks, Japan Islands region is one of the most suitable area to

study the dynamics of the subduction zone.

Utsu (1967) first found the existence of the laterally heterogeneous structure along subduction zones beneath the Japan Arc, and Oliver and Isacks (1967) found it beneath the Tonga-Fiji region. Utsu (1971) showed many seismological and geophysical evidences that indicate lateral heterogeneity in the deep structure of the Japan Arc system. He presented an upper mantle model beneath the Japan Arc, in which there is a high-Q, high-velocity zone of about 100 km thick dipping toward the arc from the vicinity of the trench at depths down to several hundred kilometers. The model includes two low-Q, low-velocity zones in the upper mantle on the inner (continental) and outer (oceanic) sides of the dipping zone. This high-Q, high-velocity dipping zone, which corresponds well to the Wadati-Benioff zone, is now regarded as a convincing evidence of the subducting slabs.

Because of the existence of the Philippine Sea plate (PHS plate), the structure in the Japan Islands region is more complicated. Both of the PAC and PHS plates subduct underneath the Eurasia plate (EUR plate) in this region. We can know from the contour map showing the depth of the Wadati-Benioff zone around Japan that the PAC plate is subducting roughly westward to a depth of 400 - 600 km along the Kuril trench in the Kuril arc, along the Japan trench in the northeast and central Japan arc, and along the Izu-Bonin trench in the Izu-Bonin arc. On the other hand, the PHS plate is subducting northwestward to a depth of 60 - 150 km along the Sagami trough in the Kanto region, along the Nankai trough in the southwest Japan arc from the Tokai to Kyushu regions, and to a depth of 200 km along the Ryukyu trench in the Ryukyu arc.

Many authors delineate the complicated structure of subduction zones through the studies of seismic tomography, seismic later phase

analyses, and seismic profiling using active sources such as airgun or dynamites. In the Kuril and Hokkaido region, Takanami (1982), Miyamachi and Moriya (1984) obtained 3-D P-wave velocity structure models at the Hidaka mountain range, Hokkaido. They found an inclined low-V zone with a seismic velocity 10 % slower than the surrounding volume extending to a depth of 65 km or more. Miyamachi and Moriya (1984) interpreted this inclined low-V zone as a subducted crust caused by a collision between the Kuril and northeastern Japan arcs. Furumura and Moriya (1990) obtained 3-D attenuation structure of the same region and found an inclined low-Q region that corresponds to the low-V zone. Miyamachi et al. (1994) obtained a velocity structure model in northern Japan and reported that the upper boundary of the subducting PAC plate distributes in the depth range from 50 km to 170 km in their study area. The dip angle of the plate boundary in the Kuril arc (Hokkaido region) is slightly larger than that in the northeastern Japan arc (Tohoku region). Okada (1971) found an ScSp phase, which is S-to-P converted wave of the ScS wave at the plate boundary, and located the plate boundary beneath Hokkaido. The estimated conversion plane has a dip of 35 ° - 39 ° which is nearly parallel to the deep seismic zone. It was attributed to the upper boundary of the subducting PAC plate beneath Hokkaido region.

In the Tohoku district, it is well known that the double-planed deep seismic zone is clearly seen (Umino and Hasegawa, 1975; Hasegawa et al. 1978a). This region has been most successfully investigated among several regions in the Japan Islands. Hasemi et al. (1984) and Obara et al. (1986) investigated fine-scale 3-D P-wave velocity and P- and S-wave velocity structures beneath the region, respectively. They found the inclined high-V PAC slab subducting beneath this region and overlying low-V zones dipping westwards just beneath

active volcanoes. Zhao et al. (1992) developed a new tomographic method that can deal with a structure having complex shaped seismic velocity discontinuities such as the upper boundary of PAC plate, Moho and Conrad discontinuities of the crust. They applied it to the increased dataset in the Tohoku region. Later, Zhao and Hasegawa (1993) obtained a 3-D P-wave velocity structure beneath the whole Japan Islands by applying their method. In addition to the tomographic technique, seismic later phases are also employed to locate the seismic velocity discontinuity. Hasegawa et al. (1978b) observed ScSp waves converted from ScS waves and located the upper boundary of the subducting PAC plate. Matsuzawa et al. (1986, 1990) located the upper boundary of the PAC plate (UBP) using PS and SP waves and found the existence of a low velocity layer at the UBP, which was attributed to the subducting oceanic crust at the top of the PAC slab. Attenuation structure is also investigated in this region. Based on the S to P spectral ratio method, Umino and Hasegawa (1984) obtained 3-D Q structure and showed that inclined high-V Pacific slab has high-Q and the overlying mantle wedge has low-Q. Matsumoto and Hasegawa (1989) obtained two-dimensional coda Q structure beneath Tohoku region and reported that Qc distribution is consistent with S-wave velocity distribution; low Qc regions have a tendency to correspond to the regions with low S-wave velocity and vice versa. Recently Tsumura et al. (1996) obtained 3-D P-wave attenuation structure of the crust and upper mantle in this region by simultaneously estimating attenuation structure, source parameters, and site response spectra.

In the Kanto and Tokai region, the PHS plate is subducting beneath the EUR plate northwestwards from Sagami and Suruga troughs. The PAC plate is also subducting beneath both of the EUR and PHS plates westwards from the Japan trench. Horie and Aki (1982) first investi-

gated 3-D Vp structure beneath the Kanto region, and later Ishida and Hasemi (1988) obtained the fine scale 3-D Vp structure with block size about 25 km beneath the Kanto-Tokai region. According to Ishida and Hasemi (1988), the high-V PHS slab with a thickness of only about 30 km is subducting at the Sagami and Suruga troughs, correlating well with the inclined zone of high seismicity. Hashida and Shimazaki (1985) obtained 3-D Q structure by inverting seismic intensity data. Sekiguchi (1991) used the amplitude spectral ratio method to obtain 3-D Q structure beneath the Kanto-Tokai area. They revealed the existence of a high-Q zone corresponding to the PHS slab and an extremely low Q region at the continental side of the volcanic front in the upper mantle. Obara and Sato (1988), and Obara (1989) found S-to-S reflected waves in the Kanto area and calculated the location of the reflector. It was located just above the inclined seismic zone. They attributed it to the upper boundary of the PAC plate beneath the Kanto district.

In central Japan, Hirahara et al. (1989) investigated 3-D Vp structure. They showed the existence of low V bodies just beneath the active volcanoes in the mantle wedge portion and the high-V PHS and PAC slabs subducting beneath it. The PHS slab beneath southwest Japan was investigated by Nakanishi (1980), Hirahara (1981), and Tanaka (1987). Nakanishi (1980) suggested the aseismic subduction of the PHS slab beneath the Chugoku region using ScSp phase analysis. Hirahara (1981) supported Nakanishi's result from 3-D velocity structure analysis. He concluded that the aseismic slab extends to a depth between 100 km and 150 km beneath the Kinki region and probably beneath the Chugoku region. Tanaka (1987) investigated the seismic velocity structure beneath the Chugoku-Shikoku region and reported that thin low velocity layer exists just above the high

velocity zone and earthquakes occur within the low velocity layer.

1.2 Scope of this Study

In this study, we focus our attention to the Kanto district, central Japan, which is characterized by its quite complex tectonic environment. The PHS plate is subducting beneath the EUR plate, and the PAC plate also underthrusts both of the EUR and PHS plates. There exists the Izu peninsula to the west which is considered to be a collision zone between the PHS and the EUR plates. The trench - trench - trench triple junction of the PAC, PHS, and EUR plates exists to the east (McKenzie and Morgan, 1969).

In this region, the National Research Institute for Earth Science and Disaster Prevention (NIED) operates a high density observation network of seismic stations (Hamada et al., 1982). It is possible to study the seismic structure of the crust and the upper mantle in this area by applying various methods such as a 3-D tomography technique, stress field analysis using focal mechanism solutions, and later phase analysis to many P and S arrival time data compiled through the long term observation.

In chapter 2, a high resolution seismic tomography method is applied to local earthquake data to delineate a fine 3-D structure of the oceanic plates beneath the Kanto area. In chapter 3, we analyze seismic conversion waves generated near the upper boundary of the PAC plate to know the location of the PAC plate precisely. In chapter 4, the results of the fine 3-D velocity structure analysis and of the seismic conversion wave analysis are compared with the seismicity and the earthquake generating stress field in this region. The seismotectonics in this region is discussed with focusing mainly on the upper boundary of the PAC plate.

Chapter 2

Detection of Subducting Crusts on the Top of Oceanic Plates

2.1 Introduction

The existence of thin low velocity layer on the surface of subducting plates has been discussed mainly from analyses of later phases and focal mechanisms. Hurukawa and Hirahara (1980) investigated the structure of the subducting Philippine Sea (PHS) plate beneath the Kinki district in western Japan. They analyzed the later P phases obtained from a small seismic array deployed in the target region, and reported the existence of a thin low velocity zone at the interface between the Eurasia (EUR) and PHS plates. Fukao et al. (1983) found remarkable later P phases in seismograms of earthquakes beneath the Kinki region observed by the seismic network in the Tokai area, central Japan and interpreted it to be channel waves. These waves propagate in the basaltic layer which remained as a low velocity layer at the surface of the subducting PHS plate. Hori et al. (1985) found a low velocity channel in the uppermost mantle beneath southwest Japan, where there is a slab-like seismic zone, based on the analysis of distinct later phases that were observed for particular source-receiver geometries. They concluded that the thin low velocity layer is the untransformed basaltic oceanic crust subducted with the underlying lithosphere. Lo-

cal tomographic studies were also conducted for those regions since Hirahara (1981) (See a review of Hirahara and Hasemi, 1993). For example, Hirahara et al. (1989) obtained a three-dimensional velocity structure model beneath central Japan which demonstrated the presence of the high velocity PHS slab subducting in the central Japan region. However, they could not detect the low velocity layer at the top of the PHS plate.

In the Tohoku district, the northeastern part of Japan, Matsuzawa et al. (1986) determined the upper boundary of the descending Pacific (PAC) plate by using PS converted waves. They concluded that the descending plate has a two-layered structure that consists of a thin low-velocity upper layer and a thick high-velocity lower layer. Zhao et al. (1992) developed a new seismic body wave tomography method that can calculate accurate travel times for a structure having complicated-shaped seismic velocity discontinuities. They applied it to the dataset obtained in the Tohoku district and found a high velocity zone corresponding to the subducted PAC plate and low velocity regions in the mantle wedge. However, they did not detect the two-layered structure of the descending PAC plate discussed by Matsuzawa et al. (1986).

In the Kanto district, central Japan, the velocity anomaly at the plate boundary has been also investigated. In this region, the PHS plate subducts under the EUR plate and the PAC plate also underthrusts beneath the PHS plate (Figure 2.1). Hori (1990) analyzed later phases of upper mantle earthquakes and presented a model of a subducting oceanic crust beneath the Kanto district. Hurukawa and Imoto (1990, 1992) determined the focal mechanisms of mantle earthquakes in the Kanto district and suggested that there are subducted oceanic crusts in the mantle along the interface not only between the

EUR and PHS plates but also between the PHS and PAC plates. Obara and Sato (1988), Obara (1989) analyzed phases in coda waves of shallow local earthquakes in the Kanto district and pointed out that they are reflected S-to-S waves at the plate boundary. The location of the reflection points for these phases are near the upper plane of the double seismic zone, showing the existence of a very large S wave impedance contrast. They suggested that these reflectors might be on the upper surface of the low velocity layer attached to the PAC plate. Three dimensional velocity structure inversion has been also conducted in the Kanto region (e.g. Horie and Aki, 1982; Ishida, 1984; Ishida and Hasemi, 1984; 1988, Lees and Ukawa, 1992). Ishida and Hasemi (1988) obtained a three-dimensional velocity model of the Kanto-Tokai district and found the high-velocity zone with a thickness of about 30 km and with a gradual dip. It extends to the northeast and west of the Izu peninsula. They interpreted it as the PHS plate. However, they did not discuss the velocity anomaly at the plate boundaries. Lees and Ukawa (1992) conducted a high resolution travel time tomography in the south Fossa Magna region. Since their target region was above the Moho at 30 - 40 km depth, they did not resolve the velocity anomaly of the plate boundaries.

Generally, the existence of low velocity layer near the surface of the subducting plates has not been reported in the previous travel time tomography studies, although it was shown in some of the later phase analyses. It is possibly due to the lack of resolution of the tomography analyses. However, there are some studies of tomographic inversion that reported the velocity anomaly associated with subducting crusts. In Hokkaido, northern Japan, Miyamachi and Moriya (1984) found an inclining low velocity zone, that was interpreted as a subducted crust of the northeastern Japan arc beneath the Kuril arc. Roecker (1982)

investigated the velocity structure of Pamir-Hindu Kush and reported the existence of a subducting low velocity continental crust. Comte et al. (1994) conducted the 2-D P-wave velocity analysis in the northern Chile region and detected a low velocity oceanic crust attached to the top of the subducting Nazca plate.

In this section, we applied a high resolution tomographic inversion method of Lees and Crosson (1989) to a large amount of earthquake data and determined a fine P-wave velocity model in the Kanto district. Then we compared the obtained velocity model with other geophysical features in the target region to delineate the existence of the low velocity crust that attaches to the top of the subducting plate.

2.2 High Resolution Seismic Tomography

2.2.1 Method of analysis.

We present here an outline of the inversion technique used in this study. A detailed account can be found in Lees and Crosson (1989). A one-dimensional, layered P-wave velocity model was used as an initial reference model. We determined hypocenters independently. Ray paths from the sources to stations are calculated through the initial model, with taking into account the effect of refractions along interfaces. Travel time perturbations were calculated by taking the difference between the observed travel times minus the theoretical ones. These travel time perturbations represent the line integrals of the slowness perturbation along the ray path. Then the target region is divided into small blocks within which the slowness perturbation is assumed to be constant. Denoting the length of the i th ray path in the j th block by a_{ij}, the travel time perturbation for the particular ray path b_i becomes

$$b_i = \sum a_{ij} x_j$$

or in matrix form,

$$\boldsymbol{Ax} = \boldsymbol{b} \tag{2.1}$$

where x_j is the slowness perturbation in the j th block. The least squares solution of (2.1) satisfies the normal equation

$$\boldsymbol{A^t Ax} = \boldsymbol{A^t b} \tag{2.2}$$

where A^t is the transpose of A. It minimizes the function $\|Ax - b\|^2$. Usually A^tA is singular and the solution of (2.2) is nonunique. To deal with this singularity we introduce Levenberg-Marquardt method (Crosson, 1976) that introduces additional constrain to the system in the following manner,

$$\begin{bmatrix} \boldsymbol{A} \\ \boldsymbol{\lambda I} \end{bmatrix} = \begin{bmatrix} \boldsymbol{0} \\ \boldsymbol{b} \end{bmatrix} \tag{2.3}$$

which minimize the weighted sum of the residual and solution vector, that is

$$\|Ax - b\|^2 + \lambda^2 \|x\|^2 \tag{2.4}$$

where λ is a weighting coefficient to be adjusted with the requirement of the problem. This trade-off between adherence to data misfit reduction and model smoothness was determined by trial and error. The modified normal equation is

$$(\boldsymbol{A^t A} + \boldsymbol{\lambda^2 I})\boldsymbol{x} = \boldsymbol{A^t b} \tag{2.5}$$

Since the slowness field we are inverting for is a discrete version of a continuously varying slowness, neighboring blocks should be related to one another by excluding solutions with gradients which are too large. Lees and Crosson (1989) introduced the second differential operator (Laplacian operator ∇^2) in the horizontal plane as a smoothing

constrains. Then the system is expressed as follows by replacing I with L

$$\begin{bmatrix} \boldsymbol{A} \\ \boldsymbol{\lambda L} \end{bmatrix} = \begin{bmatrix} \boldsymbol{0} \\ \boldsymbol{b} \end{bmatrix} \tag{2.6}$$

where L is the laplacian operator applied over horizontal planes. Using this system, they will minimize the following function

$$\|Ax - b\|^2 + \lambda^2(x^t L^t L x) = \|Ax - b\|^2 + \lambda^2 \|Lx\|^2 \tag{2.7}$$

To solve the above system, which is large and sparse, LSQR algorithm (Paige and Saunders, 1982) is applied. In Lees and Crosson (1989), iterative step, in which the ray paths and hypocenters are recalculated using the obtained three-dimensional model as a new initial model, is not performed.

In this paper, inversion results are given as slowness perturbations in percent, defined as

$$((u - u_0)/u_0) \times 100 \tag{2.8}$$

where u_0 and u are values of the initial and final slowness, respectively. From this definition, positive slowness perturbations indicate lower velocities than the initial reference model and negative slowness perturbations signify higher velocities.

2.2.2 Resolution and error analysis.

The resolution of the inversion is primarily a function of the ray distribution and of smoothing parameters imposed by regularization. Ideally, we should obtain resolution kernel at every point of the model. However, it is not practical for the inversion of this scale with thousands of parameters. According to the method by Lees and Crosson (1989), we calculate the resolution for one block by placing a unit spike in the block. We compute the theoretical travel time data from the

spike model and invert them with using the same way used in the real data analysis. The result is the impulse response (point spread function) of the system for that block. If the ray coverage in the vicinity of the block is homogeneous and isotropic, then the impulse response will be uniform and representative over the region (Humphreys and Clayton, 1988). Resolution impulse responses used in conjunction with ray distribution descriptions can thus be used as qualitative substitutes for full resolution analysis when model parameters are very numerous.

The standard errors are estimated using the jackknife (Efron, 1982; Lees and Crosson, 1989). This method involves partitioning the data into subsets so that each partition excludes a different, non-overlapping portion of the data. Inversions are performed for each data partition and statistics (e.g. the standard error) are accumulated for each model parameter. To obtain a jackknife estimate an inversion is performed using all the data and the result is stored as a vector, $\hat{s}_{all}$. The data is then divided into k sets, each leaving out a random $1/k$ th portion of the data, selected without replacement. A separate inversion is performed for each of the k subsets and the slowness model derived from each inversion is denoted $\hat{s}_j$. From these "mini-inversions" a "pseudo-inversion" $\tilde{s}_j$, is formed by the following linear combination:

$$\tilde{s}_j = k\hat{s}_{all} - (k-1)\hat{s}_j \tag{2.9}$$

The pseudo-inversions thus represent information about the model that is explained by that portion of the data that was removed. Since each of the k subsets has a different nonoverlapping set of excluded data, the variability of the model due to all the data is contained in the pseudo-inversions. The jackknife estimate of the slowness is simply the average of the pseudo-inversions:

$$\tilde{s} = \frac{\sum^k \tilde{s}_j}{k} \tag{2.10}$$

which has variance,

$$v = \frac{\sum \tilde{s}_j^2 - \frac{1}{k}(\sum \tilde{s}_j)^2}{k(k-1)} \tag{2.11}$$

From this the standard error is $E_\sigma = \sqrt{v}$. This will be an estimate of the variability of the model (due to variability of data) and can be used to project how large the errors are in each block of the target.

2.3 Data

2.3.1 Initial hypocenters.

The data were selected from the catalogue of events provided by National Research Institute for Earth Science and Disaster Prevention (NIED). First we selected earthquakes in the target region (Figure 2.2) which was located in the range 0 km < x < 188 km, 0 km < y < 228 km, and 0 km < depth < 110 km by the NIED in the period from January 1980 to September 1991. The origin of (x, y) coordinate is (138.80°E, 34.96°N). Then we relocated these events, using a one-dimensional layered P-wave velocity model. This layered model is also used as an initial model of the inversion procedure with a slight modification (Table 2.1 and Figure 2.3). Hypocenters were relocated with the technique developed by Hurukawa and Ohmi (1993), which use only P-wave arrival time data. In the method, hypocenter determination is conducted with using station corrections that are obtained as a function of the hypocenter coordinates (x, y, and z) to correct the travel time delay in the lateraly heterogeneous media. It means that a set of station corrections changes according to the location of earthquakes. Detailed account is described in Hurukawa and Ohmi (1993). Since we do not relocate hypocenters in the inversion procedure described above, it is very important to get the initial hypocenter locations accurately. Arrival time data used in the hypocenter reloca-

tion procedure were weighted according to values of the observation quality showing clearness of onsets, which are determined at the time of picking. Routinely determined hypocenters and relocated ones are shown in Figure 2.4 for comparison. Depths in relocated hypocenters are systematically shifted compared to those routinely located.

Then we eliminated the poorly determined events which do not satisfy the following earthquake location criteria: (1) azimuthal gap < 270 °; (2) root mean square residual < 0.3 sec; (3) location error < 6 km; and (4) number of P picks ≥ 8. This step yielded 3,038 earthquakes giving 40,763 P-wave arrival times. Though the value of the criterion for azimuthal gap (270 °) is large, about 2,400 events (80 %) have azimuthal gap less than 180 °. Those events with large gaps are located near the edge of the target region and northern Tokyo Bay area. Figure 2.5 shows the relocated hypocenters and station distribution used in this study. Station codes and coordinates are shown in Figure 2.6 and Table 2.2 for reference. Ray density diagrams are shown in Figure 2.7. In general, we can expect reliable result for the region with high ray density.

A set of station delays was then determined to remove the effect of local structure in the vicinity of each station. Since we applied the method of Hurukawa and Ohmi (1993) for the relocation procedure, we assume that the large effect of lateral heterogeneity such as the deep structure is already removed. However, the effect of local structure near the station may still remain. Therefore we determined a set of station delays to remove it. We computed the travel time residuals of relocated events with using the initial velocity model. We calculated the travel time residuals for each station and plotted their histograms to determine the average, non-zero offsets. Figure 2.8 shows the station delay distribution and each value is listed in Table 2.2.

Histograms of station residuals for P-arrivals are shown in Figure 2.9. The present station residuals are those subtracted the station delays in Figure 2.8 from the original station residuals.

2.3.2 Initial velocity model.

The target area was divided into $47 \times 57 \times 18$ blocks measuring 4 km per side and 4 - 10 km thicknesses in depth. As we described above, the one-dimensional P-wave velocity model based on Hurukawa and Ohmi (1993) was used as an initial model (Figure 2.3 and Table 2.1). Since the depths of layer boundaries in their model are different from those of layer boundaries in this study, we slightly modify their model. Originally, the crust and upper mantle structures in this model are from Hurukawa and Imoto (1990) and Ukawa et al. (1984), respectively. Each velocity discontinuity in the model corresponds to each block boundary in our block modeling.

2.4 Results

2.4.1 Resolution analysis.

We located four unit spikes in the target area and calculated the resolution. The horizontal resolution (Figure 2.10 (a-d)) is generally good, though with smearing into neighboring parts of the model. The lateral resolution length ranges from 8 - 12 km (2 - 3 blocks) near the center of the model and 12 - 16 km (3 - 4 blocks) near the edge. Figure 2.10(e) represents the vertical resolution change calculated for a unit spike at the same location shown in Figure 2.10(d). It is clear that smearing into vertical neighboring block is very little.

2.4.2 Error analysis.

Results of the jackknife estimate with 30 partitions are presented in Figure 2.11. The maximum standard error for each layer is also listed in Table 2.1. While the errors are generally small for the most part, there are some localized areas that exhibit slightly large errors which will be taken into consideration in the interpretation. In layers 5-7 (25-40 km) there is a region where the estimates of the standard error have more than ± 2.0 % perturbation in Boso peninsula area. In layer 9, there is a wide area where the estimates of the standard error are up to ± 1.5 % around Ibaraki-Chiba border area. In layers 10-13 (50-70 km), about 2.0 % standard error of the estimated parameters are observed along the eastern edge of the target area. However, the errors are generally small, less than 2.4 % in all regions. The errors are not large enough to wipe out the extreme anomaly for each layer. Though we cannot constrain the absolute value of the P-wave velocity by this technique since it slightly depends on the reference model, we infer that the sense (positive or negative) of the velocity anomaly is well constrained in regions of low standard errors. Error estimation from jackknife analyses is not reliable when the hit count is very small, such as the regions close to the edge of the target area. These regions may exhibit a low variance but will also have a low resolution and some uncertainty.

Usually, the variance improvement is used to judge how the inversion process improved the model parameters. In this inversion, it reduced 73 % of the weighted root mean square misfit remained in the 1-D model. Therefore the obtained 3-D model parameters should explain the observed travel times. Thus the travel time difference $T_{obs} - T_{1D}$, where T_{obs} is observed travel time and T_{1D} is the calculated travel time for the 1-D initial model, should coincide to the difference $T_{3D} - T_{1D}$,

where T_{3D} is the calculated travel time for the obtained 3-D model, for each ray. Figure 2.12 shows the diagrams of $T_{obs} - T_{1D}$ against $T_{3D} - T_{1D}$. We can say the obtained 3-D model well explains the observed travel times.

2.4.3 Results of tomographic inversion.

We present the result of the inversion in Figure 2.13. Only the blocks with standard errors less than 1.2 % are shown. Vertical cross sections along the lines shown in Figure 2.5 are given in Figure 2.14. The estimated extreme perturbation values and their corresponding absolute velocity values are listed in Table 2.1.

The Kanto area is widely covered by Quaternary sediments and this feature may affect the result of the shallow layers. In the layers 1 and 2 ($<$ 12 km depth), an extreme high velocity anomaly appeared in the western part of the target area, which corresponds to the Mesozoic metamorphic rocks and sediments. A geological map in the target area reproduced from Geological Survey of Japan (1992) is presented in Figure 2.15. Although covered by Quaternary sediments, particular high velocity anomalies are recognized in the vicinity of stations in the eastern part of the Boso peninsula. We suppose this is probably due to the limitation of eliminating the effects of immediate vicinity of the station only by the station delays. Thus we should focus our interpretation below those layers. In layer 3 (12 km - 20 km depth) and layer 4 (20 - 25 km), extremely large anomalies near some particular stations are not seen.

In layer 3, Quaternary and Tertiary volcanic area north of ASO and OMM stations turned to exhibit low velocity anomaly. This trend can be observed down to the depth of layer 8 (40 km - 45 km) and this feature is also clear in the cross section along D-D' (Figure 2.14 (d)).

We suppose that this feature is associated with the deep structure of the volcanoes. It agrees with the result of Hirahara et al. (1989) and Zhao et al. (1992) that low velocity bodies exist beneath active volcanoes in central Japan and in Tohoku. In layers 4, 5 and 6, a high velocity anomaly is predominant in and around MOR and CDP area. This high velocity region is getting pronounced compared to a low velocity region south of it. This feature correlates well with the gravity anomaly in this area. The high velocity anomaly corresponds to high gravity anomaly and vice versa. A gravity anomaly map reproduced from Kono and Furuse (1989) is shown in Figure 2.16. It should be noted that Kono and Furuse (1989) did not eliminate the gravitational effects of the subducting PAC and PHS slabs.

In layer 5 (25 km - 30 km), low velocity anomalies are clearly seen in the eastern Yamanashi Pref. region and the northern Tokyo Bay area. In layer 6 (30 km - 35 km), these low velocity anomalies are observed in a band of about 25 km width in almost east-west direction. It bends to NNW direction near the border of Tokyo Met. and Yamanashi Pref. The pronounced band-like feature is recognized in the result of 45 km depth (layer 8) and this trend can be traced to the depth of about 60 km (layer 11). It gradually moves north or northwestward with depth. Here we call this low velocity layer as LV-A. At the depth of 35 km (layer 7), a clear high velocity region is observed to the south of LV-A and it also moves northward with depth. We call this high velocity layer HV-A (Figure 2.17).

Although the intensity of the anomaly is rather small, another low velocity area is seen in layer 9 (45 km) in the eastern part of the Kanto district. It can be seen at nearly the same location down to the depth of layer 12 (60 km), and it forms a north-south trending belt. Since the standard error for the low velocity zone in layers 9 - 12 (45 - 65

km) is slightly large, these images might be artifact. We thus focus our interpretations below these layers. In layers 13-15 (65-80 km) the low velocity zone gradually moves westward with depth. We call this low velocity layer LV-B. A high velocity area attached to the eastern side of the low velocity belt is recognized in layer 14. We call this HV-B. In layer 15 (75 km - 80 km), the pair of LV-B and HV-B moves westward compared with its location in layer 14. In this depth, another pair of low and high velocity belts is observed to the west of the LV-B and HV-B pair. In layer 16 (80 km - 90 km), the two pairs run roughly SSE to NNW in the southern part of the Kanto region and bend to NNE direction in the northern Kanto region. Since the ray coverage is getting worse in the deeper part ($>$ 90 km), we will not give our attention to these deeper layers.

The features described above are also recognized on the vertical cross sections (Figures 2.14). In Figure 2.14 (a), LV-A is lying at about 50 km depth with HV-A beneath it. LV-A becomes shallow and thick in the western part with a thickness as much as 25 km. This thick part of the LV-A is also seen in Figure 2.14 (d). Another inclined low velocity layer (LV-B) dipping to west is clear and it is located above the high velocity region. This high velocity region corresponds to the HV-B. In Figure 2.14 (b), we can clearly see the LV-A dipping to the NNW with HV-A below it. Beneath the pair of LV-A and HV-A, we observe another pair, LV-B and HV-B underneath it. A thick low velocity zone is observed in the middle to the northern part of Boso peninsula (right side in Figure 2.14 (b)). We suppose that this low velocity zone is made of LV-A and LV-B, and phantom image due to large error mentioned in the previous paragraph. In Figure 2.14 (c), LV-A and the corresponding high velocity layer HV-A are also recognized. Below the LV-A and HV-A pair, the LV-B and HV-B pair is observed.

2.5 Discussion

Seismic activity in the target area is generally high. The occurrence of some moderate earthquakes and swarm activities are already well investigated and discussed with consideration of the tectonic background in this region by other authors. In this section, we compare the obtained P-wave velocity model with other geophysical information in the target area. This clearly indicates that the LV-A is located at the boundary between the EUR and PHS plates, and LV-B between the PHS and PAC plates. Comparison with previous studies suggests that they are the subducting crusts on PHS and PAC plates.

2.5.1 Earthquakes near the plate boundary.

Southwestern Ibaraki swarm. The southwestern Ibaraki region is a seismically active area (hatched area along B-B' in Figure 2.18). The active swarm along B-B' is interpreted as interplate thrust events between the EUR and PHS plates. (e.g. Kasahara (1985)). Focal mechanisms for the typical events of the swarm activity are shown in Figures 2.19 (a) and (b).

It is clear that those swarm events are located in the inclined low velocity layer (LV-A) in Figure 2.14 (b). This supports the result by Hurukawa and Imoto (1992) who interpreted that these earthquakes occur in the low-velocity oceanic crust of the subducted PHS plate.

As shown in the previous section, LV-A is getting pronounced from a depth of 30 km. Ashiya et al. (1987) revealed the depth distribution of the Conrad and Moho discontinuities beneath the Kanto-Tokai district. They concluded that the Moho is located at a depth shallower than 30 km around Tokyo Bay region. Since there is a large velocity contrast for a medium in the crust and mantle, we suppose that the low velocity PHS crust becomes detectable after it subducts into the

high velocity EUR mantle.

Hori (1990) and Hurukawa and Imoto (1992, 1993) inferred that the low-density gabbro at the surface of the subducting PHS plate transformed into a high-density eclogite at a depth deeper than about 60 km based on the analyses of later phases and earthquake focal mechanisms. Thus it is expected that the low velocity layer extinguishs at this depth. However, the low-velocity layer (LV-A) seems to extend to a depth of 65 km or 70 km in our result, which does not coincide with their studies.

Tsukuba-Chiba Seismic Belt. The seismic activity along C-C' is called Tsukuba-Chiba Seismic Belt (Hurukawa and Imoto, 1990). Focal mechanisms which are considered to be typical in this activity are shown in Figure 2.19 (c) and (d). Most of these events are of low angle thrust fault type with westward slip vectors. Thus they are interpreted as interplate earthquakes between the PHS and PAC plates (e.g. Kasahara, 1985). Most of them are located in LV-B in our model (Figures 2.14 (b) and 2.14 (c)). Two moderate earthquakes that occurred in the Tsukuba-Chiba seismic belt are discussed below.

Southern Ibaraki earthquake of 1983. On February 27, 1983, an earthquake of magnitude 6.0 took place in the central part of the Tsukuba-Chiba seismic belt. Focal parameters relocated in this study are as follows: latitude = 35.976° N; longitude = 140.104° E; focal depth = 68.5 km. Focal mechanism obtained by NIED is shown in Figure 2.20. Location of the hypocenter is shown in Figure 2.18. This event is interpreted as an interplate thrust fault type earthquake between the PHS and PAC plates (Hurukawa and Imoto, 1990; Okada and Kasahara, 1990), of which fault plane dips westward at a low angle. We can see that this event is located in the LV-B, that is an

inclined low velocity layer attached to the top of a high velocity layer (HV-B) (Figure 2.14 (a)). This indicates LV-B corresponds to the boundary region between the PHS and PAC plates.

Ibaraki-Chiba border earthquake of 1985. This magnitude 6.1 event occurred on October, 4, 1985 in the central part of the Tsukuba-Chiba seismic belt. Focal parameters relocated in this study are as follows: latitude = 35.897° N; longitude = 140.104° E; focal depth = 72.9 km. Focal mechanism obtained by NIED is shown in Figure 2.20 and the epicenter location is also shown in Figure 2.18. The event was interpreted as an intraplate earthquake in the PAC plate by Hori (1986), and Hurukawa and Imoto (1990) based on its focal mechanism and hypocenter location. It is clearly seen that this intra PAC event took place in the high velocity layer (HV-B) underneath the inclined low velocity layer (LV-B) (Figures 2.14(a), 2.14(b), and 2.14 (c)). Although the eastern extension of HV-B is not very clear (Figure 2.14 (a)) because of the lower resolution, we can surmise HV-B corresponds to the high velocity mantle portion of the subducting PAC plate.

East off Chiba earthquake of 1987. On December 17, 1987, an earthquake of magnitude 6.7 took place off the east coast of Chiba Prefecture. This was the largest event in the target area in the last 60 years. Focal parameters of the event relocated in this study are as follows: latitude = 35.391° N; longitude = 140.472° E; focal depth = 43.5 km. Focal mechanism is shown in Figure 2.20 and the epicenter is shown in Figure 2.18. Okada and Kasahara (1990) suggested that it is an intra PHS plate earthquake. In our result, although it is contaminated by the phantom image in the Boso peninsula region, the event is located in the high velocity layer, HV-A (Figure 2.14 (b)). Moreover, they pointed out that a shallower seismic activity

in this region including some aftershocks occurred along the upper boundary of the PHS plate. Our result confirms their interpretation. This shallower activity and the southwestern Ibaraki swarm are both located along the low-velocity layer LV-A (Figure 2.14 (b)).

2.5.2 Subducting oceanic crust.

Comparison with hypocenter distribution and focal mechanisms described above strongly suggests that LV-A and HV-A are in the PHS plate. On the other hand, we attribute LV-B and HV-B to be the subducting PAC plate although they have slightly lower amplitude perturbations.

Hino et al. (1992) conducted a refraction seismic profiling in the Izu-Bonin arc with using ocean bottom seismographs. They estimated that the thickness of the upper crust is about 10 km and that of the lower crust is also about 10 km along the profile of latitude 33° N in the Izu-Bonin arc, that is close to the southern edge of our target area. The PHS plate is subducting under the Japan arc including this Izu-Bonin arc portion (e.g. Ishibashi, 1987; 1988a; 1988b). In the shallow layers (depth $<$ 40 km), LV-A is thick in the western part. The thickness of the relatively low velocity region is as much as 25 km in the west and less than 10 km in the central and eastern part (Figure 2.14 (a)). In deeper layers, the thickness of LV-A decreases (Figure 2.14 (d)). Therefore we suggest that LV-A is the subducting crust of the Izu-Bonin arc portion in the PHS plate at shallow depths and the pair of LV-A and HV-A is the subducting PHS plate itself at deeper depths. Since the crust has a lower density than that of the mantle portion of a continental plate (e.g. Kudo and Kono, 1993; Hino et al., 1992; Iwasaki et al., 1990), the thick Izu-Bonin arc crust can not subduct easily beneath the EUR plate. In the western part of our

target area, the crust of the Izu-Bonin arc is stacked in the shallower part, so that it shows rather thick low velocity anomaly.

The northern edge of LV-A in Layers 6, 7, and 8, which corresponds to the depth range from 30 km to 45 km, does not shift its horizontal location with depth. It is located in the western Kanto district, from 139° 25'E to 139° 55'E at 35° 55'N. Since an abrupt change of gravity anomaly is expected at this location, we compare the distribution of the velocity anomalies in the Kanto district with that of the gravity anomalies.

Kudo and Kono (1994) pointed out the lineament-like distributions of gravity anomalies in the Kanto district. They showed an EW-strike gravity lineament of about 40 km length in the western part of the Kanto plane (See Figure 2(B) in Kudo and Kono (1994)). We call it Kawagoe-Noda line from its location (Figure 2.16). The Kawagoe-Noda line is located just on the northern edge of LV-A. The low velocity zone steeply dipping to the north, which is located around the Kawagoe-Noda line, is recognized in the cross section along D-D' (Figure 2.14 (d)). Therefore this line can be interpreted as the northern edge of the subducting crust of the PHS plate at this depth range.

The crust of the PHS plate to the south of this line directly contacts with the continental crust of the overriding EUR plate, and it begins to subduct into the mantle of the EUR plate. A similar phenomena is observed in the Kinki district where the crust of the PHS plate is considered to subduct northwestward into the mantle of the EUR plate and an abrupt gravity change is seen (Hurukawa, 1983; Hori et al., 1985).

The Naoetsu-Choshi line (Kudo and Kono, 1994), which is a dominant lineament of gravity anomaly in central Japan, runs roughly from Maebashi to Choshi in the Kanto area (Figure 2.16). This line corre-

sponds well with the shape of LV-A in the depth range of 30 - 40 km. We suppose it indicates a similar feature to that we discussed for the Kawagoe-Noda line. The PHS crust may begin to subduct into the mantle of the EUR plate in these depth ranges.

The subducting PAC plate has been also investigated by a refraction seismic profiling method. Iwasaki et al. (1989) revealed the subduction structure of the PAC plate in the Kuril trench region. They clarified that the oceanic crust with a total thickness of 8 km is subducting from the Kuril trench and it can be traced at depths as deep as 25 km. If it is a common feature of the PAC plate, we expect that the oceanic crust is also subducting beneath our target area. Obara (1989), Obara and Sato (1988) detected the S wave reflector beneath the Kanto district and pointed out that amplitude data of the reflected wave requires the existence of a thin low velocity layer between PHS and PAC plates. Depth distribution of the S wave reflector corresponds well with that of LV-B at 70 - 90 km depth range. Although the observed perturbation has a slightly lower amplitude, we infer that LV-B corresponds to the subducting PAC crust.

2.5.3 Geometry of the subducting oceanic plates.

Isodepth contour map of the subducting PHS and PAC plates derived in this study is shown in Figure 2.21. If the low velocity layers can be considered to be the oceanic crusts which are at the top of the subducting plates, the fronts of the low velocity layers represent the isodepth contour of the subducting PHS and PAC plates. Ishida (1992) gave a plate configuration model of the subducting PHS and PAC plates beneath the Kanto-Tokai district based on hypocenters distribution, seismic velocity structure, and focal mechanisms. In general, our result corresponds well with Ishida's model, though, there are some

slight differences. In our model, the PHS plate shows a more complicated shape in the depth range from 30 km to 45 km. It has a very steep dip around the Kawagoe-Noda line. For the PAC plate, our model corresponds well with Ishida's model, although uncertainty is still remained because of the lower amplitude of perturbation.

2.6 Summary

We have shown the result of a high resolution velocity structure inversion beneath the Kanto district, central Japan. The result strongly suggests that the obtained low velocity layers correspond to the subducting crusts at the surface of the Philippine Sea and the Pacific plates.

The low velocity layer in the subducting Philippine Sea plate can be traced clearly at depths from 30 km to 60 km. Its location moves north or northwestward with depth. We suggest that it is the crust of the subducting Izu-Bonin arc in the Philippine Sea plate at shallow depths, and is the oceanic crust at the top of the Philippine Sea plate at deeper depths. Low density crust of the Izu-Bonin arc is probably stacking in the area from 139°25'E to 139°55'E at 35°55'N, which is observed as a thick low velocity layer to the south of the area and its steep dip angle to the north of the area. This is also recognized from the gravity anomaly.

Since the low velocity layer is recognized at depths as deep as 65 km or 70 km for the PHS plate, phase transition from gabbro to high density eclogite probably does not occur in this depth range. Another low velocity layer was observed at depths from 60 km to 90 km that moves westward with depth. We infer this is the subducting oceanic crust at the surface of the Pacific plate. Thrust earthquakes, that occur at the plate boundaries between the Eurasia and the Philippine Sea plates

and between the Philippine Sea and the Pacific plates, distribute in these low velocity layers obtained in this study.

There are several studies that shows the existence of low velocity bodies in the mantle wedge portion beneath active volcanoes, such as in central Japan and Tohoku. In these studies, the low velocity bodies are attributed to the deep structure of active volcanoes. We also found low velocity bodies located in the wedge portion beneath active volcanoes in the northwest Kanto region similarly to the cases of central Japan and Tohoku.

Layer	Depth	Reference Velocity	Minimum %Slowness	Maximum %Slowness	Maximum Velocity	Minimum Velocity	Error %Slownes
1	0.00	5.50	-17.2	8.2	6.64	5.08	1.5
2	4.00	6.00	-12.7	7.8	6.88	5.57	2.1
3	12.00	6.30	-11.2	13.4	7.10	5.55	2.4
4	20.00	6.60	-7.1	8.2	7.10	6.10	1.5
5	25.00	7.20	-9.1	12.3	7.92	6.41	2.1
6	30.00	7.80	-9.5	12.4	8.62	6.94	2.2
7	35.00	7.81	-8.2	13.0	8.52	6.91	2.1
8	40.00	7.83	-8.3	10.2	8.54	7.10	1.8
9	45.00	7.84	-6.4	9.6	8.37	7.15	1.5
10	50.00	7.85	-7.0	11.9	8.45	7.02	2.0
11	55.00	7.87	-4.0	7.1	8.19	7.35	1.7
12	60.00	7.88	-3.5	4.0	8.17	7.58	1.8
13	65.00	7.90	-4.2	4.1	8.24	7.58	1.8
14	70.00	7.91	-3.5	2.3	8.20	7.73	1.9
15	75.00	7.92	-3.2	2.9	8.18	7.70	1.3
16	80.00	7.94	-3.9	3.4	8.25	7.68	1.5
17	90.00	7.96	-3.3	3.4	8.24	7.70	1.4
18	100.00	7.99	-2.8	2.0	8.22	7.83	1.3

Table 2.1: P-wave Velocity model for the Kanto district. Column 3 represents the reference velocity. Columns 4 and 5 represent the minimum and maximum percent perturbations for the given layers. Columns 6 and 7 are the corresponding absolute velocities for the minimum and maximum perturbations, respectively. The thickness of the bottom layer is 10 km.

Station Code	Latitude	Longitude	Height	Delay
AKW	35.5201	139.3179	-0.01	0.32
ASG	35.3138	139.0279	0.39	0.14
ASO	36.6312	139.4646	0.76	0.28
CDP	36.1224	140.0932	-0.62	-0.26
CHS	35.7022	140.8550	-0.04	0.08
CKR	34.9674	139.9491	-0.66	0.06
ENZ	35.7360	138.8053	0.81	0.42
FCH	35.6507	139.4736	-2.71	-0.04
FJW	36.9833	139.6962	0.67	0.25
HAS	35.8259	140.7355	-0.78	-0.10
HDA	34.9646	138.8048	-0.05	-0.27
HHR	35.7353	139.0764	0.59	0.28
HRM	35.5508	139.6794	-0.54	0.58
HTS	35.0387	139.1715	-0.08	-0.16
ICH	35.4009	140.1768	-0.15	0.61
IWK	35.0981	139.8713	-0.01	0.35
IWT	35.9258	139.7381	-3.50	-0.53
KIB	36.8777	140.6578	0.30	0.16
KTU	35.1770	140.2689	-0.01	-0.02
MIN	35.1019	139.9901	0.11	0.24
MNB	36.1411	138.9174	0.90	0.22
MNK	36.8384	139.0588	0.77	1.14
MOR	35.9419	140.0048	0.00	0.27
MOT	36.5535	140.2167	0.14	0.15
NMT	36.3622	140.5838	-0.07	0.15
NMZ	35.1576	138.8462	0.11	0.02
NRY	35.0599	138.9628	-0.09	-0.38
OHR	36.3601	139.6923	0.24	-0.00
OMM	36.4971	139.3212	0.46	0.29
SHM	35.7934	140.0238	-2.28	-0.27
SSN	35.2622	138.8100	0.90	0.42
TRU	35.5105	138.9439	0.56	0.09
TR2	35.5120	138.8869	0.15	0.01
TYM	34.9713	139.8483	0.03	0.42
YFT	35.3675	139.6289	-0.03	1.04
YGW	35.1635	139.0928	0.14	-0.17
YKI	35.7185	140.5088	-0.14	0.22
YMI	36.0477	139.4396	-0.05	0.05
YMK	35.4870	139.0628	0.56	0.09
YSK	35.2077	139.6996	-0.19	0.75
YST	36.2530	140.2061	-0.07	-0.08

Table 2.2: Station coordinates and station delays. Station height is represented in unit of km and delays are in unit of second.

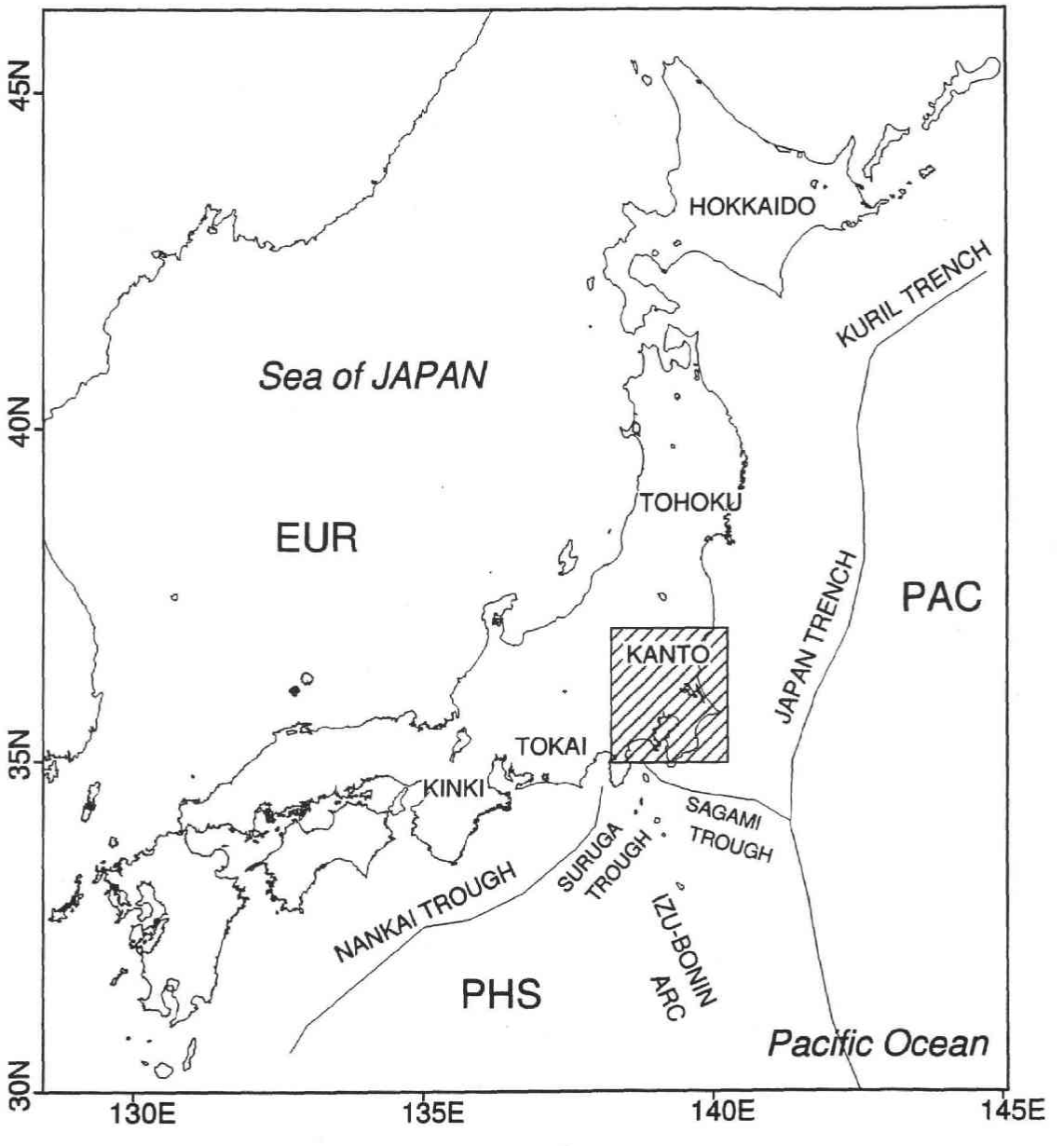

Figure 2.1: Map showing the relationship among the Philippine Sea (PHS), Pacific (PAC), and Eurasia (EUR) plates. The target area is denoted with a hatched square.

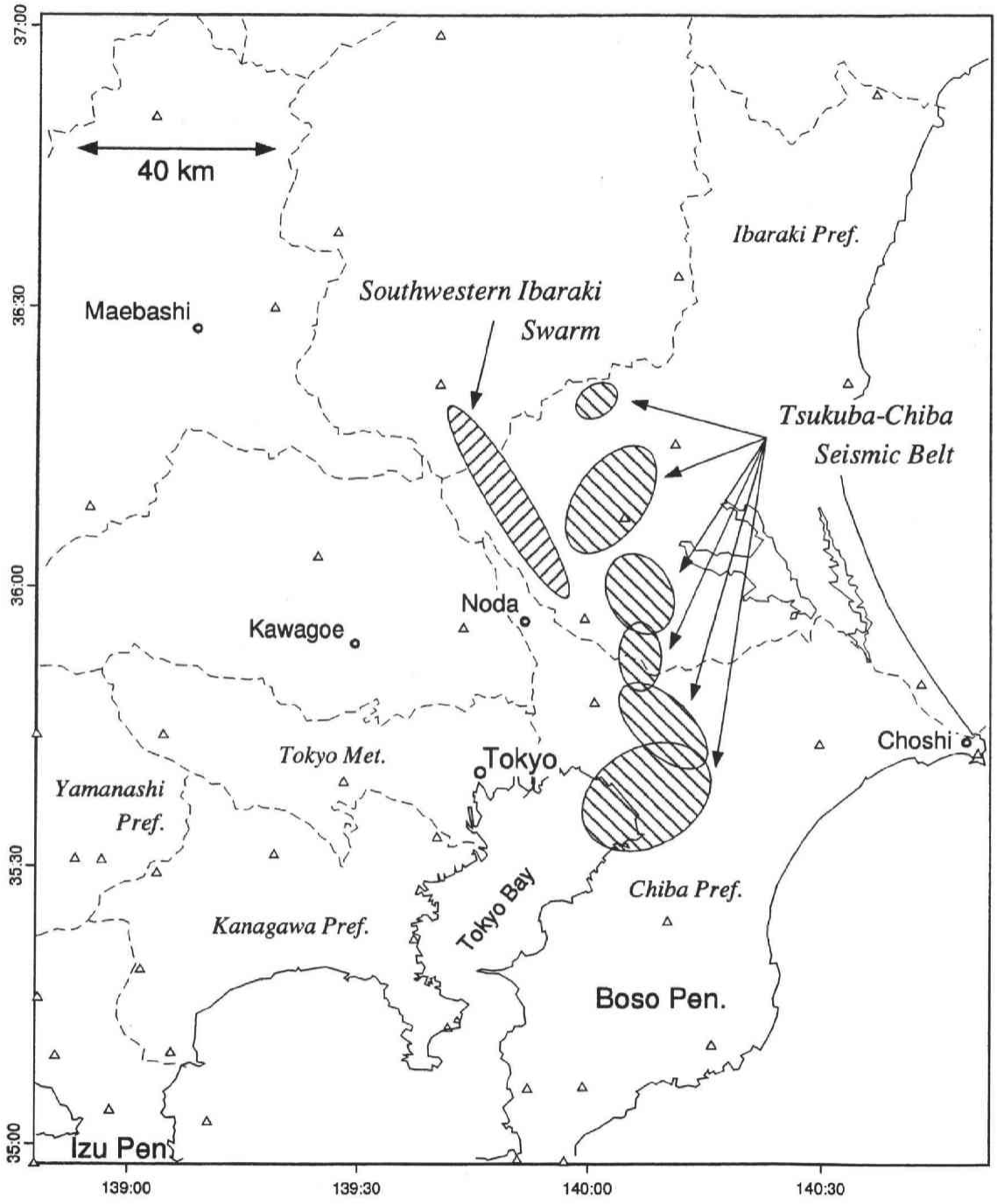

Figure 2.2: Close up of the target area. Open triangles represent seismic stations used in the study. Region names mentioned in the text are shown.

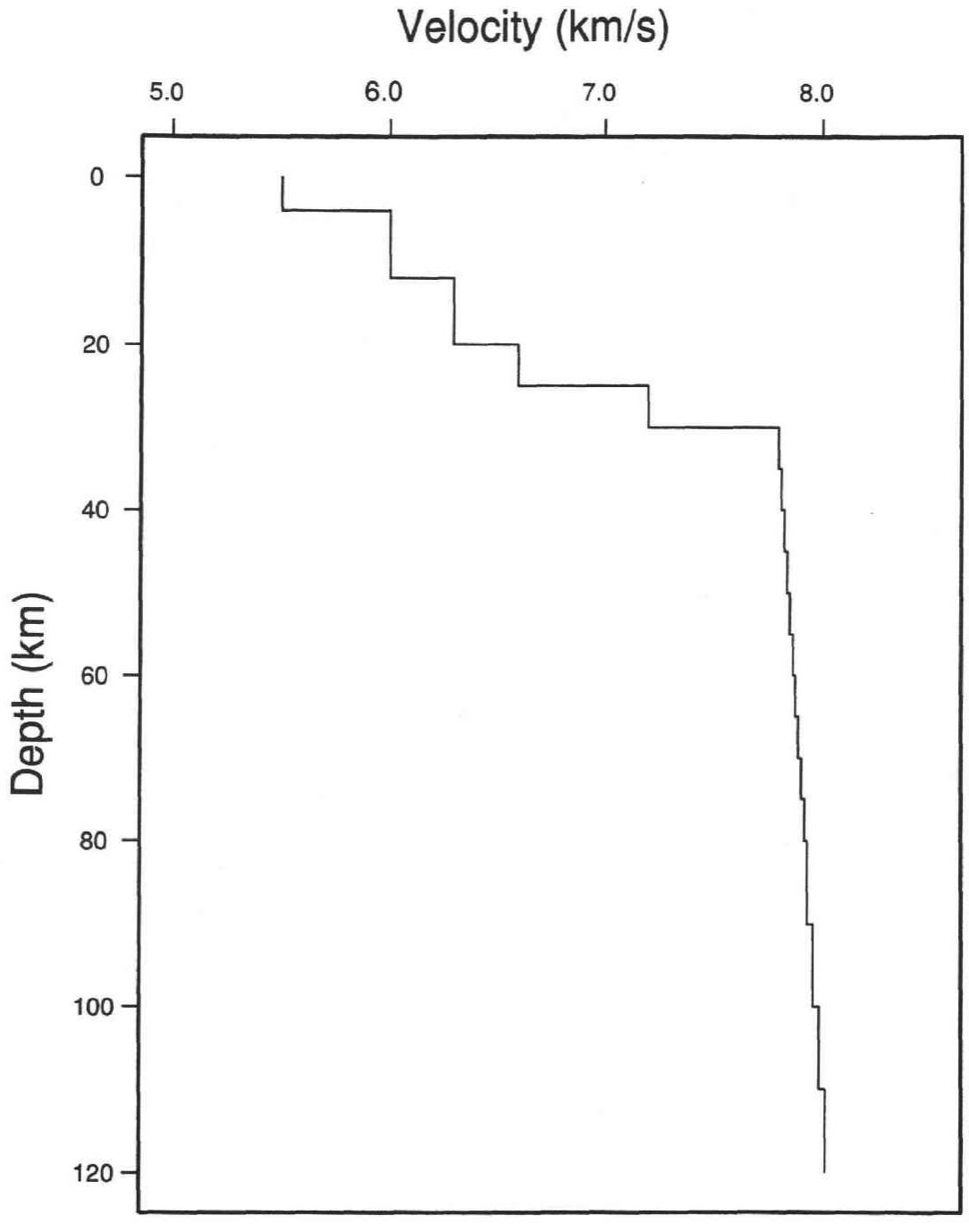

Figure 2.3: One dimensional reference P-wave velocity model. Each velocity discontinuity in this model corresponds to each block boundary in our block modeling.

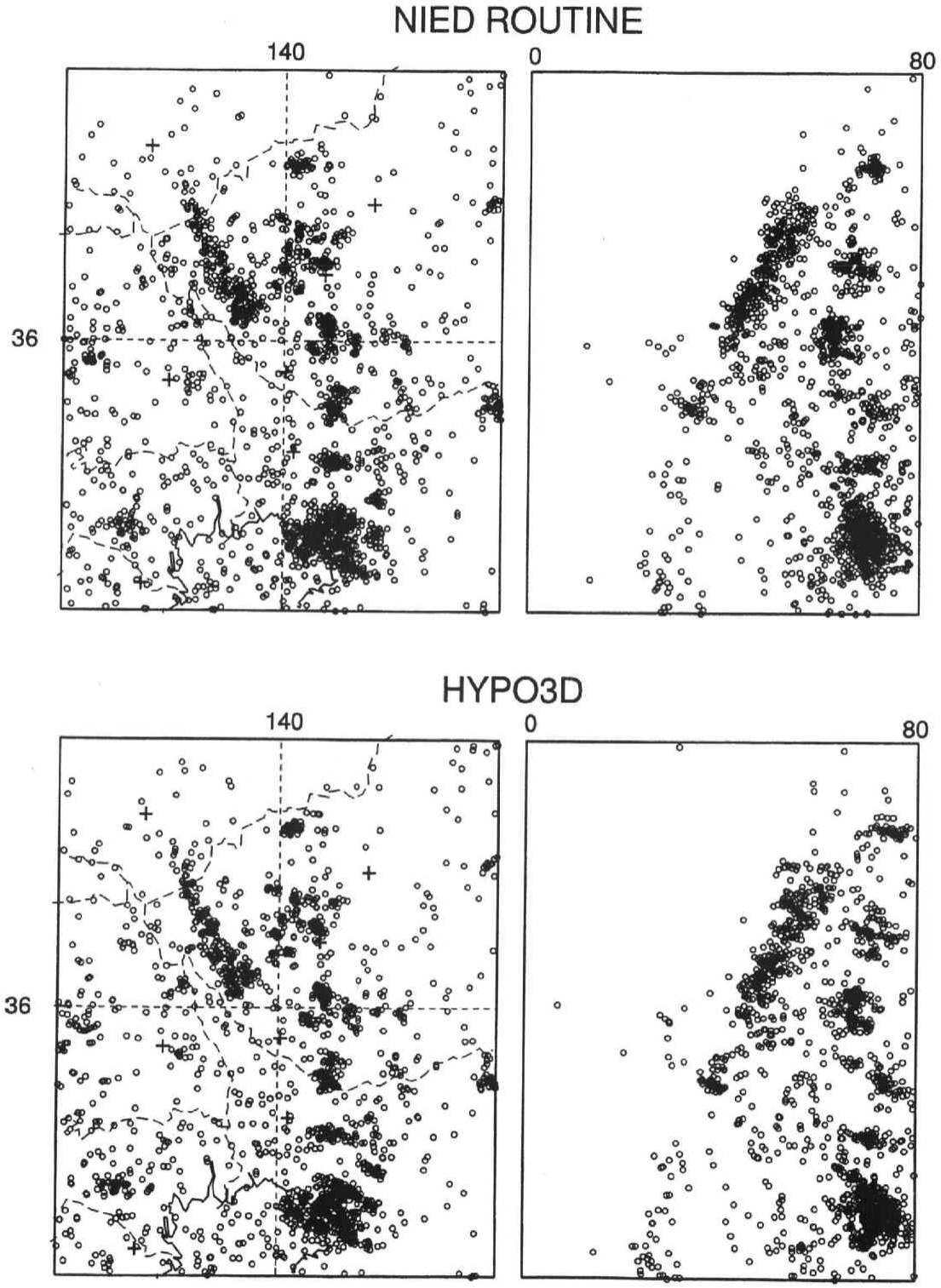

Figure 2.4: Hypocenter locations of relocated and routinely located events. Upper: Routinely located hypocenters by NIED. Lower: Relocated hypocenters using Hurukawa and Ohmi's method.

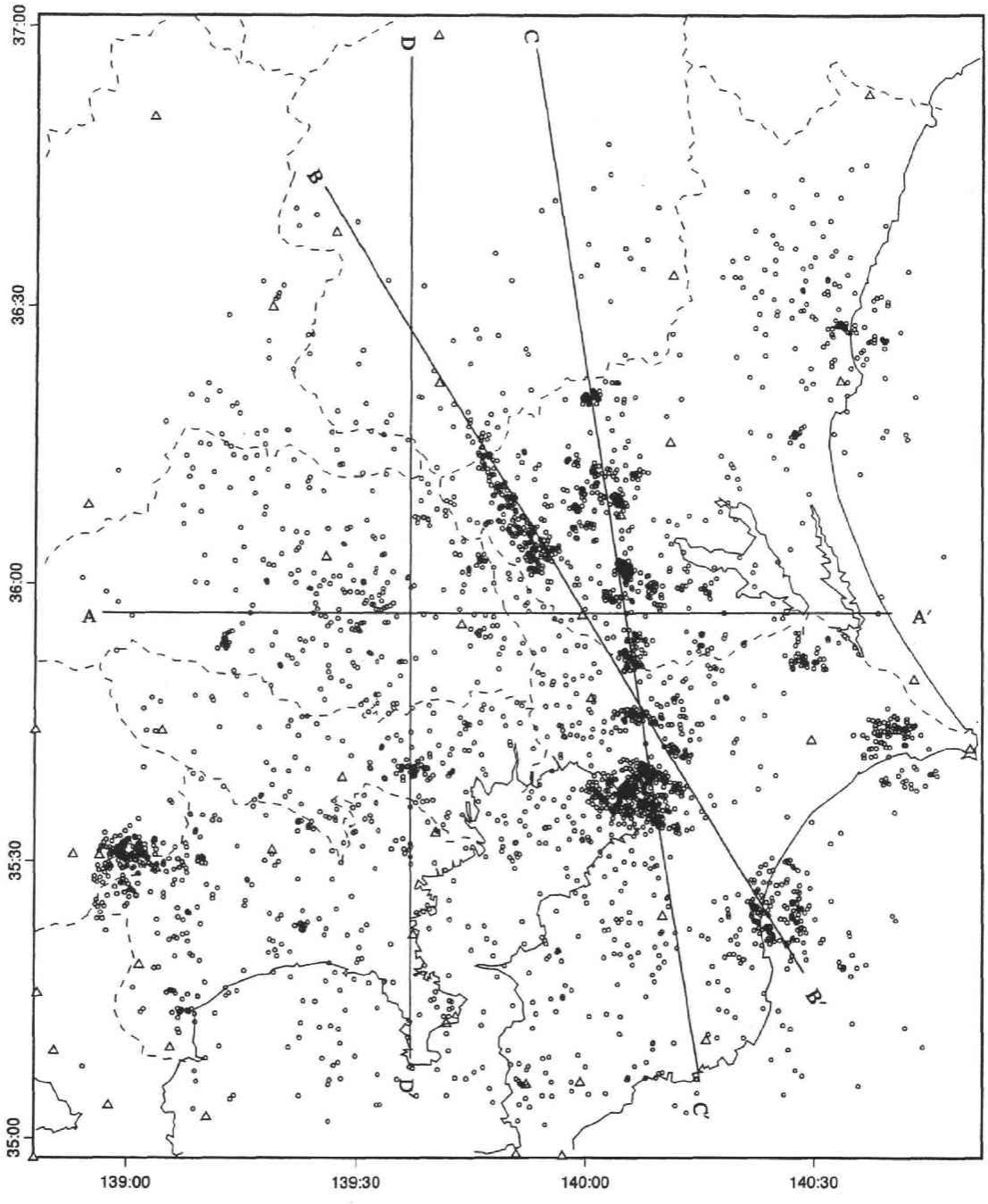

Figure 2.5: Epicenter distribution of events used in this study which are located with the reference velocity model. There are 3,038 earthquakes plotted. These events yielded 40,763 P-wave arrival times. Open triangles represent seismic stations.

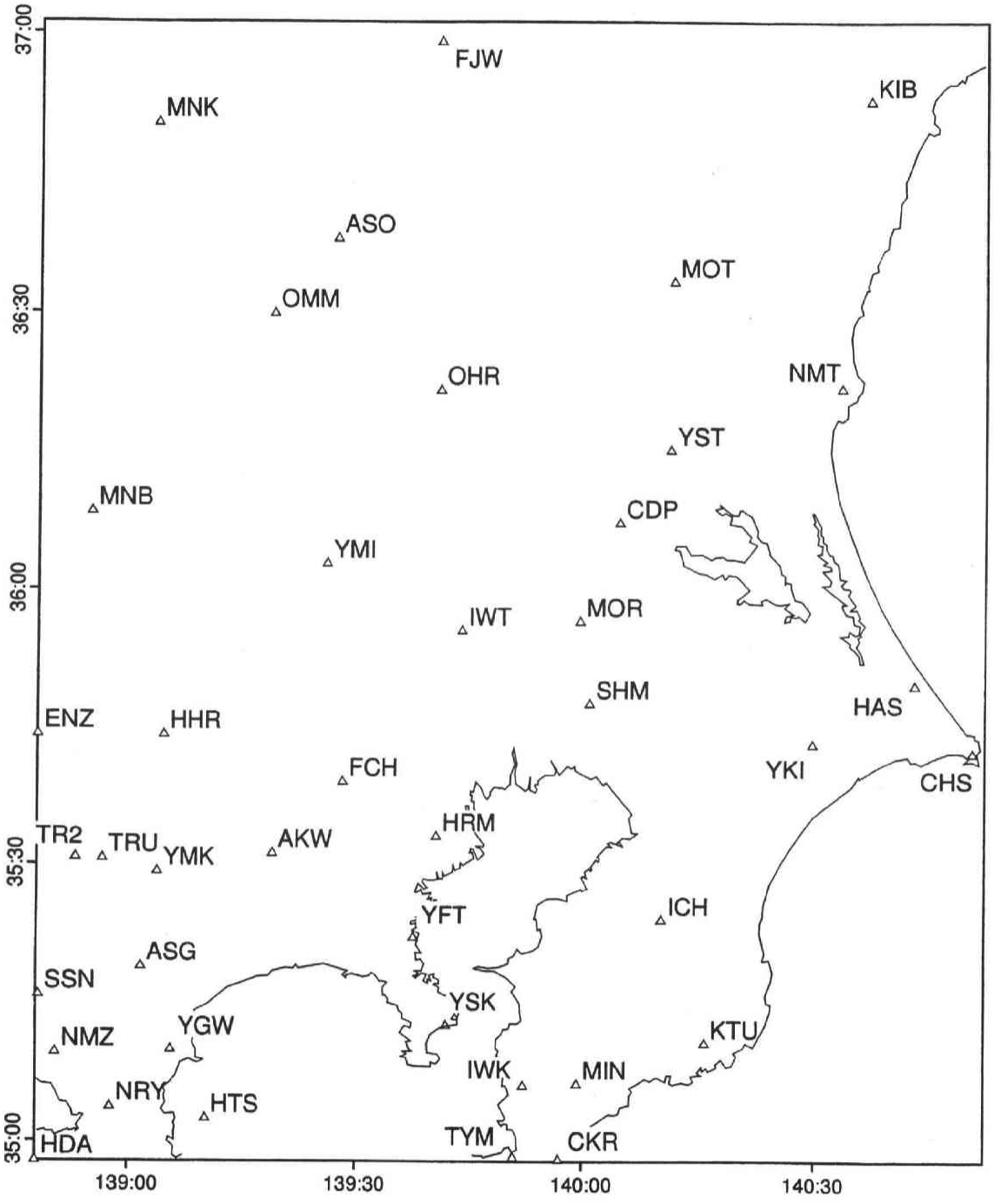

Figure 2.6: Site codes of seismic stations used in this study.

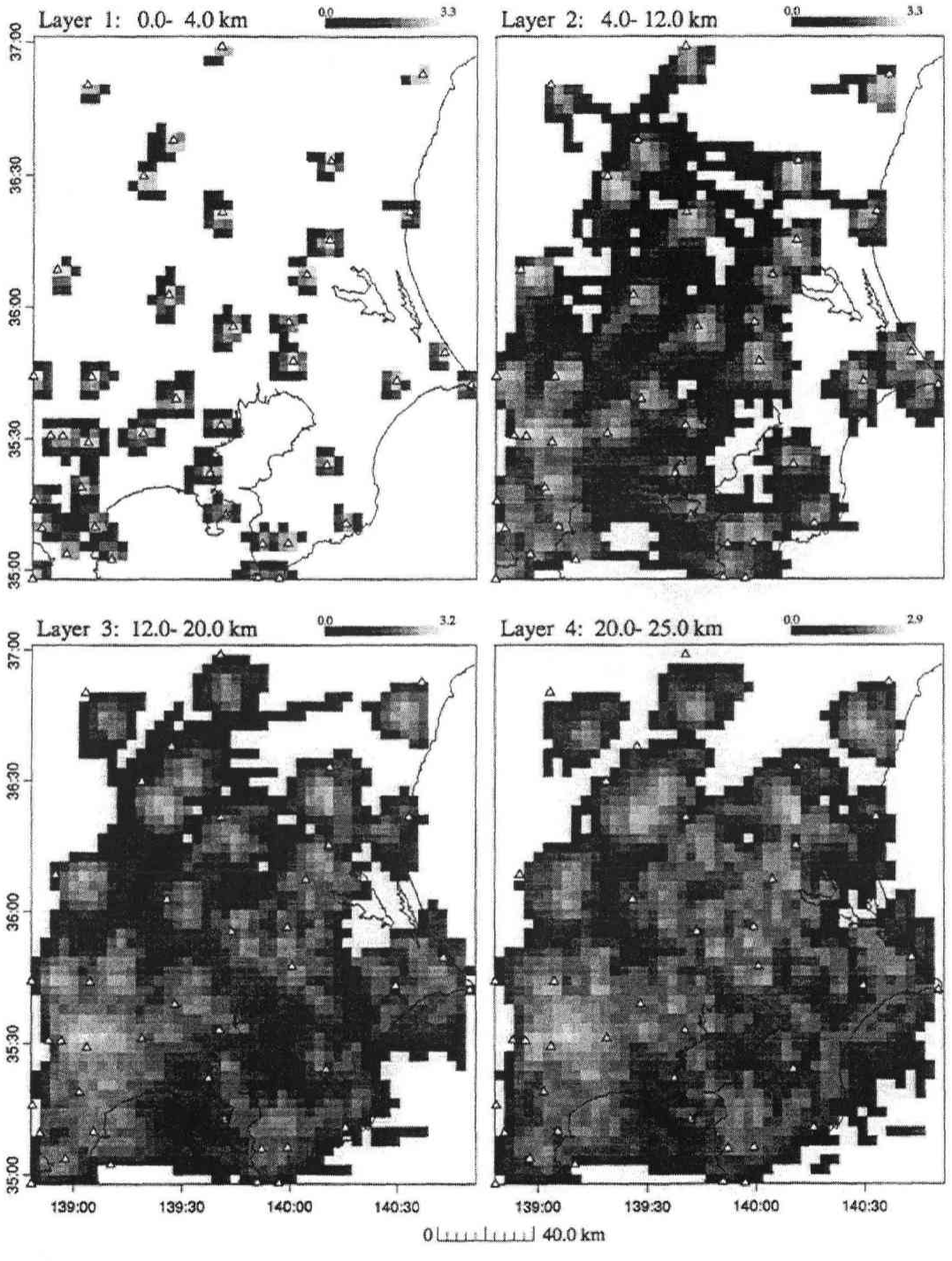

Figure 2.7: Density of ray paths in the target area. Gray scales show the number of rays that sampled each block. Numbers above the scale represent exponent of base 10.

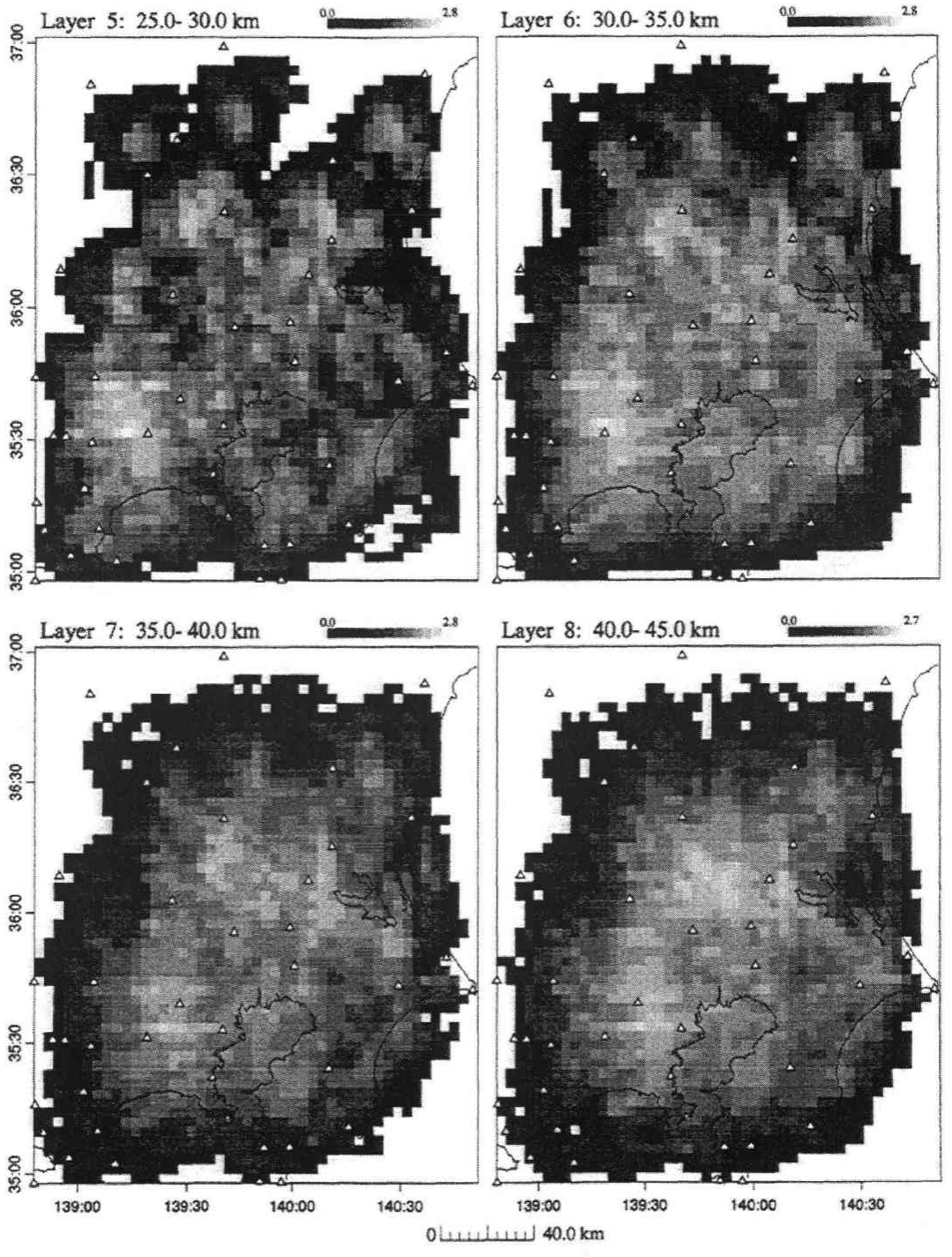

Figure 2.7: Density of ray paths in the target area (continued).

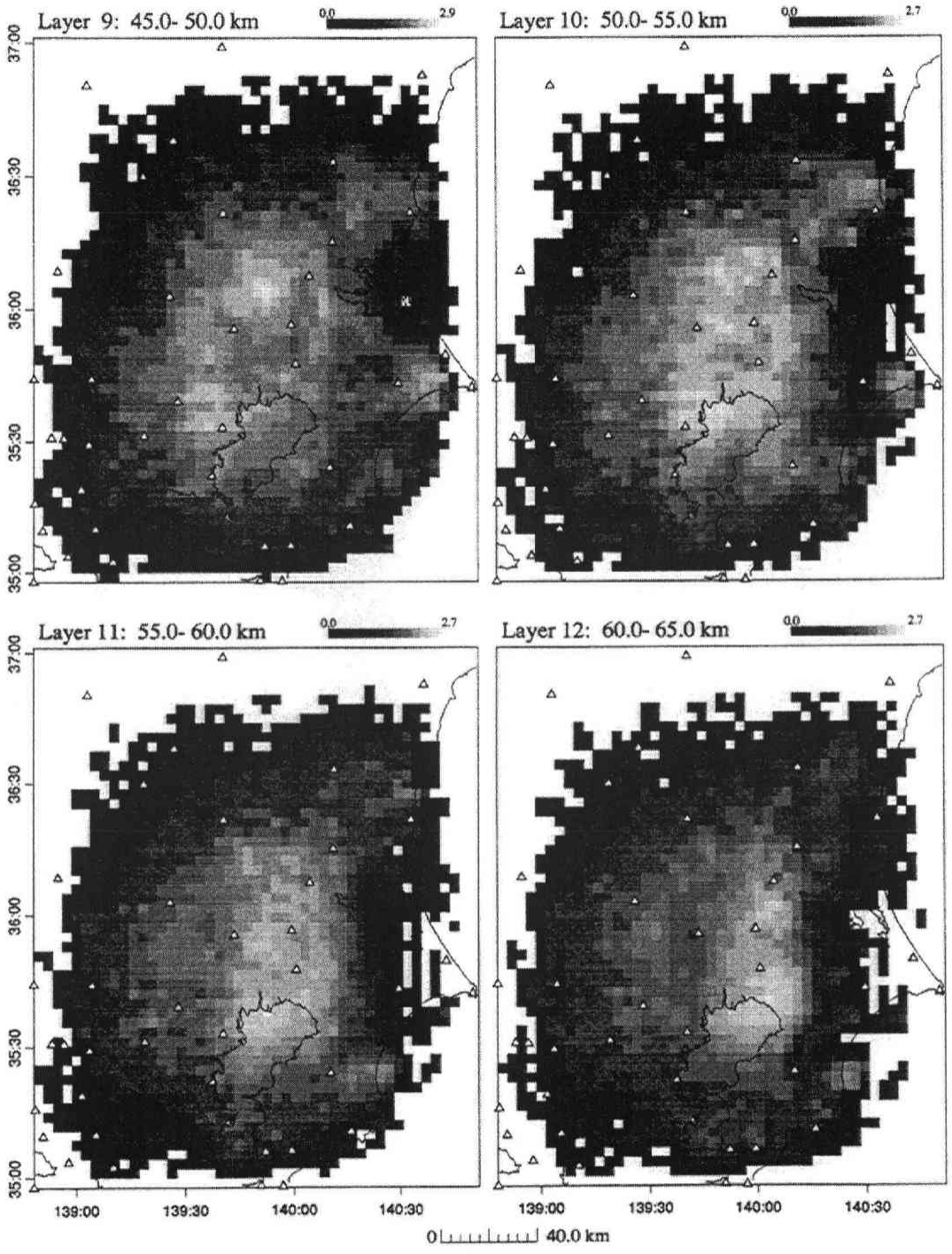

Figure 2.7: Density of ray paths in the target area (continued).

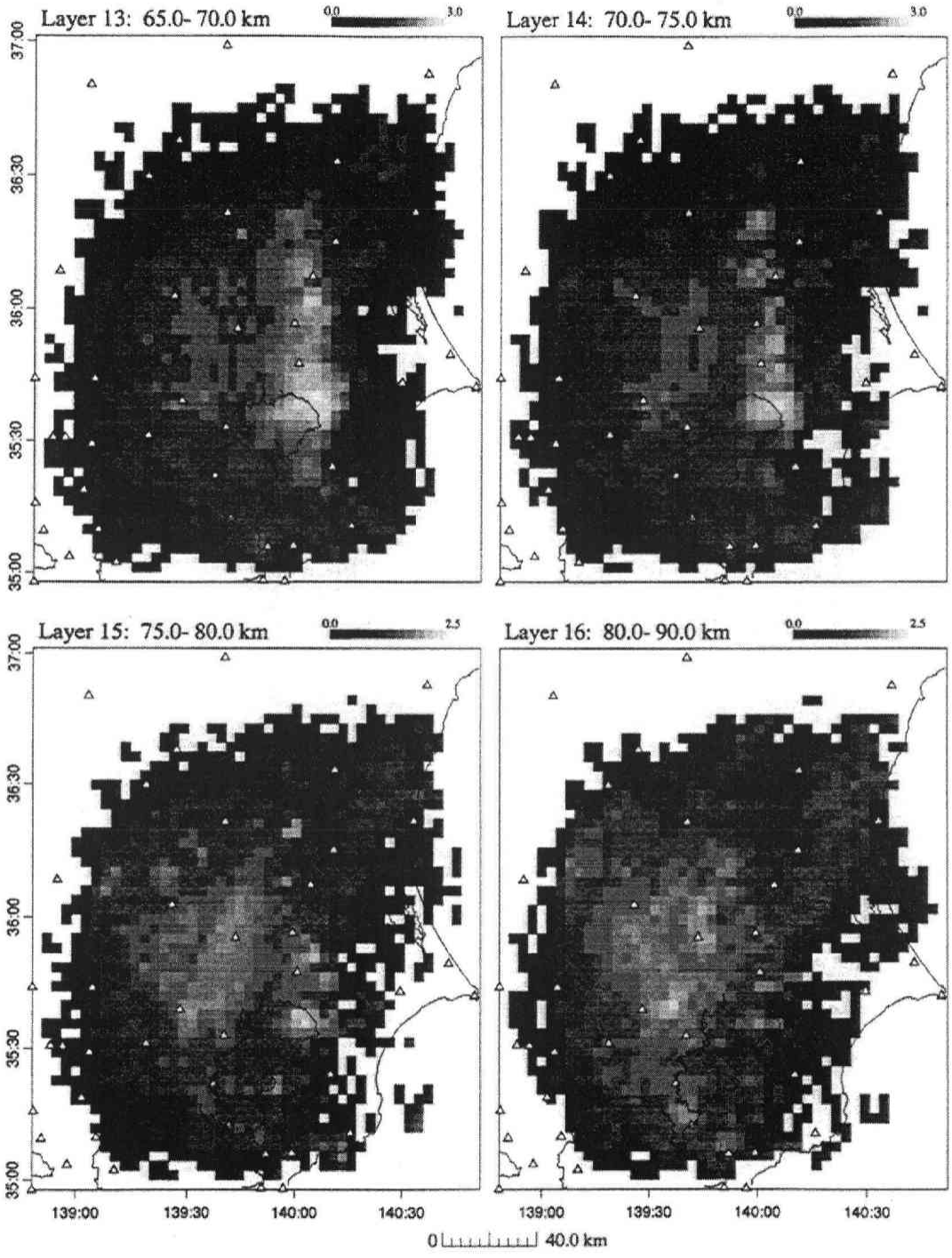

Figure 2.7: Density of ray paths in the target area (continued).

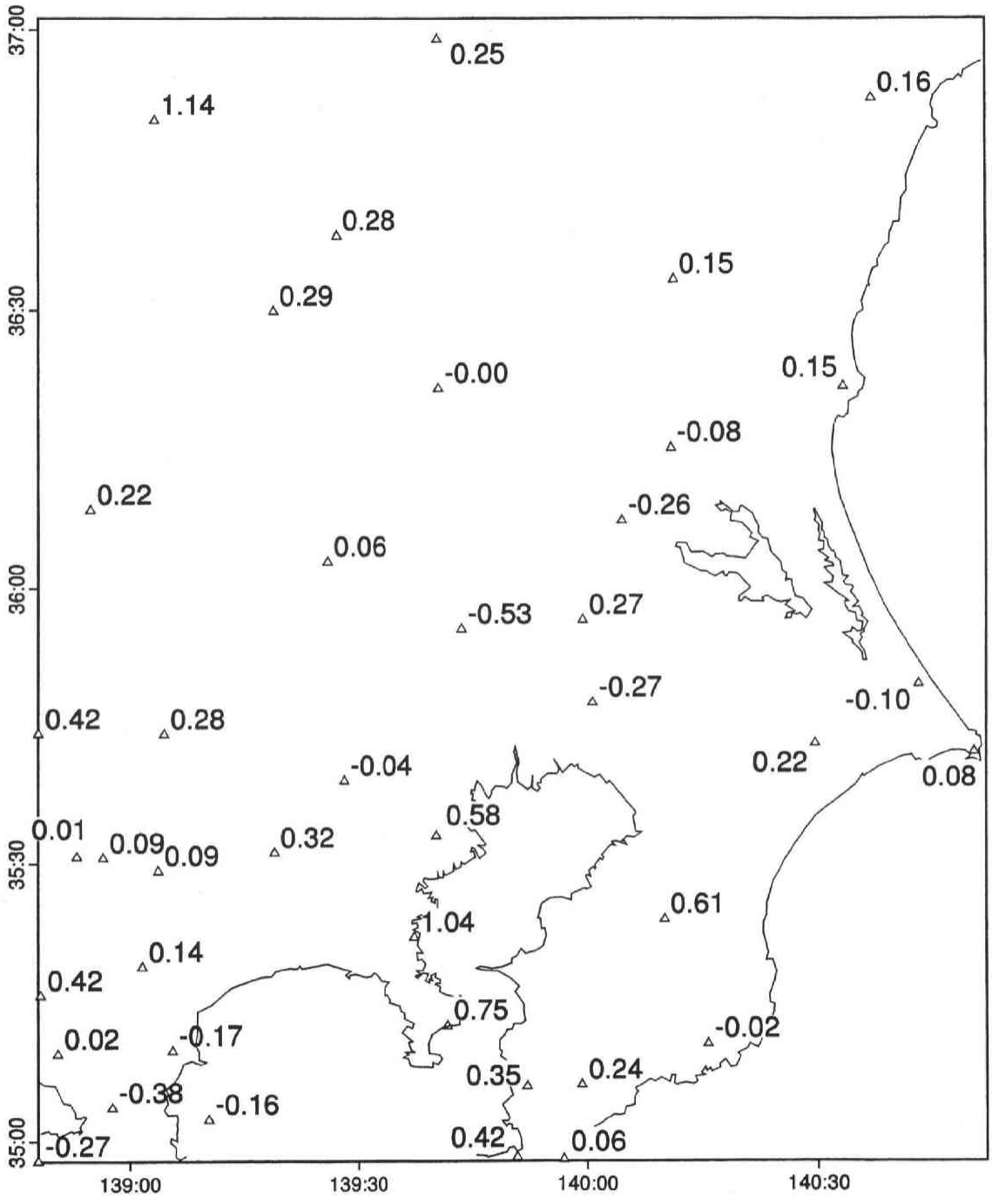

Figure 2.8: Distribution of station delays. Each number represents station delay in unit of second.

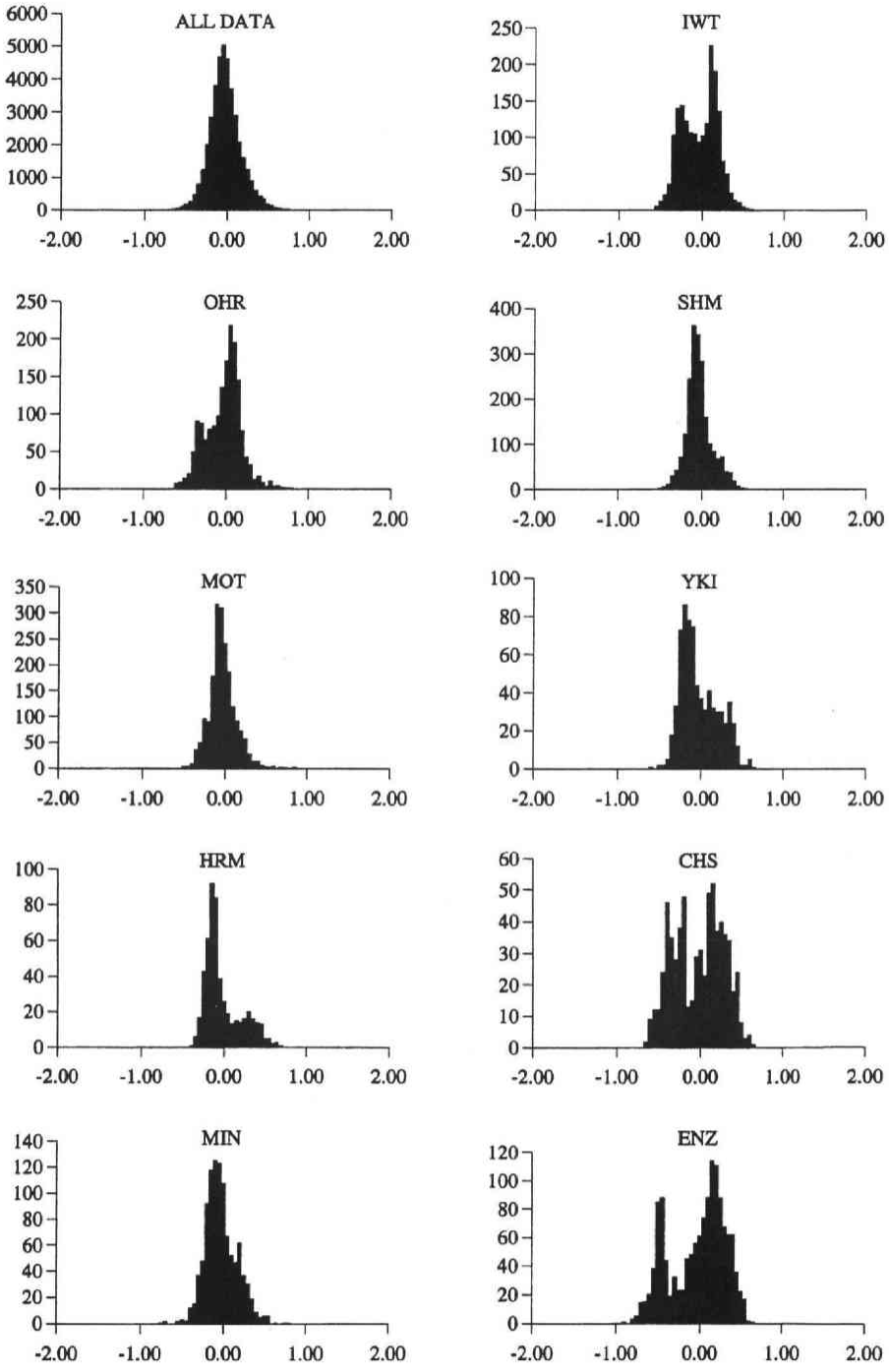

Figure 2.9: Histograms of station residuals for P arrivals. The horizontal axis is in seconds and the vertical axis represents the number of rays.

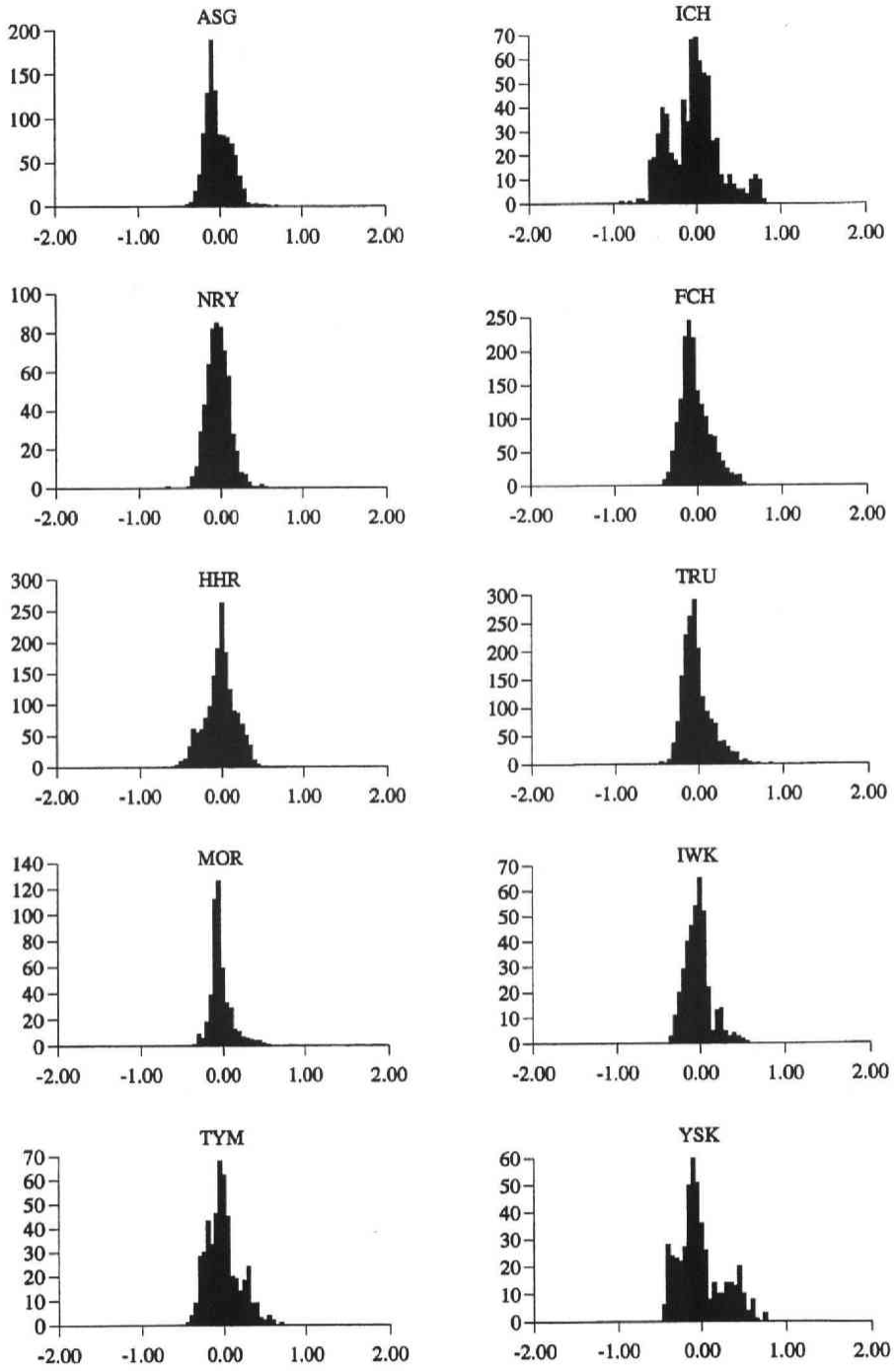

Figure 2.9: Histograms of station residuals for P arrivals (continued).

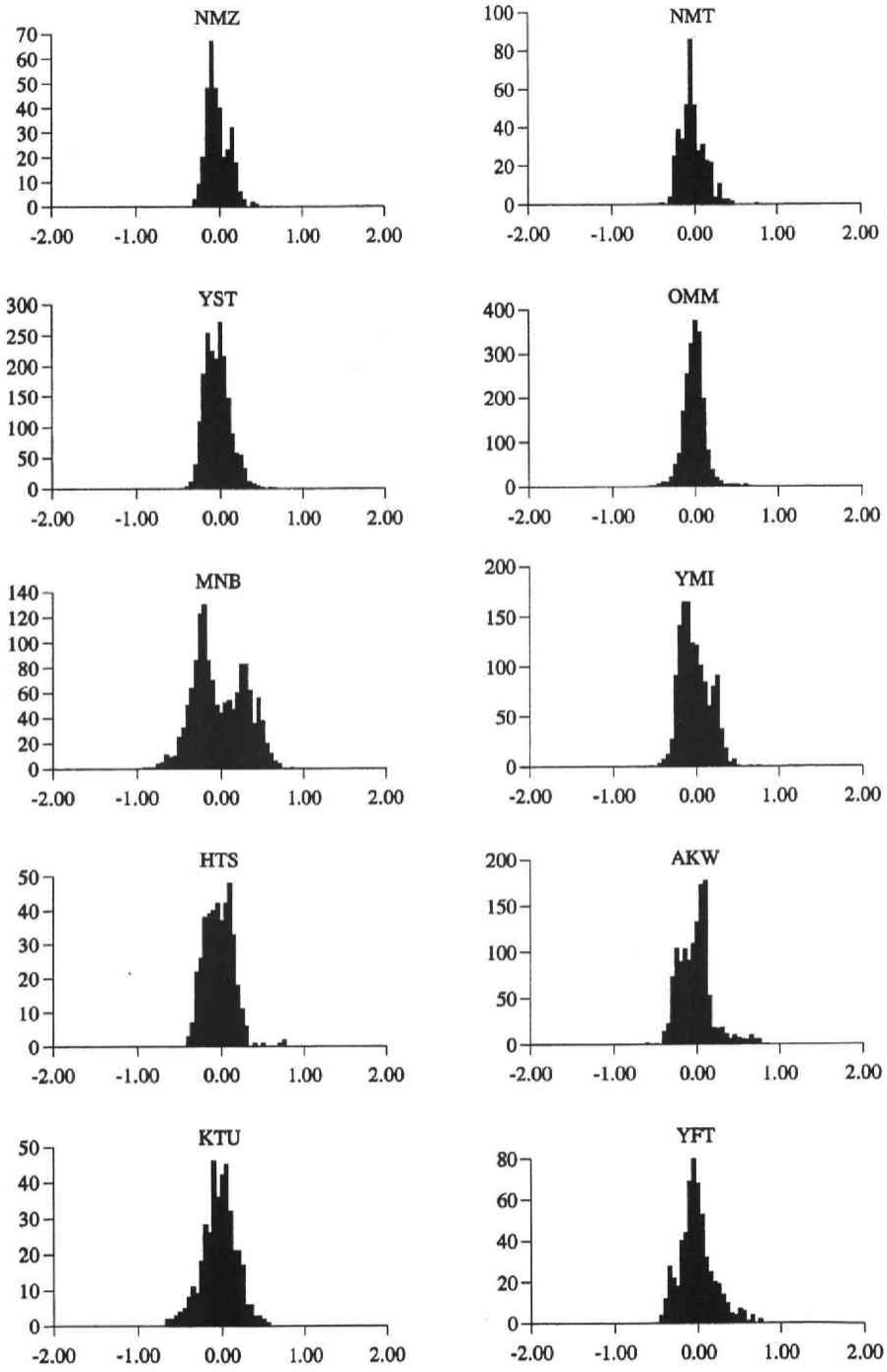

Figure 2.9: Histograms of station residuals for P arrivals (continued).

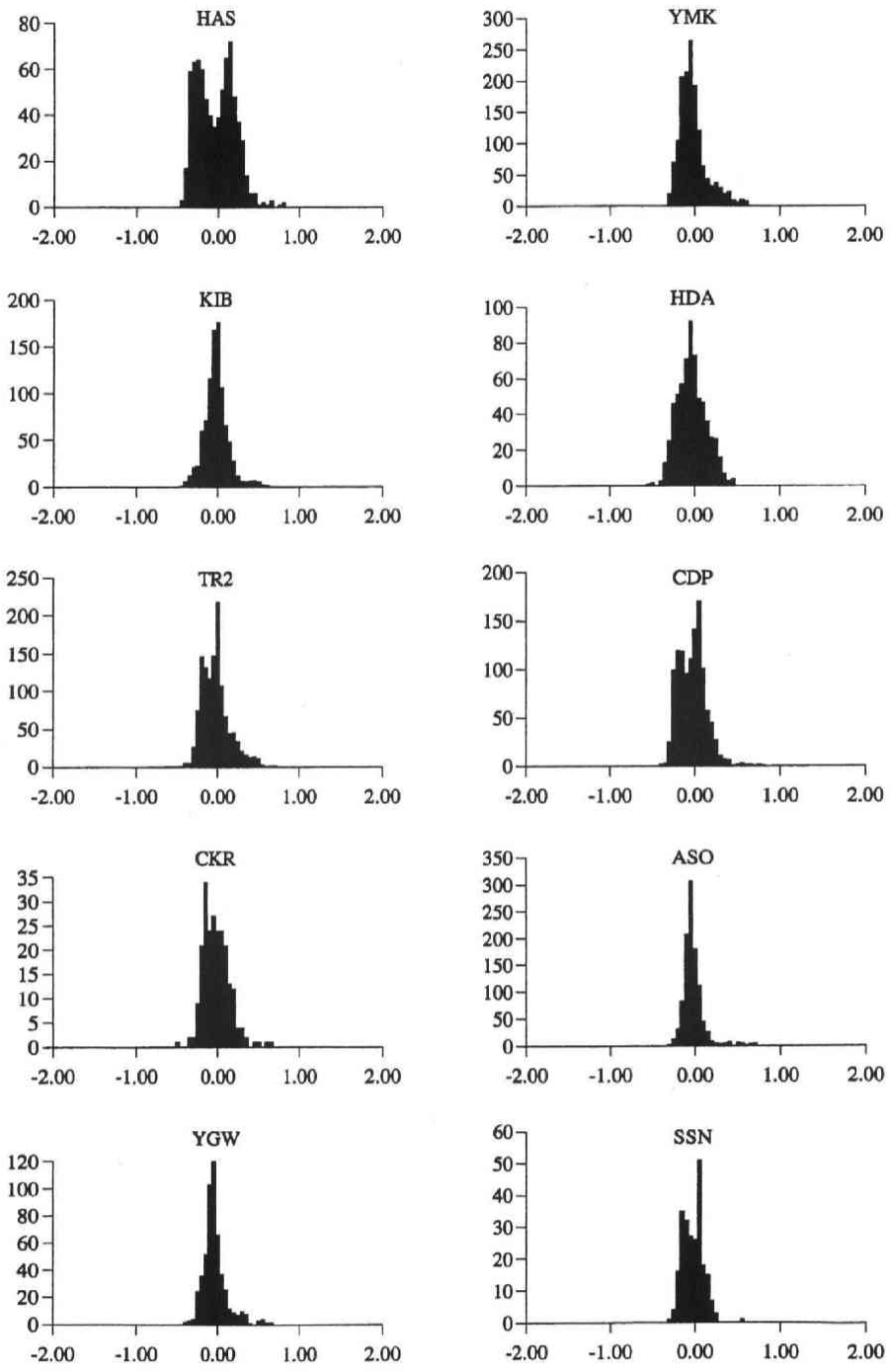

Figure 2.9: Histograms of station residuals for P arrivals (continued).

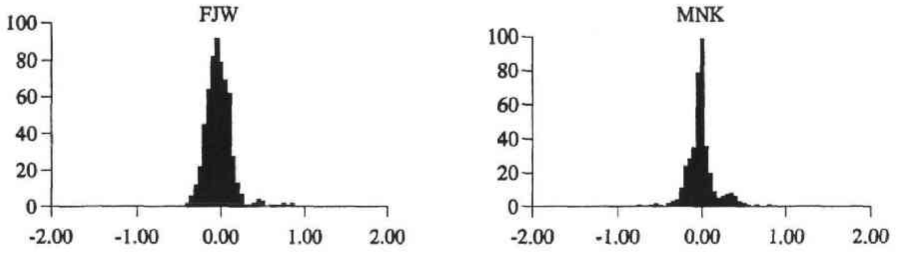

Figure 2.9: Histograms of station residuals for P arrivals (continued).

(e)

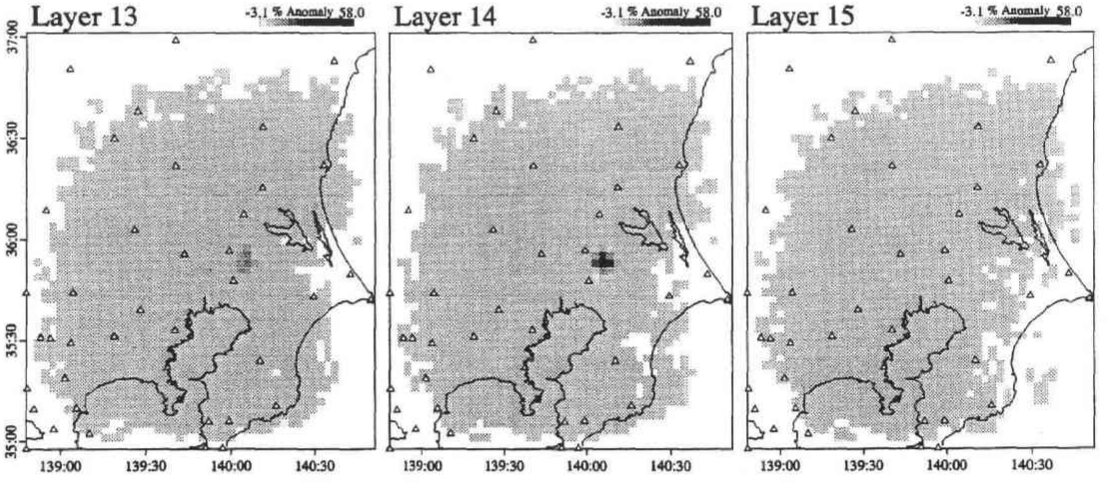

Figure 2.10: Estimated resolution kernels located in well resolved regions. (a) hypocenter area of Dec. 17, 1987 earthquake; (b) hypocenter area of Southwestern Ibaraki swarm; (c) hypocenter area of Feb. 27, 1983 earthquake; (d) hypocenter area of Oct. 4, 1985 earthquake. The lateral resolution length ranges from 2 or 3 blocks (8 km $\sim$ 12 km) near the center of the model and 3 or 4 blocks (12 km $\sim$ 16 km) near the edge of the model. (e) represents an example of vertical resolution change. The spike is located at the same block as that of (d).

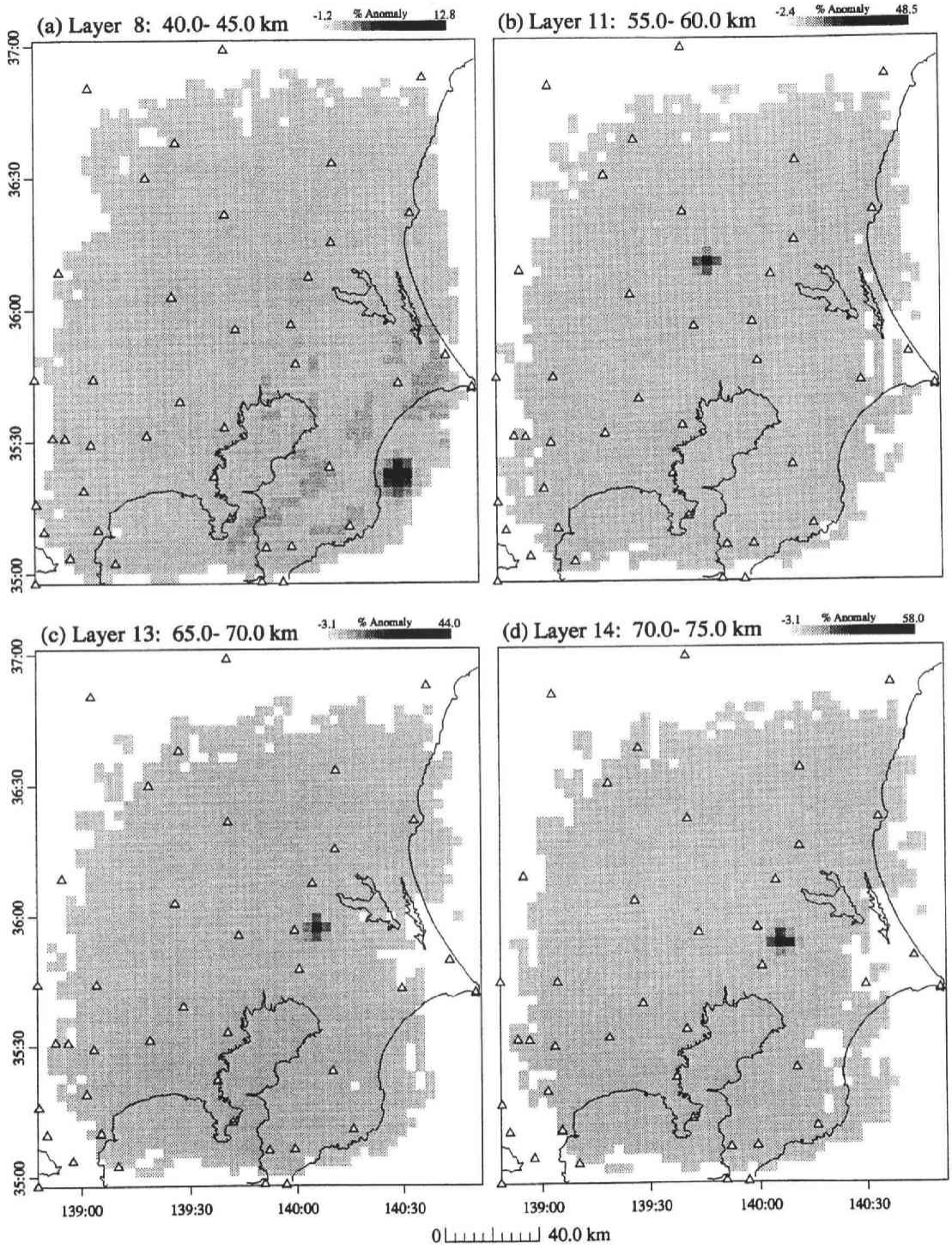

Figure 2.10: Estimated resolution kernels located in well resolved regions (continued).

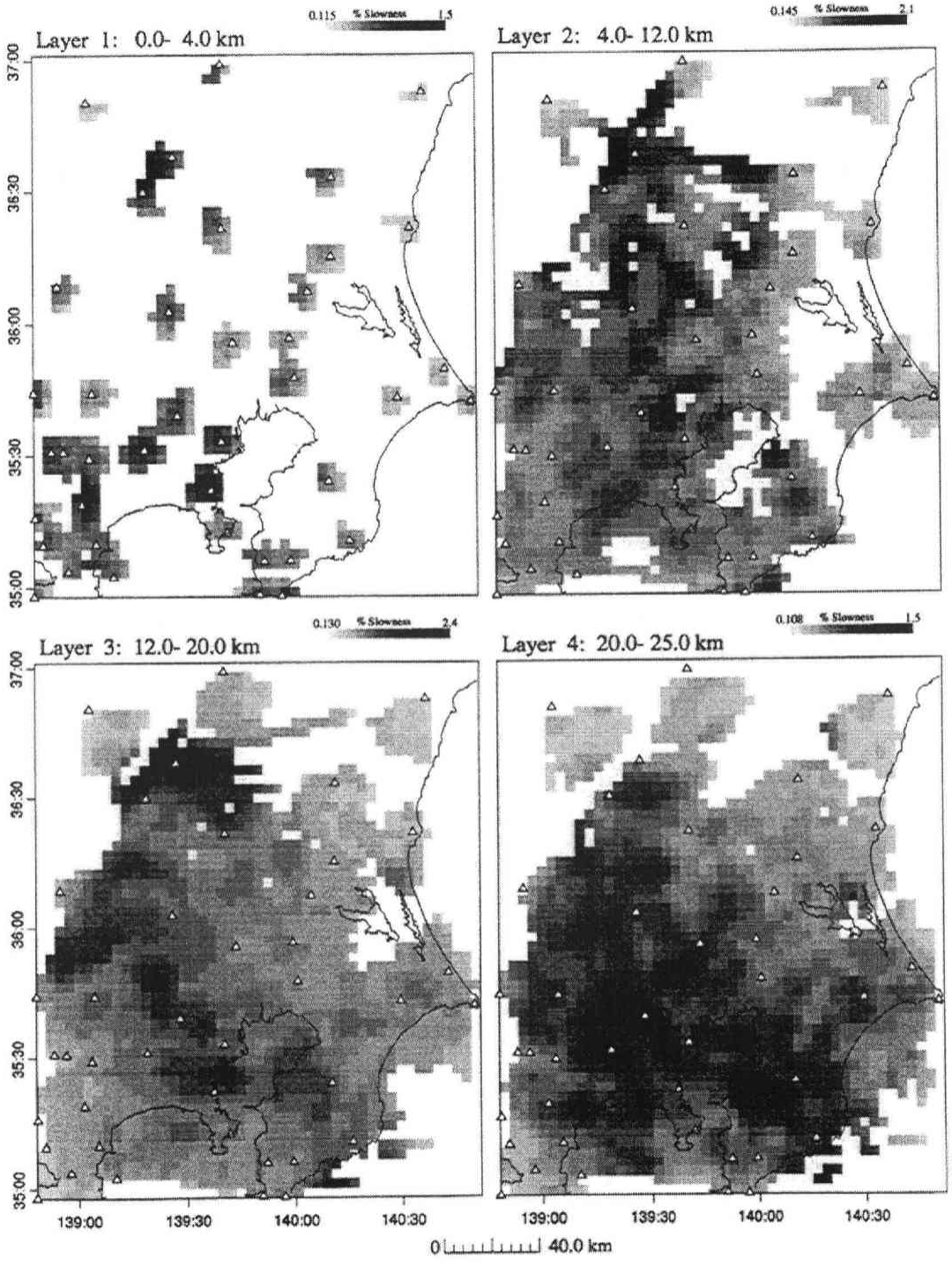

Figure 2.11: Jackknife estimates of standard errors. Errors are generally less than 2.4% perturbation.

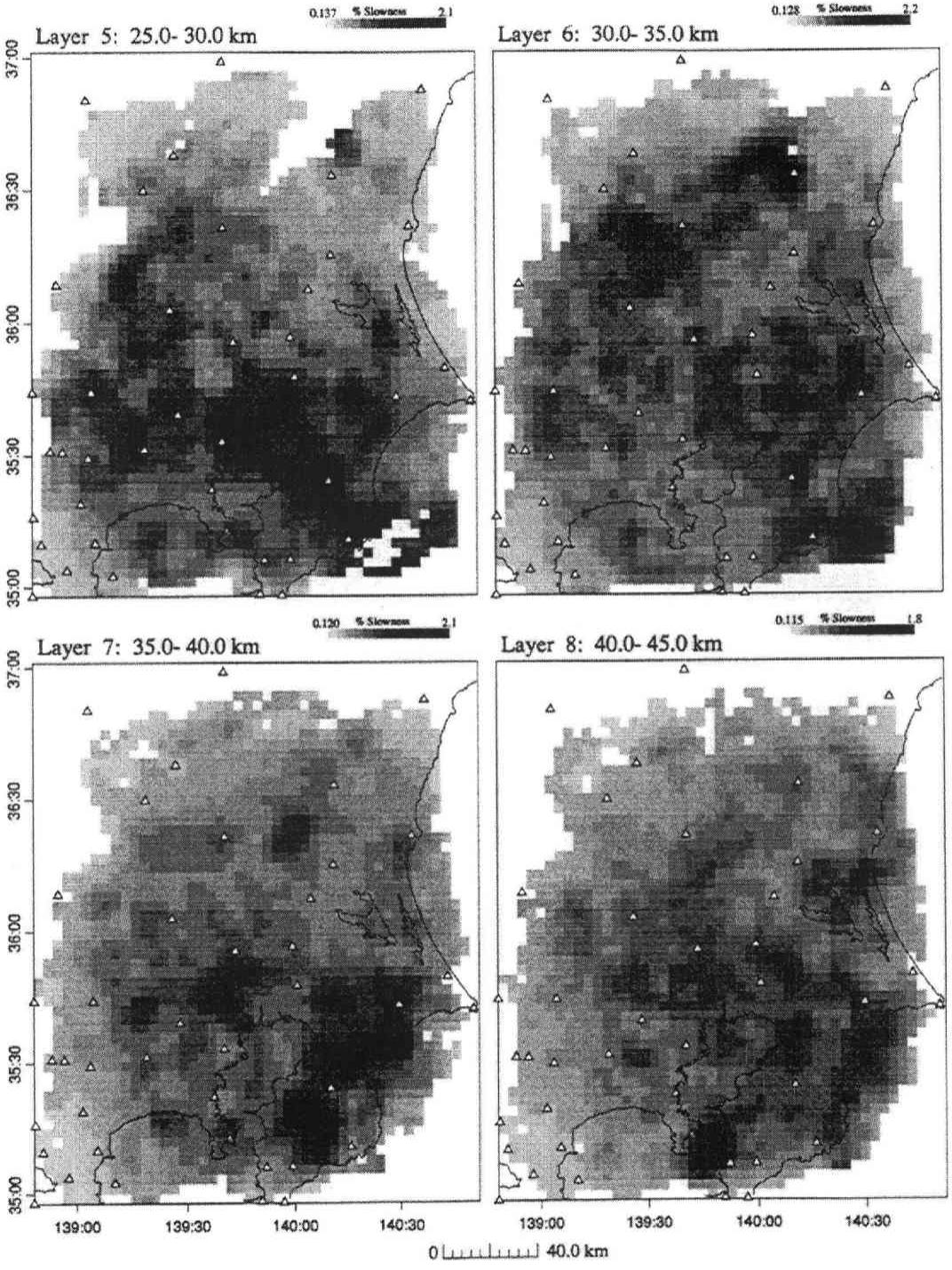

Figure 2.11: Jackknife estimates of standard errors (continued).

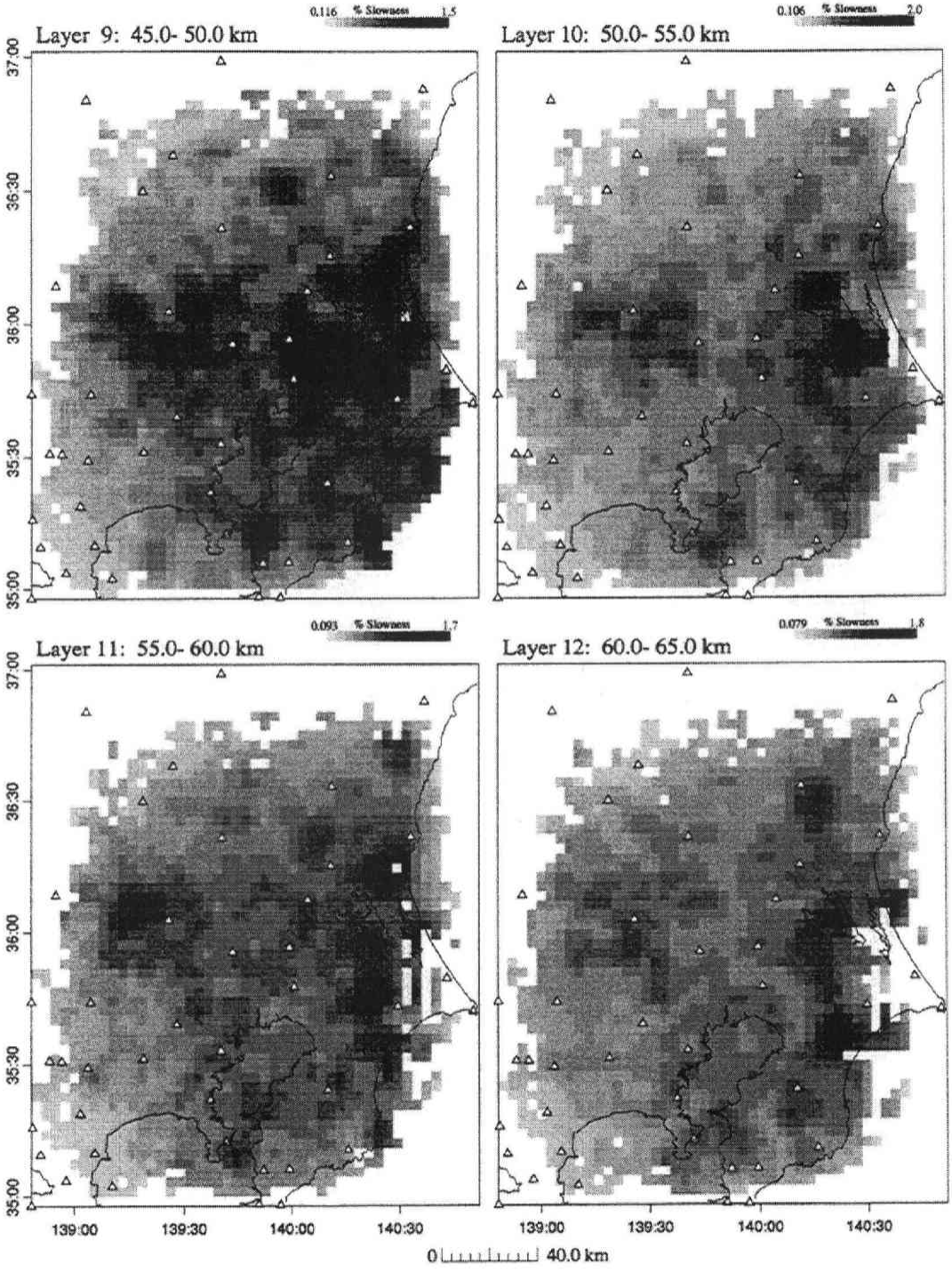

Figure 2.11: Jackknife estimates of standard errors (continued).

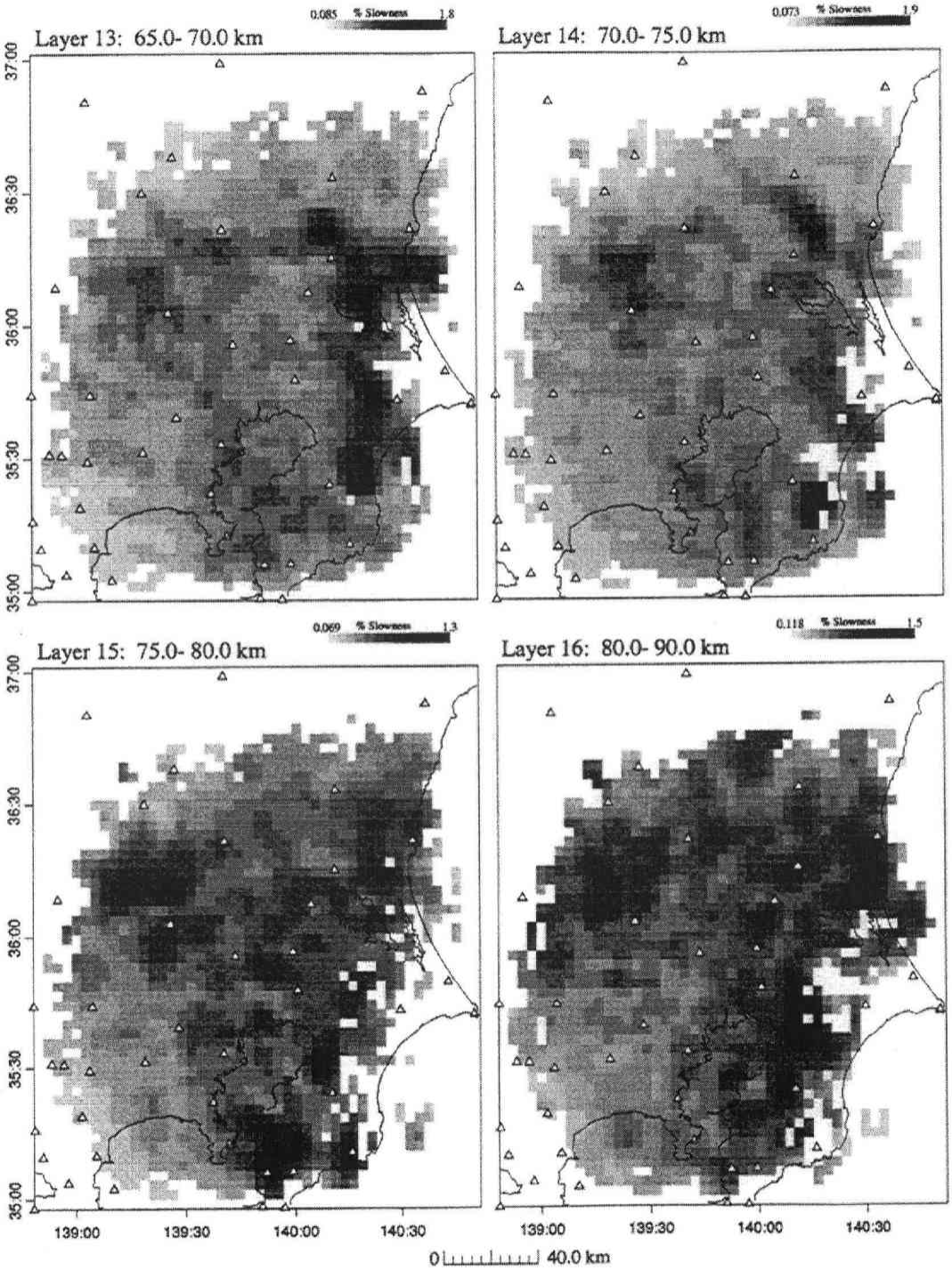

Figure 2.11: Jackknife estimates of standard errors (continued).

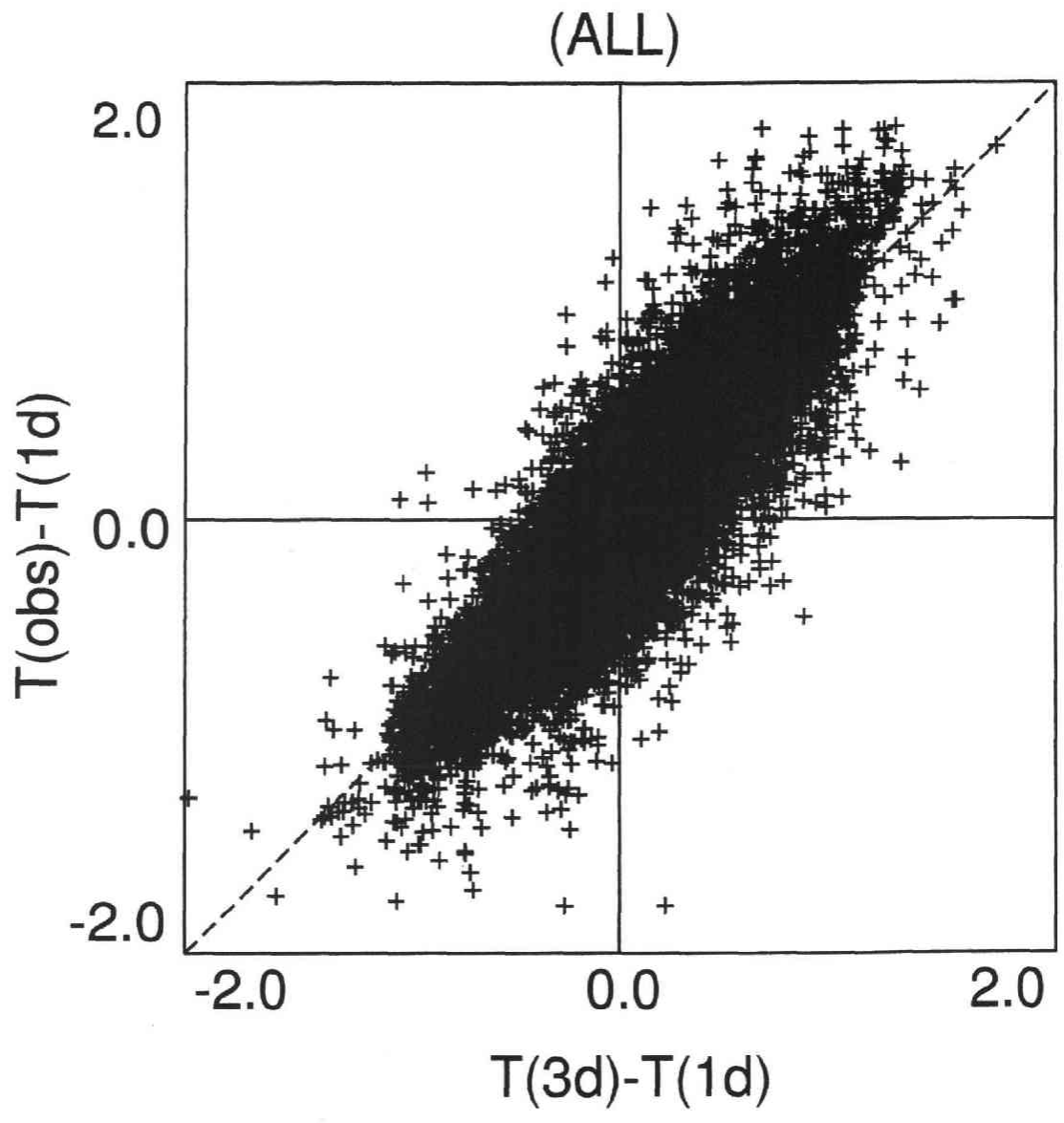

Figure 2.12: (a) Check of travel time residual improvement of all rays..

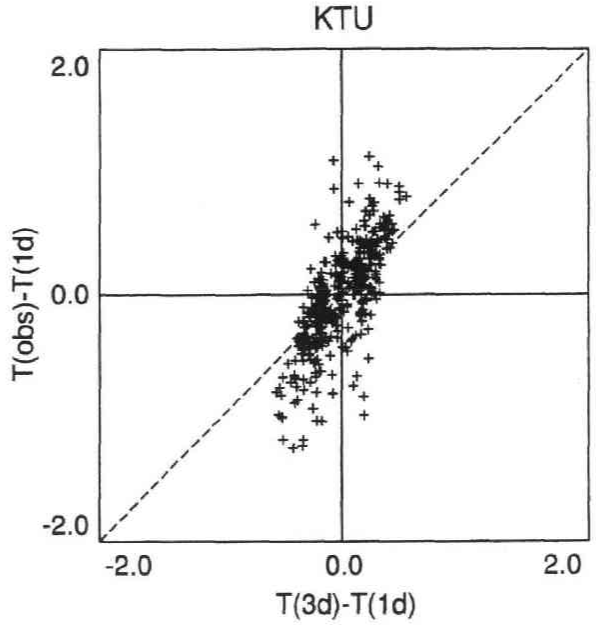

Figure 2.12: (b) Check of travel time residual improvement of the rays observed at KTU station.

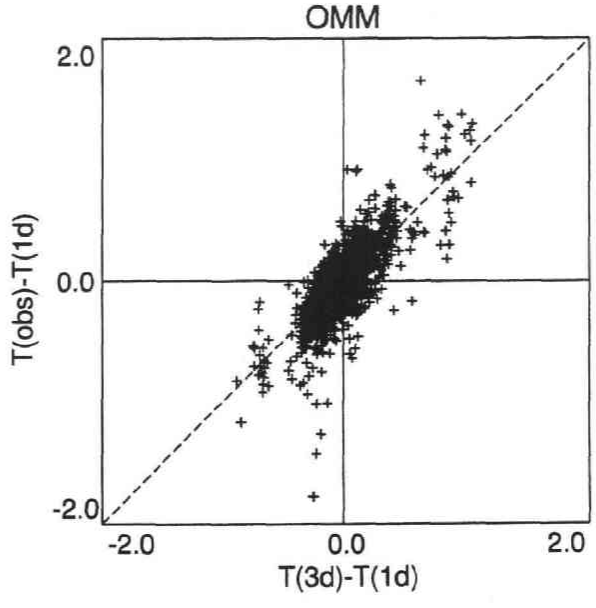

Figure 2.12: (c) Check of travel time residual improvement of the rays observed at OMM station.

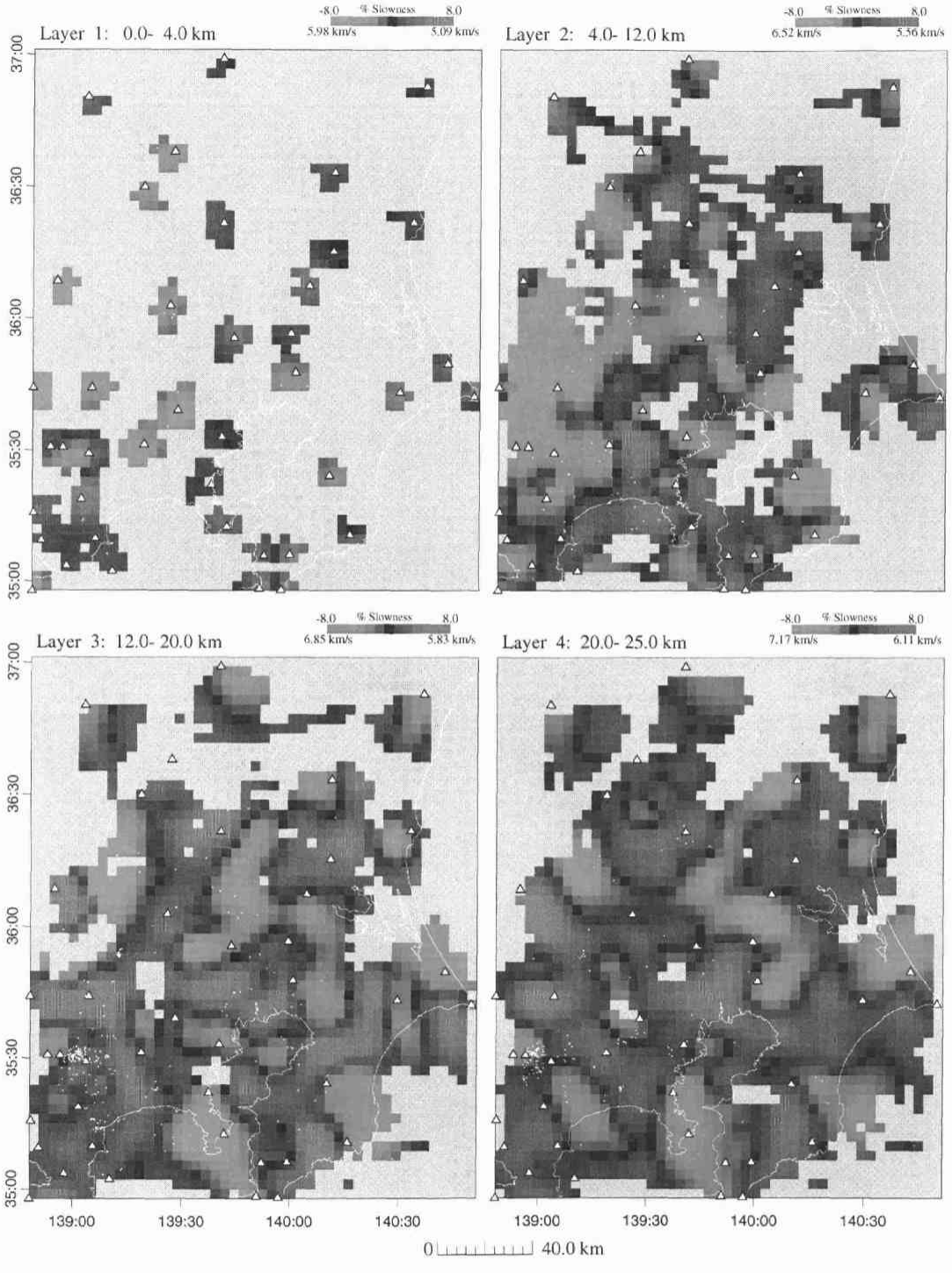

Figure 2.13: P-wave slowness perturbations in %. Slowness perturbations are shown in color scales. Blue and red colors correspond to high and low velocities, respectively. Open triangles are station locations. Yellow dots are hypocentral locations within each layer.

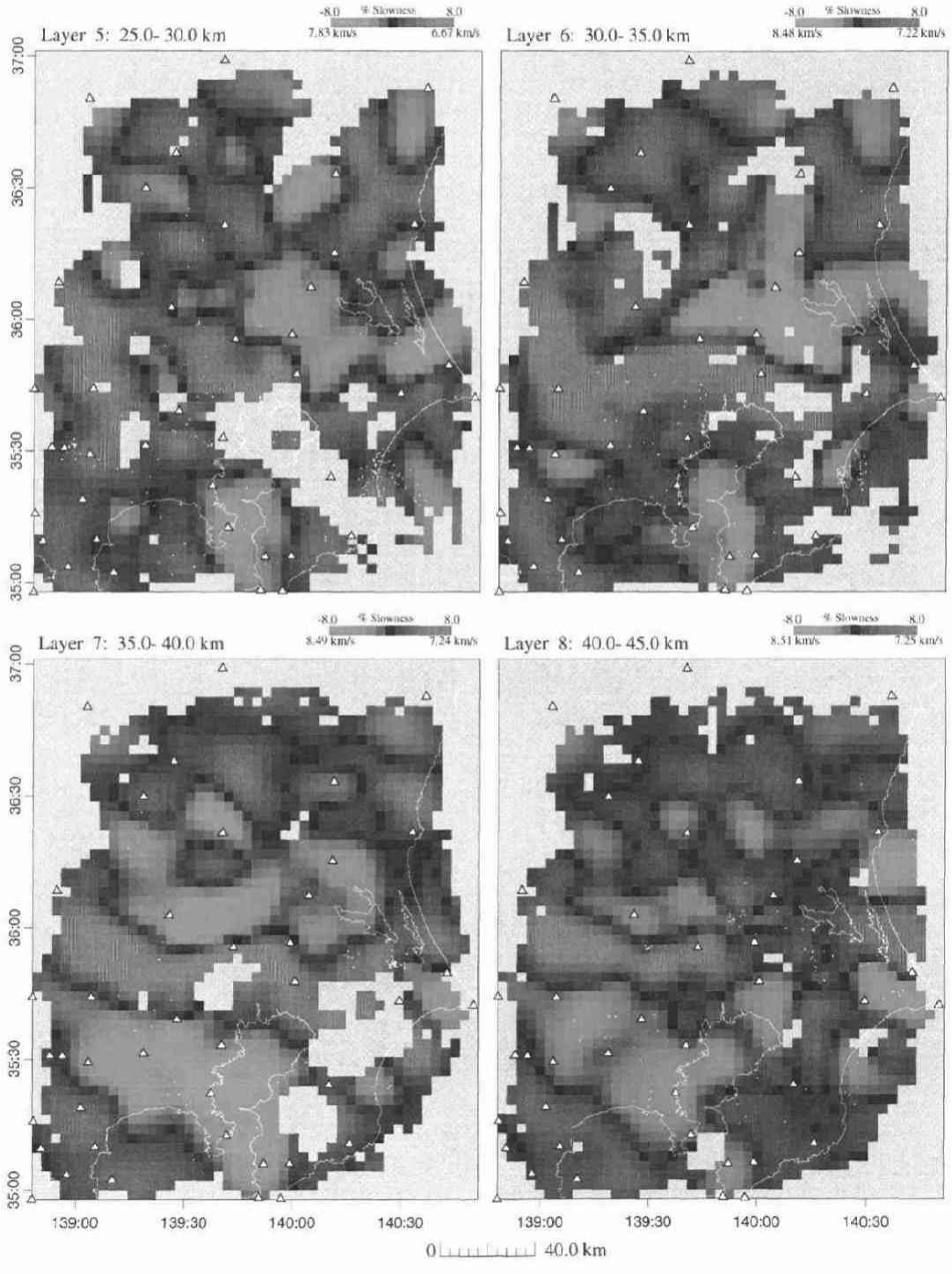

Figure 2.13: P-wave slowness perturbations in % (continued).

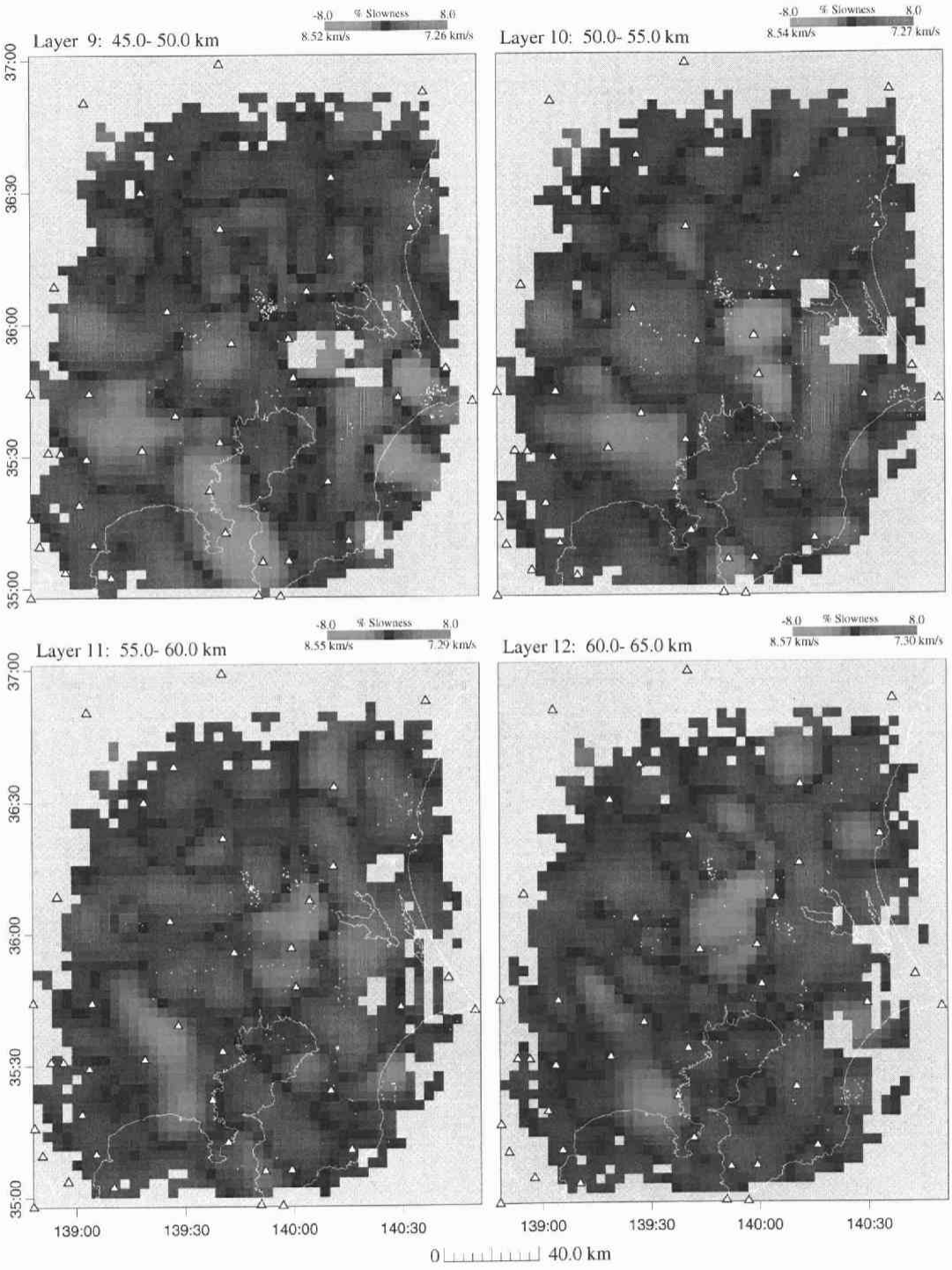

Figure 2.13: P-wave slowness perturbations in % (continued).

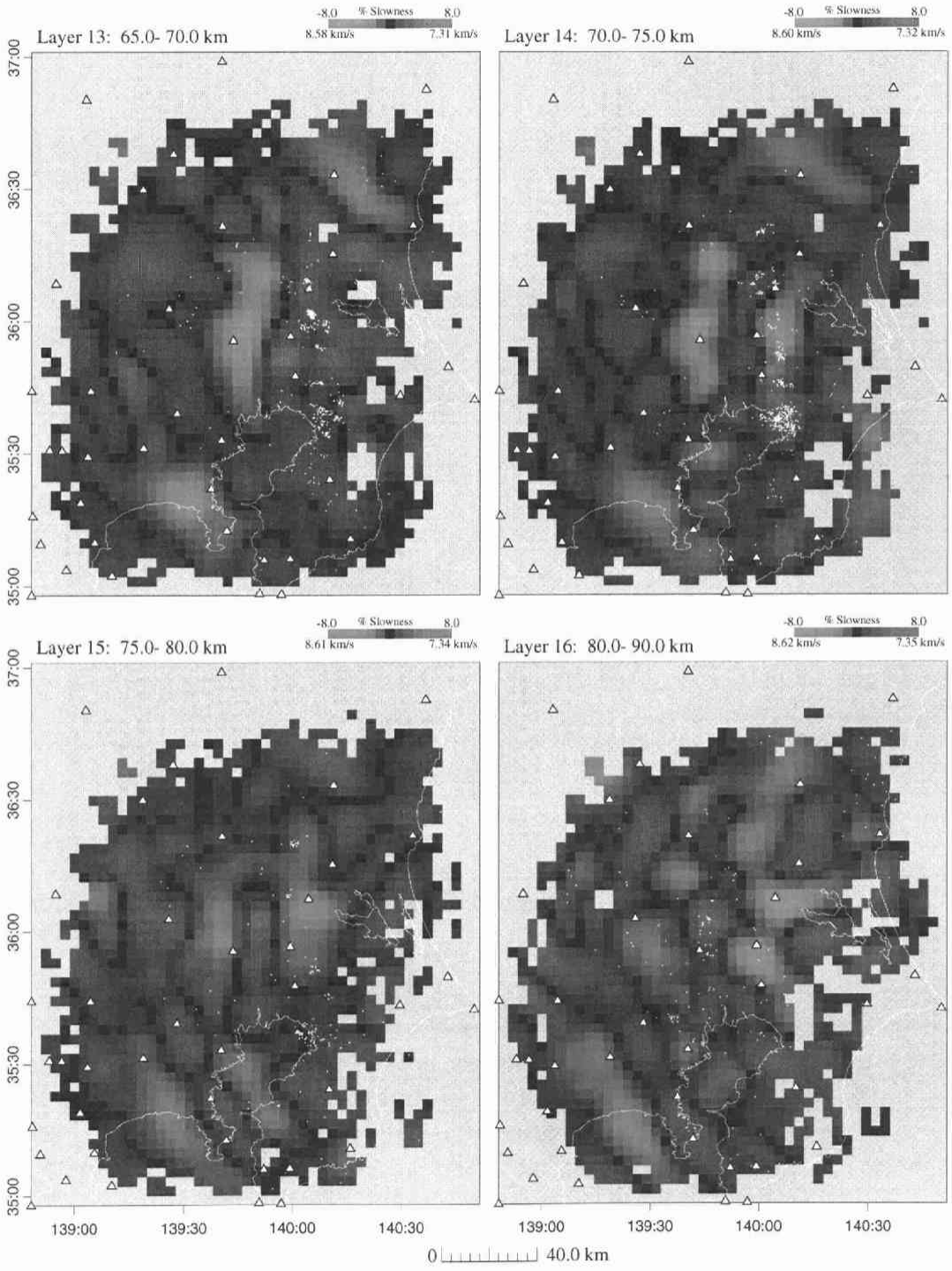

Figure 2.13: P-wave slowness perturbations in % (continued).

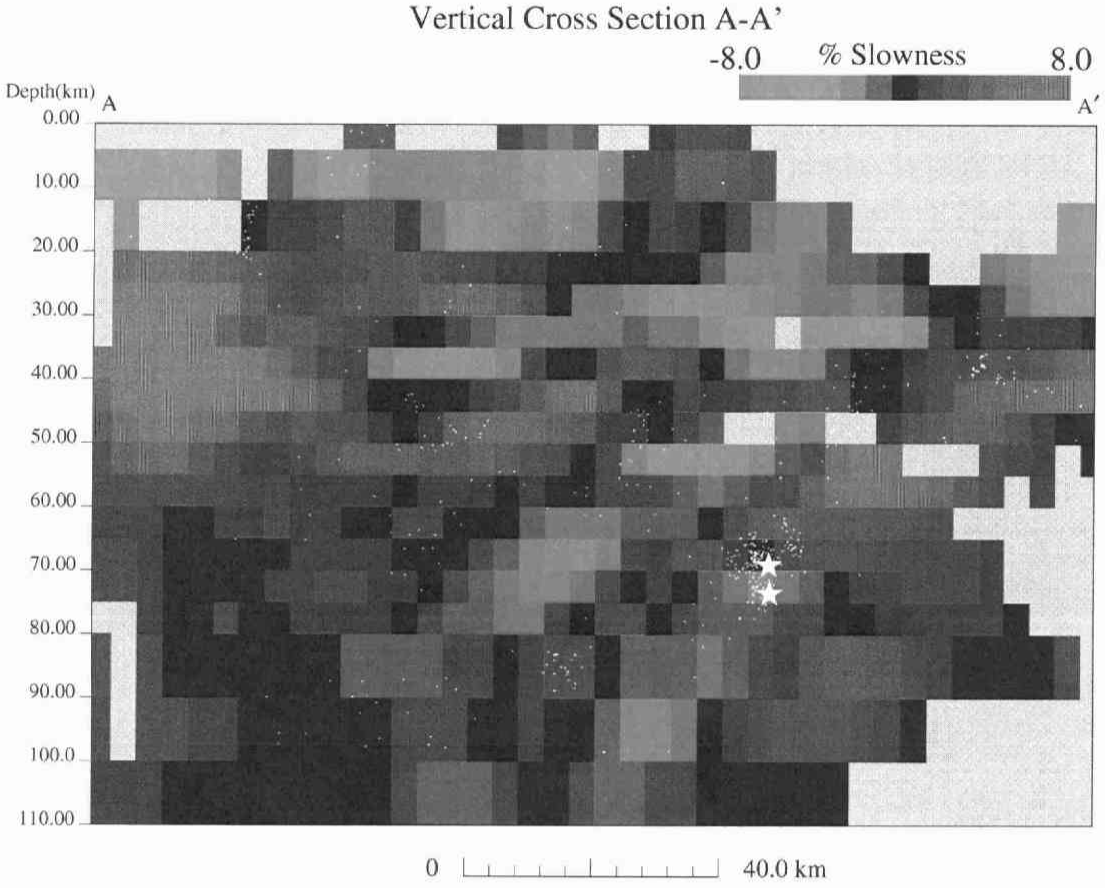

Figure 2.14: Vertical cross sections of P-wave velocity anomalies. Map view of cross section locations is in Figure 2.5. Slowness perturbations are shown by color scale. Yellow dots represent hypocenters projected along a 10 km swath. (a) upper star denotes the Feb. 27, 1983 interplate earthquake while lower star shows the Oct. 4, 1985 intra PAC earthquake.

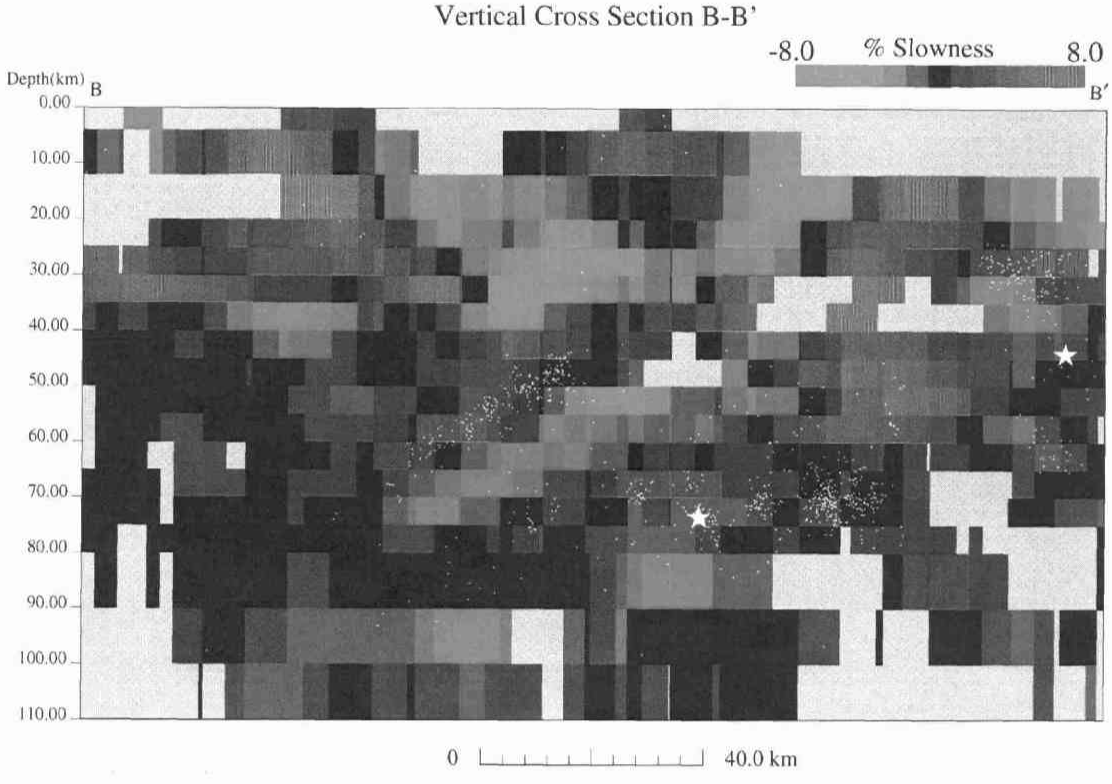

Figure 2.14: Vertical cross sections of P-wave velocity anomalies (continued). (b) left hand star represents the Oct. 4, 1985 earthquake and right hand star is the Dec. 17, 1987 intra PHS earthquake.

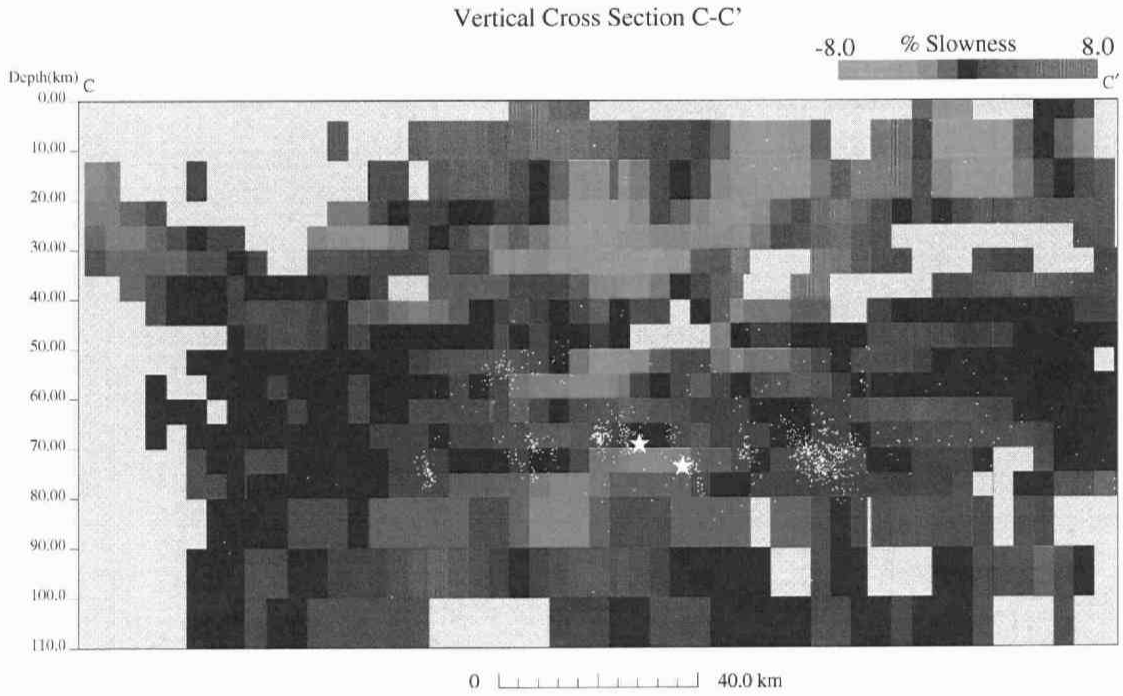

Figure 2.14: Vertical cross sections of P-wave velocity anomalies (continued). (c) upper star denotes the Feb. 27, 1983 earthquake while lower star represents the Oct. 4, 1985 earthquake.

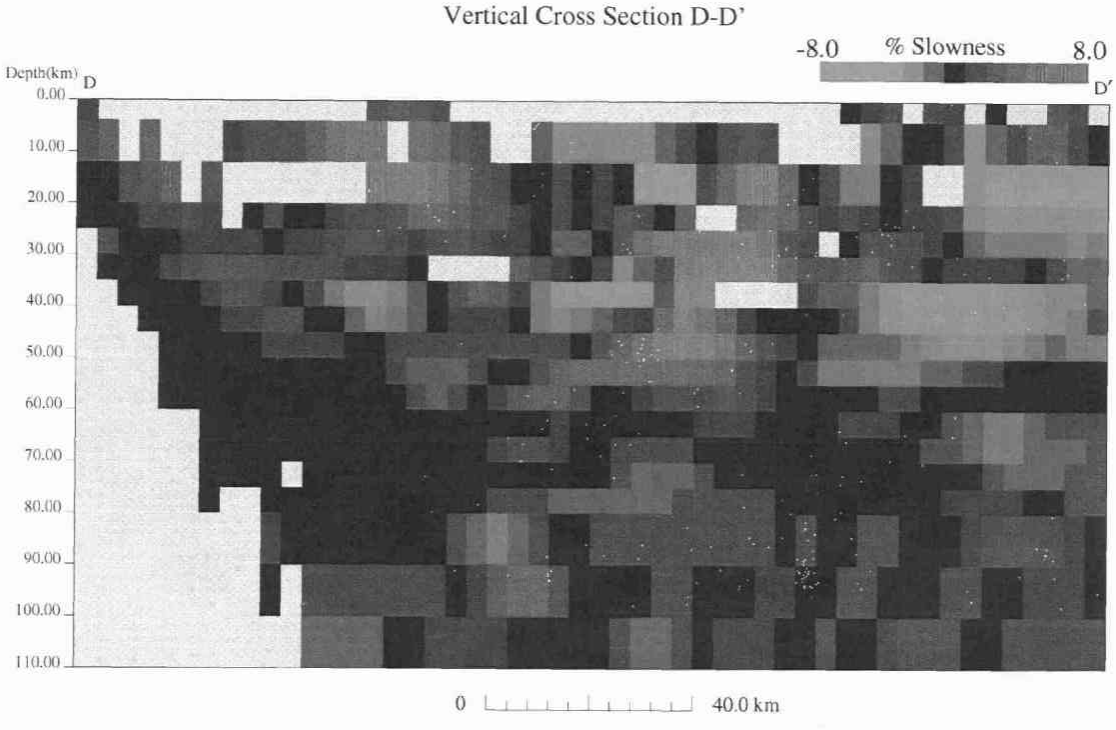

Figure 2.14: Vertical cross sections of P-wave velocity anomalies (continued).

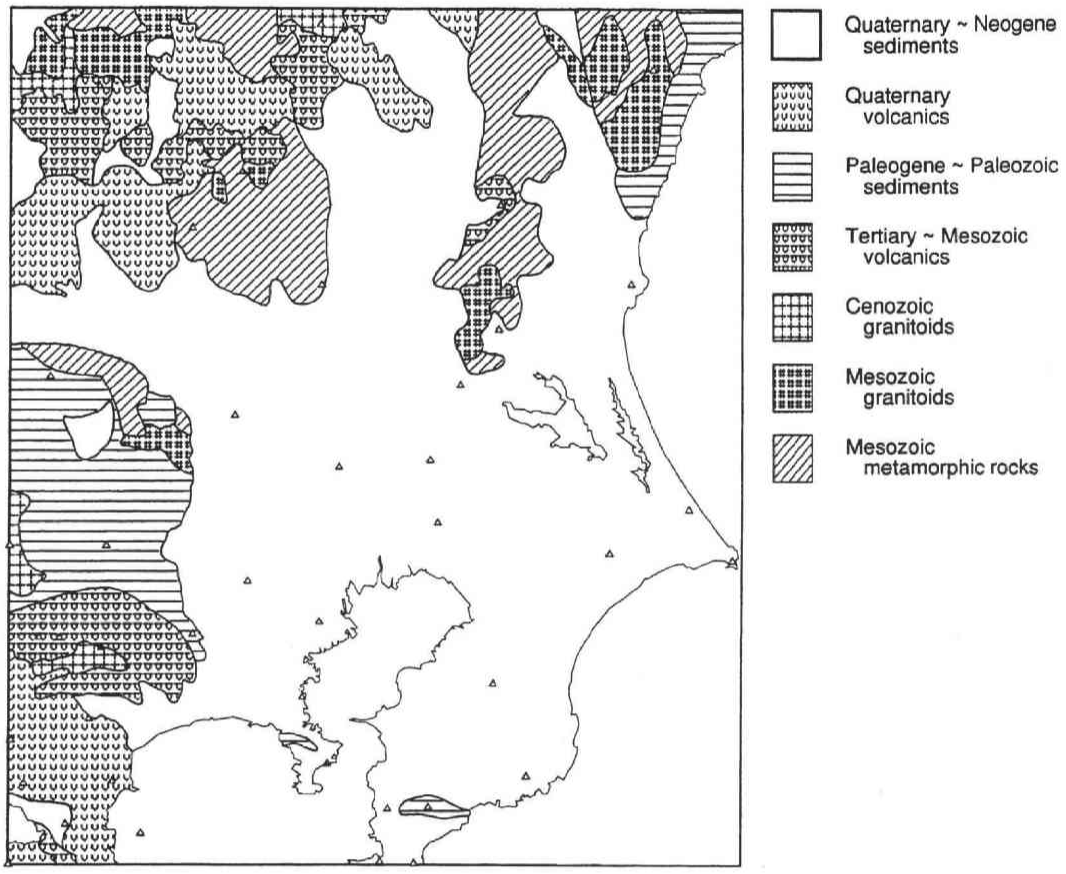

Figure 2.15: Geological map around the Kanto region reproduced from Geological Survey of Japan (1992).

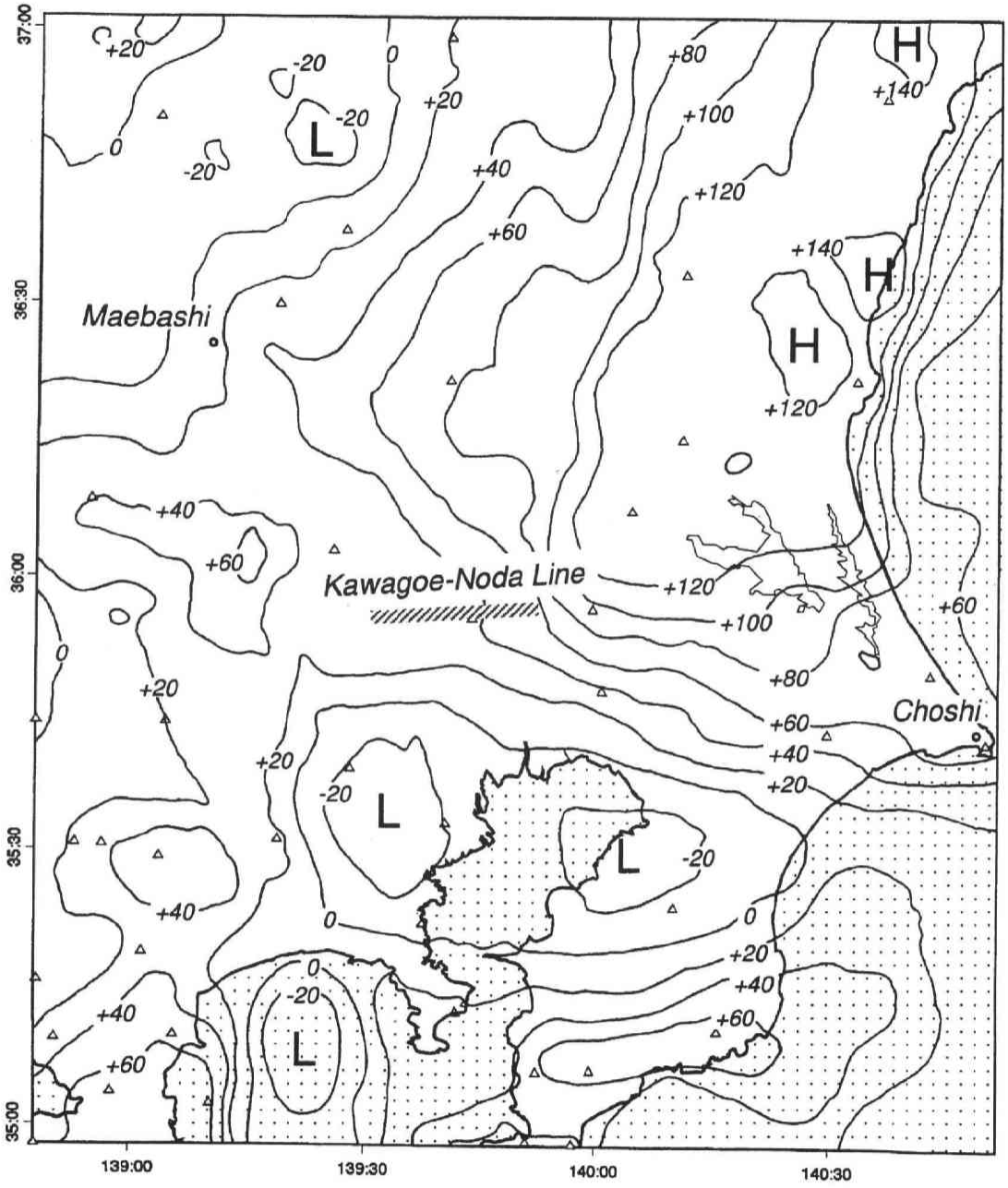

Figure 2.16: Gravity anomaly map in the target area reproduced from Kono and Furuse (1989). This anomaly map includes gravitational effects of the subducting PHS and PAC slabs. The contour interval is 20 mgal.

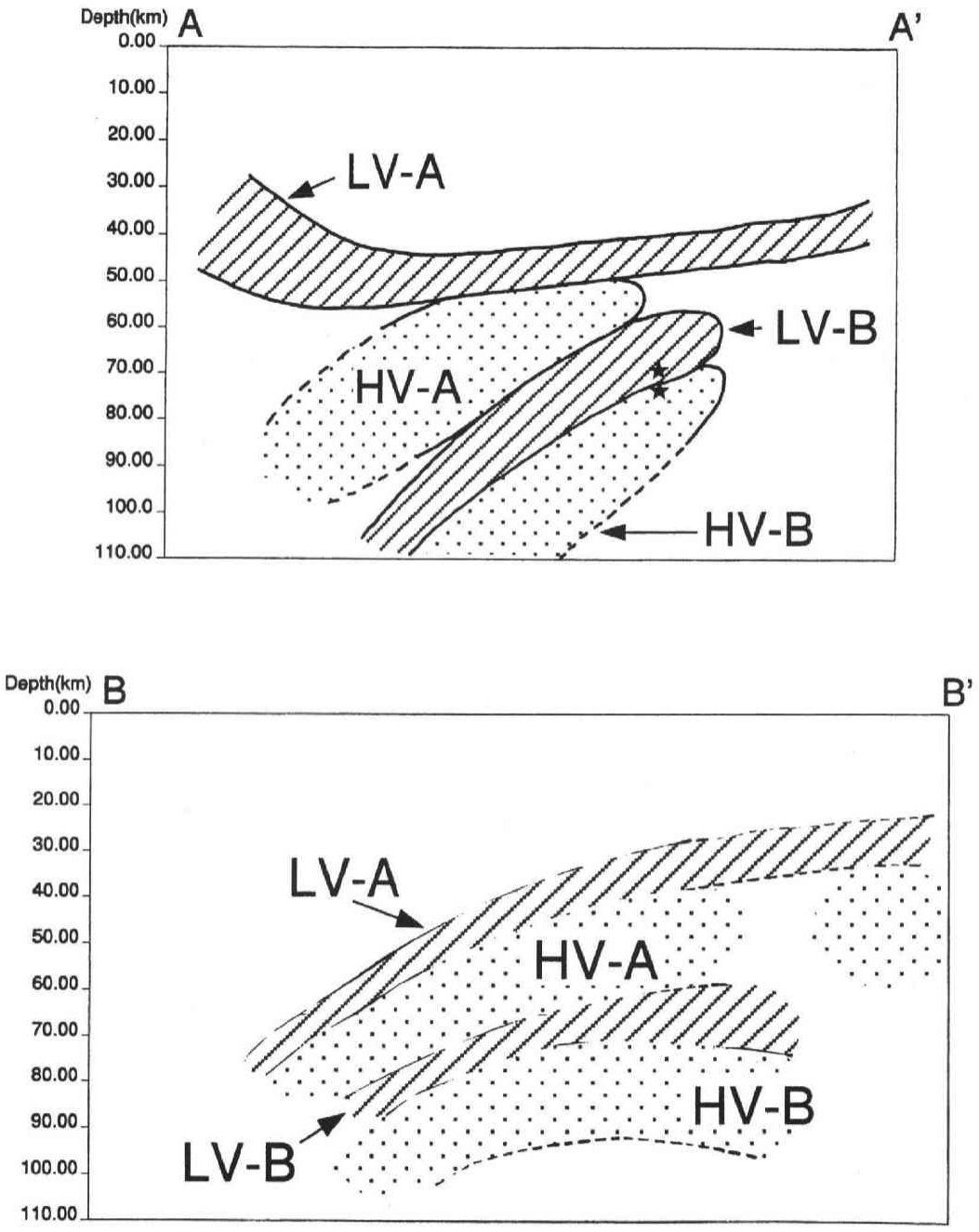

Figure 2.17: Identification of LV-A, HV-A, LV-B, and HV-B cited in the text.

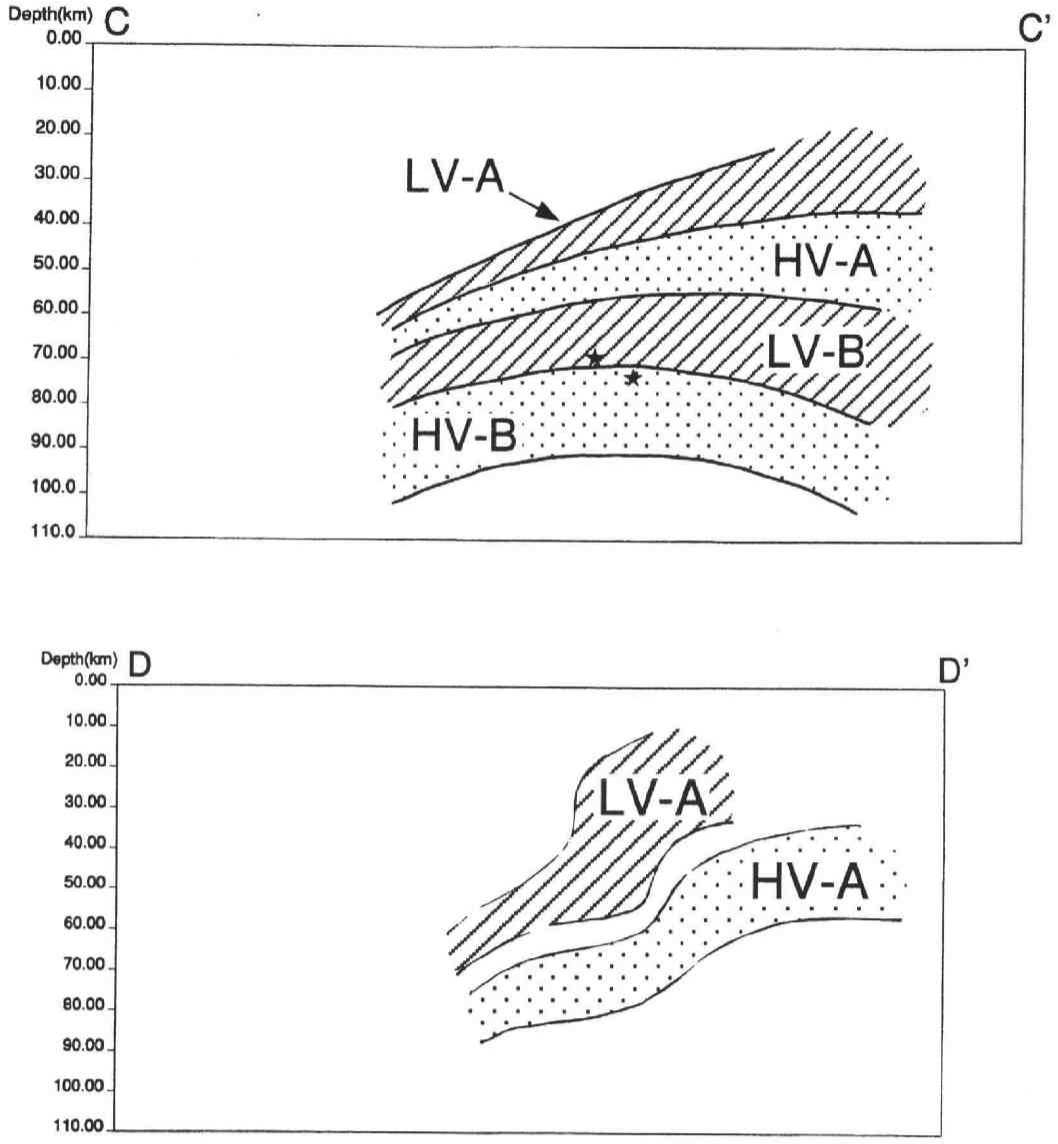

Figure 2.17: Identification of LV-A, HV-A, LV-B, and HV-B cited in the text (continued).

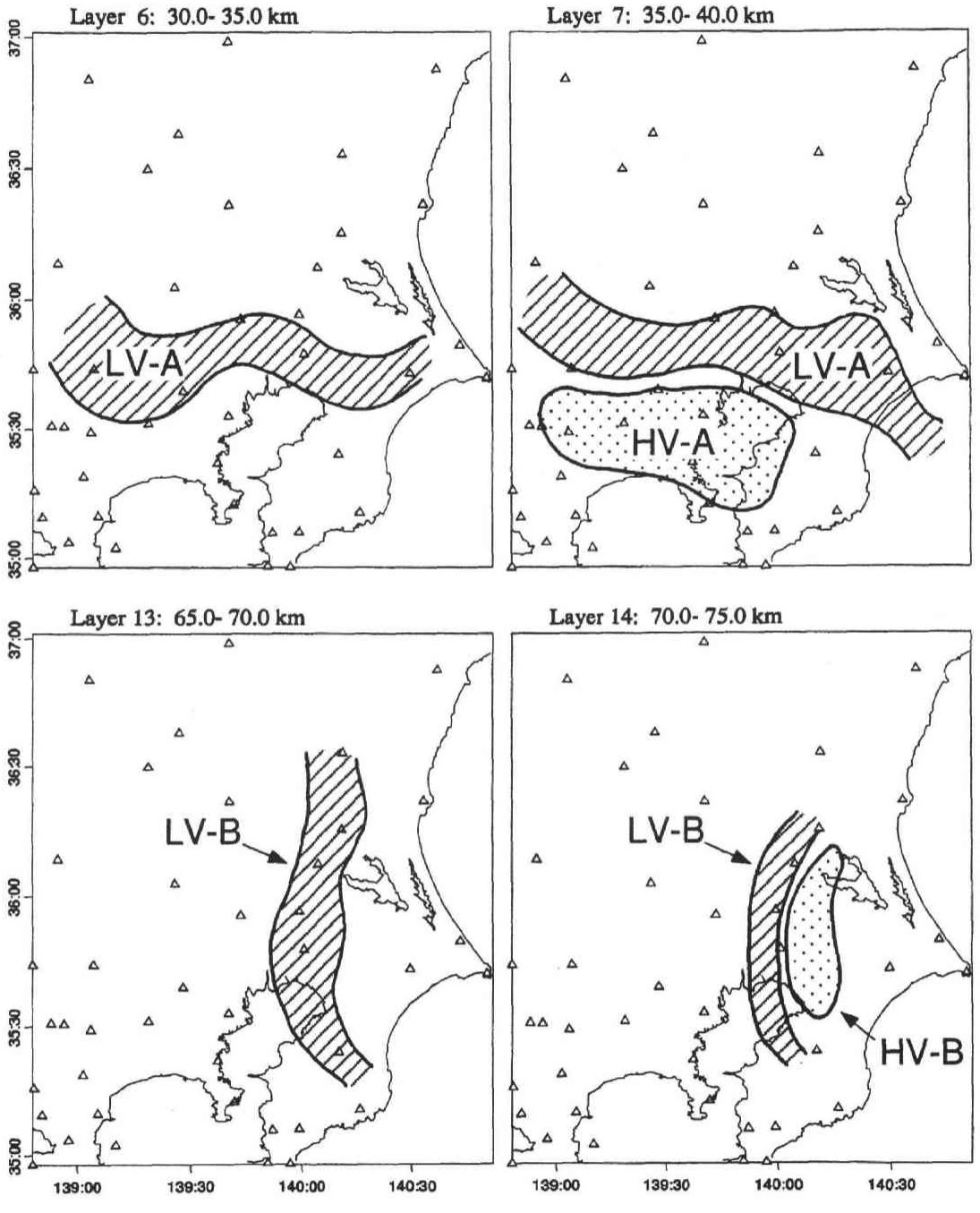

Figure 2.17: Identification of LV-A, HV-A, LV-B, and HV-B cited in the text (continued).

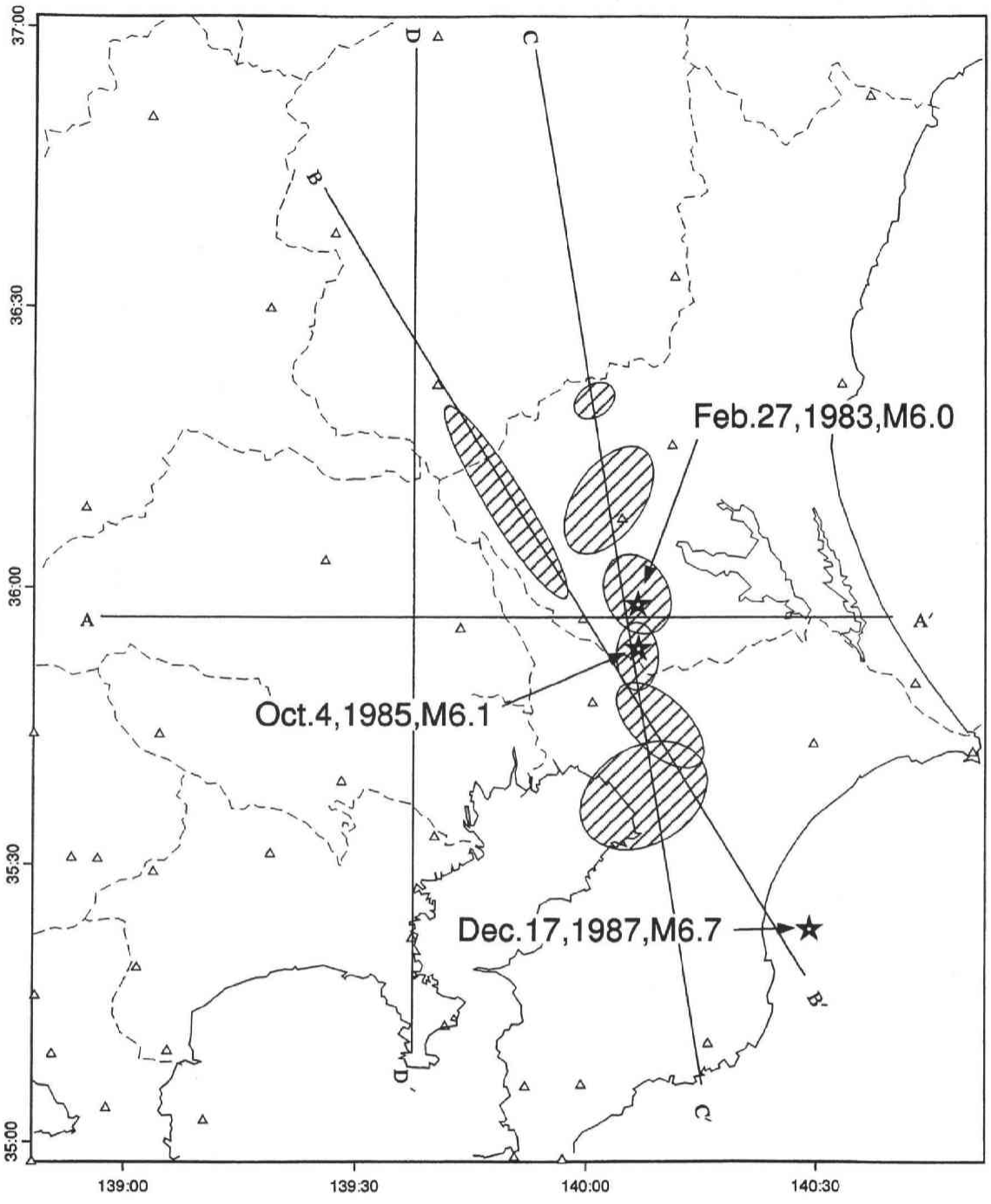

Figure 2.18: Epicenter locations of the particular earthquakes in the target area. Feb. 27, 1983 earthquake is an interplate event between the PHS and PAC plates. Oct. 4, 1985 event is an intra PAC earthquake and Dec. 17, 1987 event is an intra PHS one. Hatched area along B-B' denotes the source region of Southwestern Ibaraki swarm that is interpreted as the interplate thrust events between the EUR and PHS plates. Six hatched regions along C-C' represent the source regions of the Tsukuba-Chiba seismic belt which is an interplate thrust zone between the PHS and PAC plates.

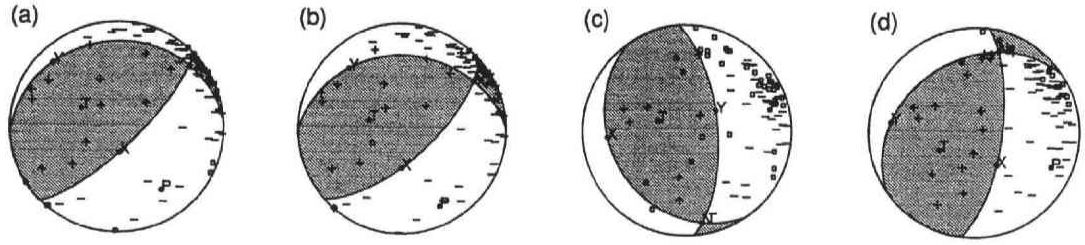

Figure 2.19: Typical focal mechanisms of the swarm activities. (a) and (b) are focal mechanisms of Southwestern Ibaraki swarm, while (c) and (d) are those of Tsukuba - Chiba seismic belt.

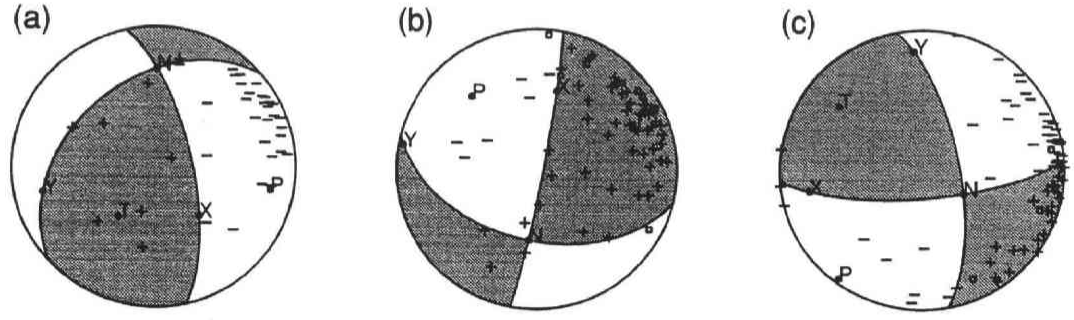

Figure 2.20: Focal mechanisms of moderate earthquakes. (a) Southern Ibaraki earthquake of 1983; (b) Ibaraki-Chiba border earthquake of 1985; (c) East off Chiba earthquake of 1987.

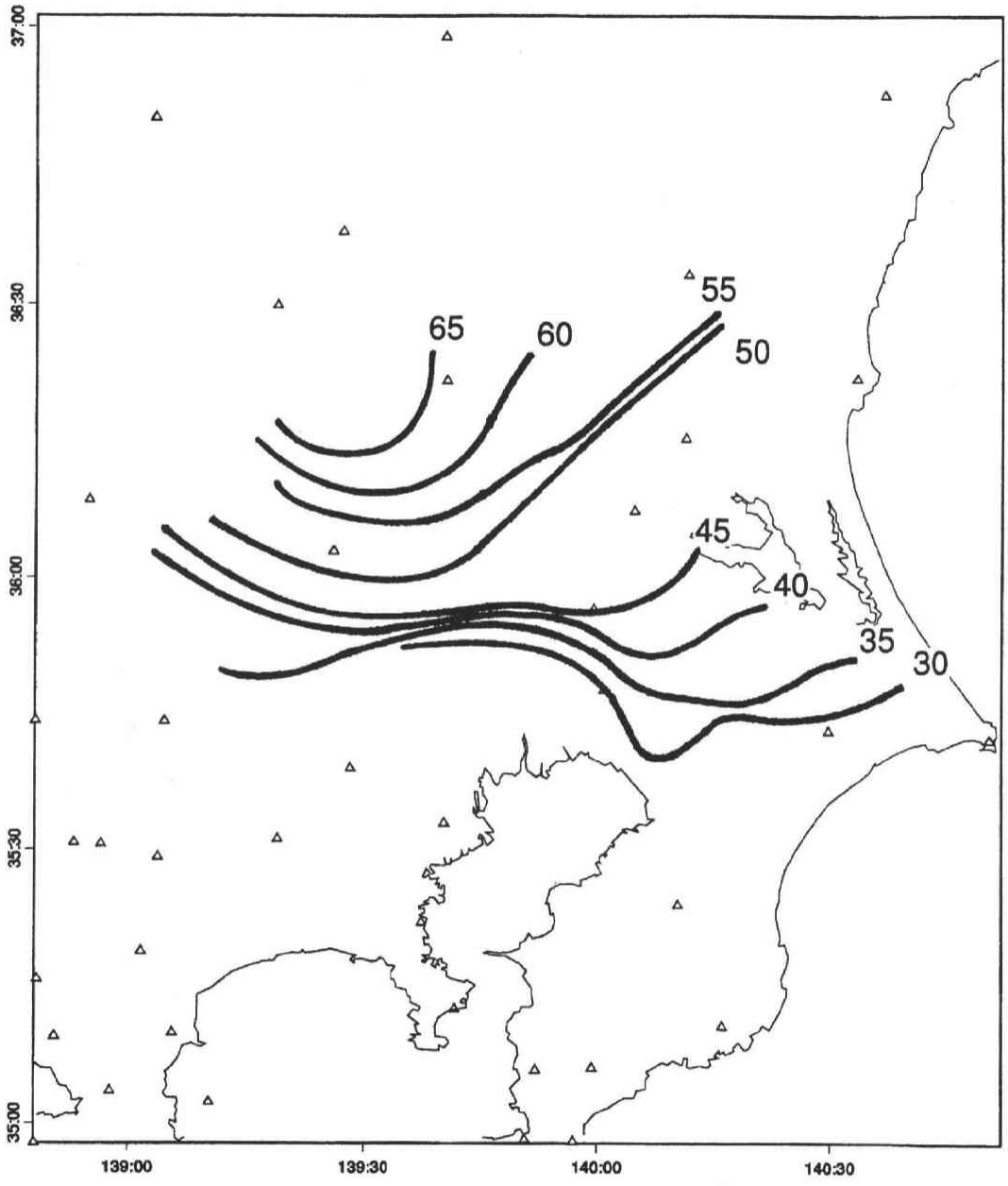

Figure 2.21: Contour map of the subducting plates derived in this study. Each number denotes the depth to the top of the plates in unit of km. (a) Philippine Sea (PHS) plate.

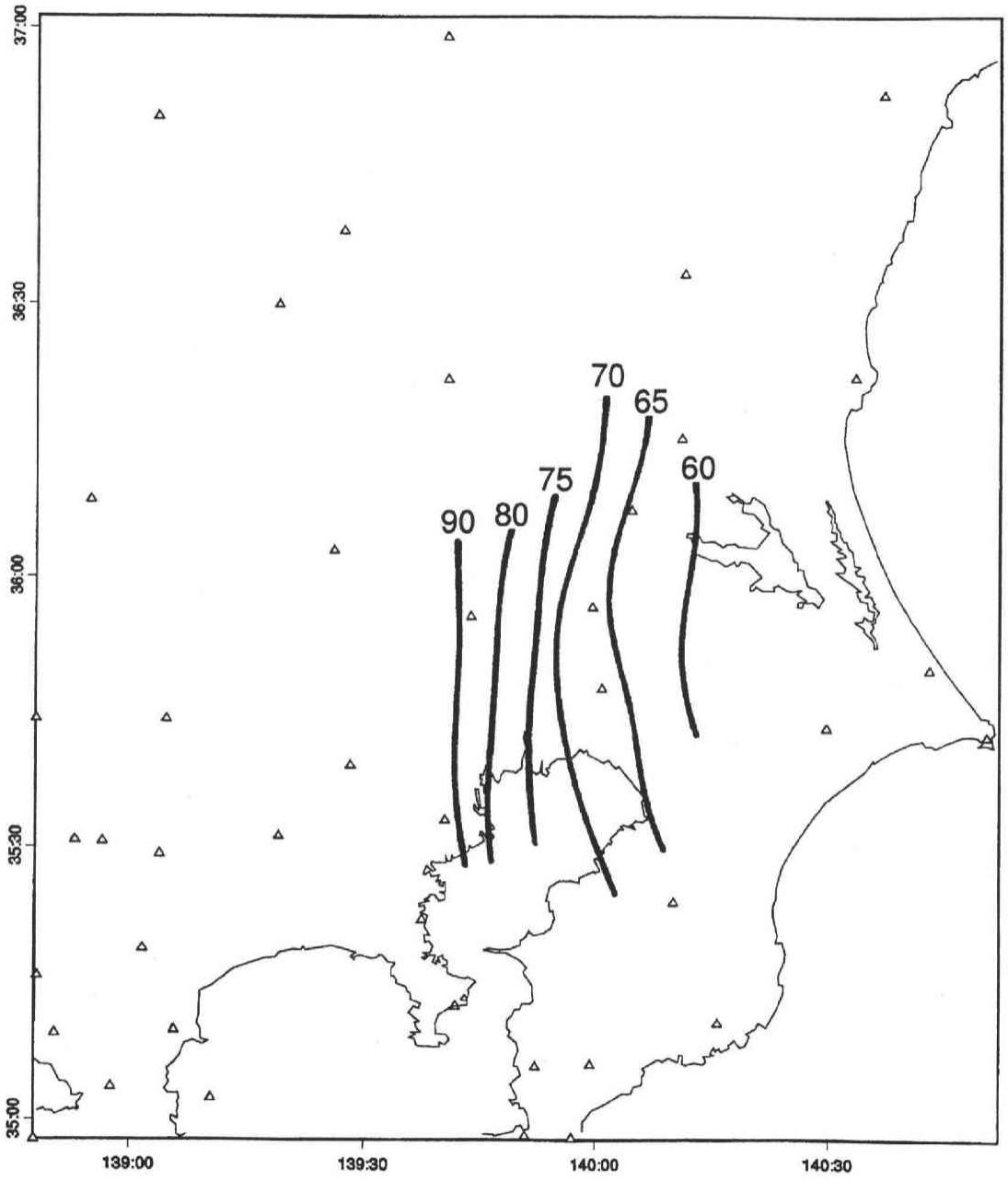

Figure 2.21: Contour map of the subducting plates derived in this study (continued). (b) Pacific (PAC) plate.

Chapter 3

Seismic Wave Conversion near the Upper Boundary of the Pacific Plate

3.1 Introduction

The Pacific and the Philippine Sea plates are subducting beneath the Kanto district, central Japan, and a number of interplate and intraplate earthquakes take place associated with this subduction. (e.g. Maki, 1984; Kasahara, 1985; Ishida 1986). Many P and S wave arrival time data compiled by the NIED enable us to study the local structure of the crust and the upper mantle in this area using various methods such as a 3-D tomography technique described in the previous chapter.

Another approach to obtain a fine structure of the subducted plate is to analyze 'slab-related' seismic phases (e.g. Matsuzawa et al., 1986). Most of the phases (so-called X phases) appearing as P or S later arrivals are strongly related to the velocity discontinuity at the plate boundaries. For example, Obara and Sato (1988) and Obara (1989) pointed out that a clear phase found in the S wave coda is the SS wave reflected at the upper boundary of the subducting Pacific plate. Hori (1990) found a pair of P and S later phases which are considered to be guided waves propagating the crustal part of the subducting

Philippine Sea plate. From the later phase analysis, they estimated the configuration of the slabs beneath the Kanto-Tokai district.

Hori (1988) found another phase between P and S arrivals for earthquakes occurring in the lower part of the double seismic zone. His preliminary analysis suggested that the later phase is an SP wave, which is S-to-P converted wave at the plate boundary. In the present study, we show the remarkable later phases to be the SP wave converted in the vicinity of the upper boundary of the Pacific plate by examining the travel time of the later phase more quantitatively. In the next step, the observed SP-P time data are inverted to locate the conversion interface. We make comparison of our result with previous studies on the configuration of the upper boundary of the Pacific plate in conjunction with the seismotectonics in this region.

3.2 Later Phase and Its Origin

A prominent seismic phase a few seconds after the first P arrival in seismograms for the upper mantle earthquakes is observed at stations distributed in the Kanto district. Figure 3.1 shows an example of the record section showing this phase. Seismograms are pasted up in the order of epicentral distances. The locations of the source and the stations for this record are shown in Figure 3.2. This later phase is dominant in the vertical component. Its apparent velocity is comparable to or slightly lower than that of the initial P phase. Three component seismograms and the particle motion of the phase are shown in Figure 3.3 and Figure 3.4, respectively. From this observation the later phase is regarded as a seismic wave arriving at stations as a compressional wave. The travel time difference between the initial and the later arrivals is in the range from 3 to 6 s. There are no significant correlations between the travel time difference and the focal depth or

the epicentral distance. The later phase is well observed for events in the lower plane of the double seismic zone in the Pacific plate but not for the other upper mantle earthquakes.

As pointed out in the previous chapter, the subducted slab can be regarded as a region having large velocity anomaly. The upper and lower boundaries of the slab, therefore, may generate reflected or converted seismic waves. Taking into account the velocity structure of the subducting slabs beneath this region, we think that the followings are the possible origins of the later phase: SP wave reflected and converted at the lower boundary of the Pacific plate (case I), SP wave converted at the upper boundary of the Pacific plate (case II), SP wave converted at the lower boundary of the Philippine Sea plate (case III), SP wave converted at the upper boundary of the Philippine Sea plate (case IV), and PP wave reflected at the lower boundary of the Pacific plate (case V). The Philippine Sea plate becomes shallower to the west of the Kanto district. On the other hand, events having the later phase become deeper toward this direction. Therefore, the travel time difference between the initial P and later phases in cases III and IV should become large with increasing depth. As mentioned above, such tendency is hardly seen from the observation. In cases I and V, the distance between the source and the reflection or conversion interface is estimated to be more than 70 km with the assumption that the thickness of the Pacific plate is 100 km. The travel time differences relative to the initial P phase becomes about 8 s for PP and 15 s for SP phases. The observed travel time difference is, therefore, not compatible with these cases. On the other hand, the travel time difference between the initial P and the later phases in case II is roughly estimated to be 3 s. Computed travel time for Case II is shown in Figure 3.5. Theoretical travel time is calculated using

SEIS83 program (Červený and Pšenčík, 1984). Calculated travel time differences well agree with the observed ones.

Thus we can conclude that the later phase is an SP wave converted near the upper boundary of the Pacific plate which is subducting beneath the Kanto district. In the following section, we determine the structure of the conversion interface with assuming the later phase to be the SP wave.

3.3 Data Analysis and Results

Forty-nine earthquakes occurring in the lower plane of the double seismic zone were selected from the earthquake catalogue of NIED for the SP wave analysis. We picked onsets of both the initial P and SP phases for 347 traces recorded at 44 stations for these events. Locations of the epicenters and the stations used in this study is shown in Figure 3.6.

The S-to-P conversion interface is determined by using the method by Matsuzawa et al. (1986) and Horiuchi et al. (1982). Taking into account the previous studies on the configuration of the Pacific slab beneath the Kanto district, we assume that the S-to-P conversion interface is expressed by a curved surface,

$$\begin{aligned} h_p &= C_0 + C_1 x + C_2 y + C_3 xy + C_4 x^2 + C_5 y^2 \\ &= \sum_{k=0}^{5} C_k H_k(x, y) \end{aligned} \tag{3.1}$$

where h_p is the depth of the conversion interface at a point (x, y). x and y are horizontal distances (km) from the local origin. $+x$ and $+y$ axes are set to the north and east direction, respectively. The local origin of (x, y) coordinate is taken at a point (140.09°E, 36.12°N).

The difference between the observed and calculated SP-P time T_{SP-P} is expressed by

$$\begin{aligned} T^{obs}_{SP-P} - T^{cal}_{SP-P} &= (\frac{\partial T_{SP}}{\partial x_e} - \frac{\partial T_P}{\partial x_e})\delta x_e \\ &+(\frac{\partial T_{SP}}{\partial y_e} - \frac{\partial T_P}{\partial y_e})\delta y_e \\ &+(\frac{\partial T_{SP}}{\partial h_e} - \frac{\partial T_P}{\partial h_e})\delta h_e \\ &+\sum_{k=0}(\frac{\partial T_{SP}}{\partial C_k} - \frac{\partial T_P}{\partial C_k})\delta C_k + e \end{aligned} \tag{3.2}$$

where

T^{obs}_{SP-P}	= observed SP-P time,
T^{cal}_{SP-P}	= calculated SP-P time,
T_{SP}	= calculated travel time of SP-wave,
T_P	= calculated travel time of initial P-wave,
x_e, y_e, h_e	= location of hypocenter,
$\delta x_e, \delta y_e, \delta h_e$	= determination error of hypocenter,
δC_k	= correction of unknown parameters,
e	= error.

If the hypocenter location is accurately determined, δx_e, δy_e, and δh_e are negligibly small. In this case, equation (3.2) becomes

$$T^{obs}_{SP-P} - T^{cal}_{SP-P} = \sum_{k=0}(\frac{\partial T_{SP}}{\partial C_k} - \frac{\partial T_P}{\partial C_k})\delta C_k + e \tag{3.3}$$

Partial derivatives of T is expressed as

$$\frac{\partial T}{\partial C_k} = \frac{\partial T}{\partial h_p}\frac{\partial h_p}{\partial C_k} = \frac{\partial T}{\partial h_p}H_k(x_p, y_p) \tag{3.4}$$

$$\frac{\partial T}{\partial h_p} = \frac{\cos\theta_1}{\upsilon_1} - \frac{\cos\theta_2}{\upsilon_2} \tag{3.5}$$

where υ_1 and υ_2 are the velocities above and below the conversion interface, θ_1 and θ_2 are the emergent and incident angle measured

from the vertical. x_p and y_p denote the horizontal coordinates of the hypocenter. (See Figure 3.7, which is originally from Matsuzawa et al. (1986)). Equation (3.3) is expressed in matrix form as

$$\boldsymbol{\tau} = \boldsymbol{A}\boldsymbol{x} + \boldsymbol{\epsilon} \tag{3.6}$$

where $\boldsymbol{\tau}$, $\boldsymbol{A}$, $\boldsymbol{x}$, and $\boldsymbol{\epsilon}$ represent a vector of the SP-P time residual, a matrix of partial derivatives, a correction vector of unknown parameters, and an error vector, respectively. This system can be solved by using classical least squares method as

$$\boldsymbol{x} = (\boldsymbol{A}^t\boldsymbol{A})^{-1}\boldsymbol{A}^t\boldsymbol{\tau} \tag{3.7}$$

Correction term δC_k is then added to C_k and $\delta C_k + C_k$ is used in place of C_k. The iteration step is conducted until δC_k becomes sufficiently small. The variance of h_p is expressed as

$$(\delta h_p)^2 = \sigma_e^2 \sum D_{ij} H_i(x_p, y_p) H_j(x_p, y_p) \tag{3.8}$$

where D_{ij} is the covariance between C_i and C_j, and

$$\sigma_e^2 = \sum (T_{SP-P}^{obs} - T_{SP-P}^{cal})^2/(N-6) \tag{3.9}$$

where N is the number of observation.

We use the velocity structure shown in Figure 3.8 to calculate travel times of P first arrival and SP wave. This is based on the model of Ukawa et al. (1984), which is used for routine hypocenter determination in NIED. The velocity within the slab is assumed to be 6% faster than that of the surrounding mantle (e.g. Matsuzawa et al., 1986). The S wave velocity is calculated by assuming $V_P/V_S = 1.73$. Rays are traced relative to the reference model with satisfying the Snell's law at the interface to calculate travel times of SP wave (T_{SP}) and direct P wave (T_P). Then we applied a least squares technique to estimate the

coefficients $C_i(i = 0, 5)$ so that r.m.s. of the observed T_{SP-P} minus calculated T_{SP-P} become minimum. Reading error of T_{SP-P} time is assumed to be 1.0 s for each reading. The required correction of each parameter becomes negligibly small after 4 th or 5 th iteration.

Presently estimated values of C_i with their standard deviations are as follows: $C_0 = 64.71 \pm 0.10$, $C_1 = (9.78 \pm 0.51) \times 10^{-2}$, $C_2 = (-4.65 \pm 0.05) \times 10^{-1}$, $C_3 = (1.94 \pm 0.37) \times 10^{-4}$, $C_4 = (1.35 \pm 0.05) \times 10^{-3}$, $C_5 = (1.01 \pm 0.07) \times 10^{-3}$.

Figure 3.9 shows a contour map of the conversion interface defined by the above coefficients. Locations of the conversion points are also shown by stars. Estimation error is shown in Figure 3.10. Figure 3.11 shows three vertical sections of the conversion interface together with the hypocenter locations. This result is similar to a preliminary analysis for SP waves conducted by Ohmi and Hori (1994), where a set of flat planes are assumed for the conversion interface.

3.4 Discussion

The inverted conversion interface is located above the upper plane of the double seismic zone (Figure 3.11). If we see in more detail, the separation between the interface and the upper seismic plane is slightly different from region to region. In the northern Kanto area (Figure 3.11 (a)), the interface is located about $5 \sim 10$ km shallower than the upper seismic plane in the depth range from 60 km to 110 km. On the other hand, in the central and southern Kanto region (Figures 3.11 (b) and (c)), it is located just above or on the upper seismic plane. This regional change of the separation will be discussed in more detail in the next chapter.

Iidaka et al. (1989) analyzed PS converted waves observed in the northern Kanto region and estimated the depth to the conversion in-

terface by assuming a flat plane. The location of their PS conversion interface agrees with our result. Obara (1989) detected reflected S waves from the plate boundary in this region by plotting many seismograms of shallow events and determined the S wave reflection interface. There is a slight difference between the location of the S-to-P conversion interface obtained in this study and that by him in the northern Kanto region. The dip direction of the interface by Obara (1989) is N70°W, while it is N62°W in our result (shaded area in Figure 3.11 (a)). In the southern Kanto region, our result well coincides with that by Obara and Sato (1988) and Obara (1989). Ishida (1992) obtained the contour map of the upper boundary of the Pacific plate (UBP) mainly from the analysis of seismicity in this region. There are also differences in dip direction of the boundary in the northern Kanto area between our result and that by Ishida (1992).

Next, the estimated conversion interface is compared with the result to the 3-D velocity structure obtained in the previous chapter. Since the hypocenter locating procedures used in chapter 2 and 3 are different from each other, we can not compare these results directly. In chapter 2, hypocenters are determined by the method of Hurukawa and Ohmi (1993). Routinely determined hypocenters by NIED are used in chapter 3. As mentioned in chapter 2, focal depths are systematically different between the two dataset of hypocenters. We recalculated the conversion interface by using the initial hypocenters and velocity structure used in chapter 2 in order to get rid of the biases caused by the difference of the dataset.

Figures 2.14 show the inverted location of the conversion interface plotted on the three vertical cross sections of the velocity structure along the lines in Figures 2.5. It is clear from each figure that the location of the conversion interface consists with that of the LV-B,

where low angle thrust fault type earthquakes are occurring. It was interpreted as the oceanic crust attached at the top of the subducting PAC slab. The relation between the plate boundary and the conversion interface will be discussed in detail in the following chapter.

Finally, we attempt to explain why the amplitude of the observed SP phase is large. Its amplitude in UD component is sometimes twice of that for the first P wave. To estimate the expected amplitude of the SP wave (A_{SP}) and P wave (A_P), we calculated the synthetic waveform using 3D paraxial ray tracing technique developed by Sekiguchi (1992). Focal mechanism and the curvature of the conversion interface is also taken into account in amplitude calculation. The amplitude of SP phase in synthetic waveform is very small ($A_{SP}/A_P < 0.002$) when we use the velocity structure without a low velocity layer at the top of the subducting slab. Then we introduce a thin low velocity layer at the UBP. We assumed that the velocity in the thin layer is 12% lower (this is an extreme case) than that of slab itself and the thickness of the thin layer is 5 km. With this assumption, the amplitude of SP phase becomes large, but it is still small ($A_{SP}/A_P \simeq 0.01$) compared with the observation. Therefore, there may be another mechanism which generates such a large amplitude of SP phase. In this stage, we remain it as a further problem to be solved.

3.5 Summary

We have shown the origin of a prominent later seismic phase observed in the Kanto district, central Japan. This phase is observed between P and S arrivals for earthquakes occurring in the lower plane of the double seismic zone of the subducting Pacific slab. It is identified as S-to-P converted wave (SP wave) near the upper plate boundary from the present analysis. The location of the conversion interface is

estimated by inverting the observed T_{SP-P} times. In this estimation, we assumed that the interface is expressed by a power series. The interface is located above the upper seismic plane of the double seismic zone.

The location of the conversion interface generally coincides with the results of the previous studies of the UBP, with slight differences in the northern Kanto area. Comparison to the result of the three dimensional tomographic inversion obtained in chapter 2 revealed that the conversion interface is located in the low velocity layer at the top of the PAC plate.

The observed large amplitude of the SP phase can not be explained in this stage, which is remained as a future problem.

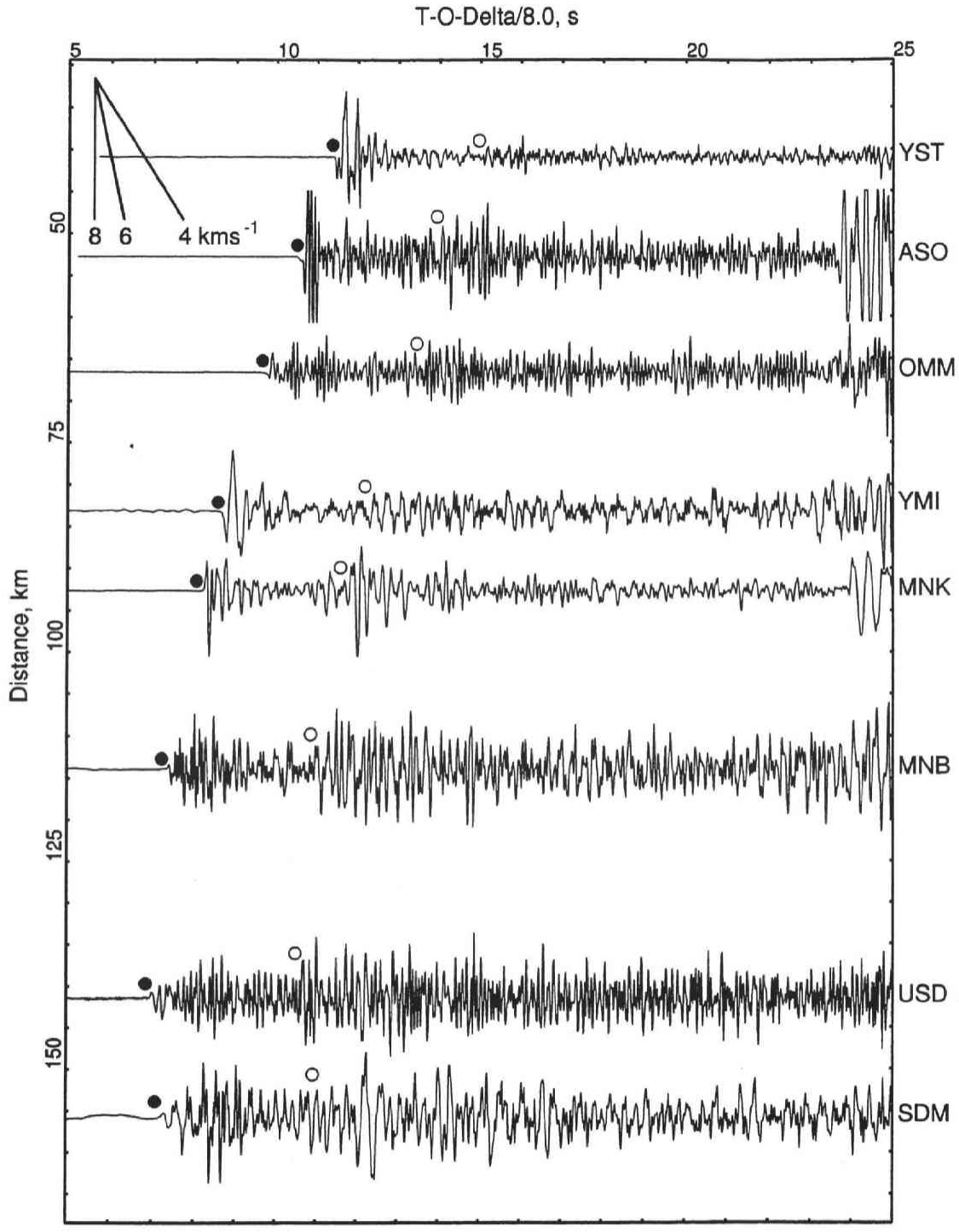

Figure 3.1: Example of vertical component seismograms showing SP phase. Record section is pasted up in order of epicentral distance. Locations of epicenter and stations are shown in Figure 3.2. Solid and open circles represent the onset of first P and SP arrivals, respectively.

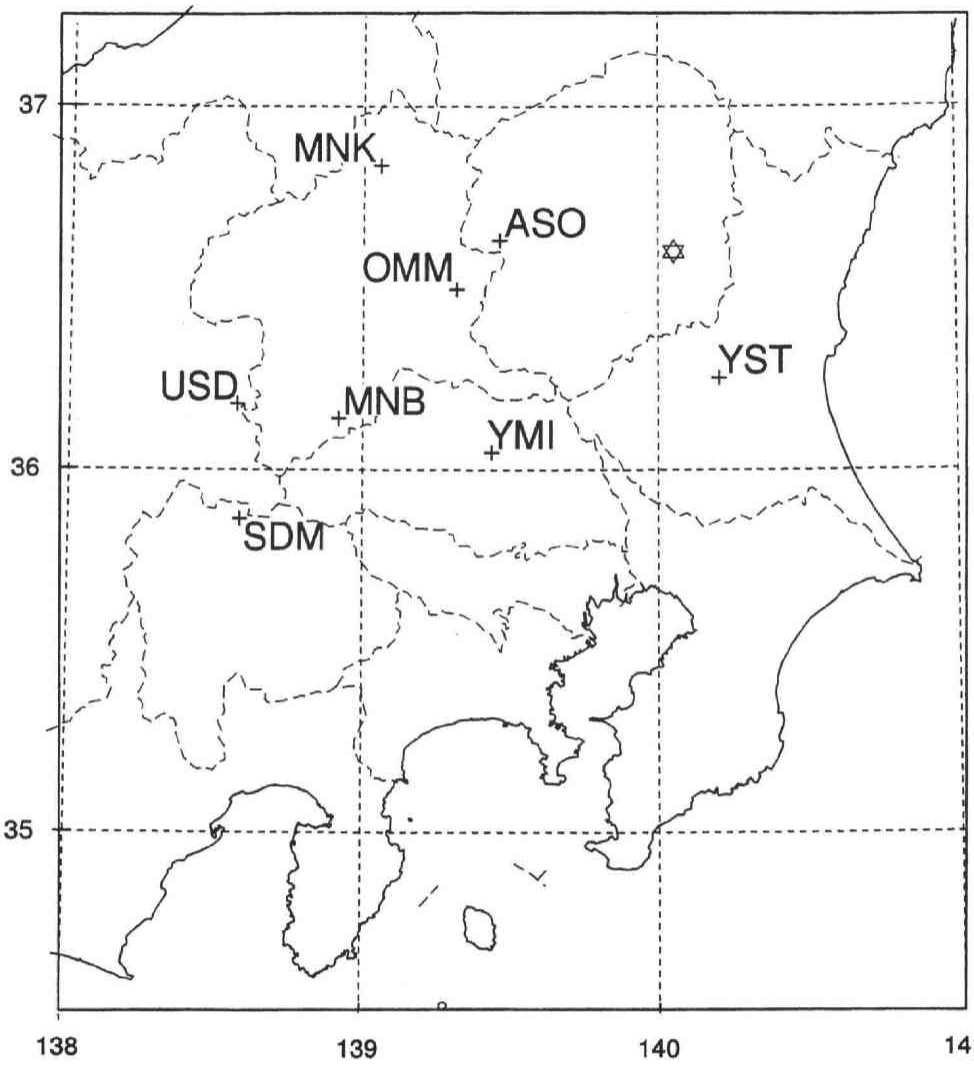

Figure 3.2: Locations of epicenter and seismic stations cited in Figure 3.1. Star denotes the epicenter and crosses represent seismic stations.

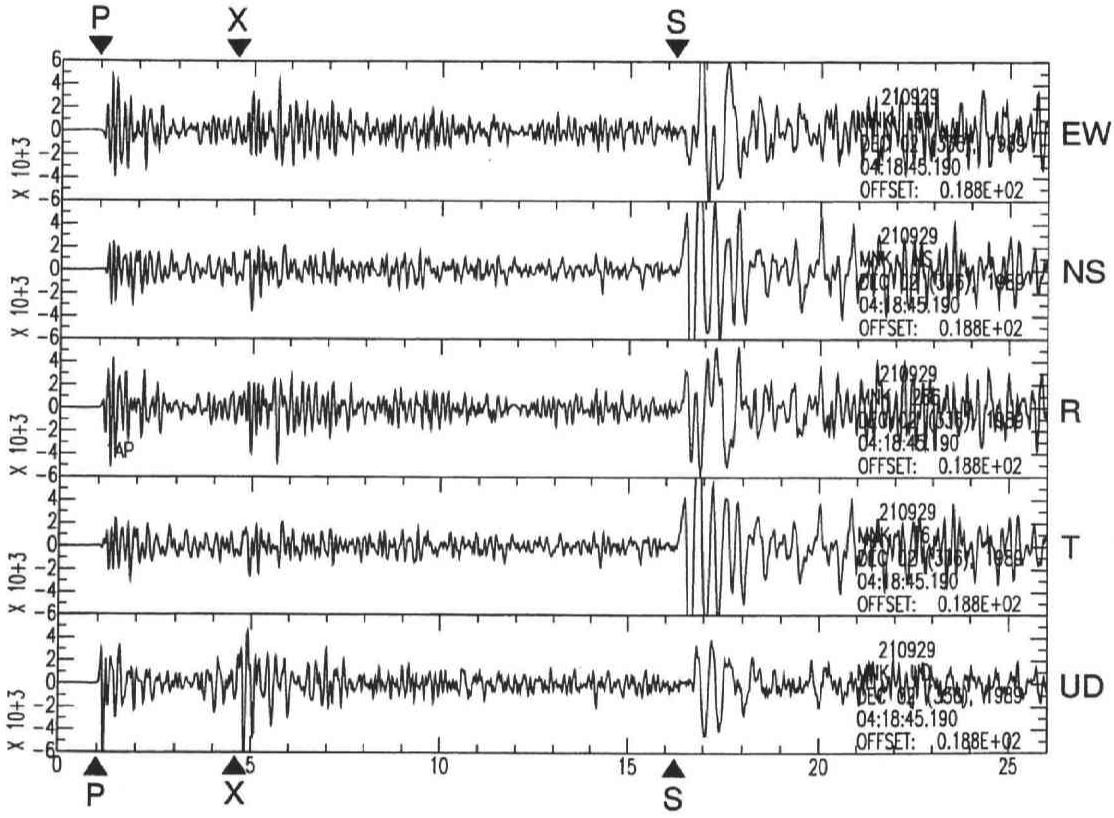

Figure 3.3: Three component seismogram of the SP phase. Radial and transverse components are also shown.

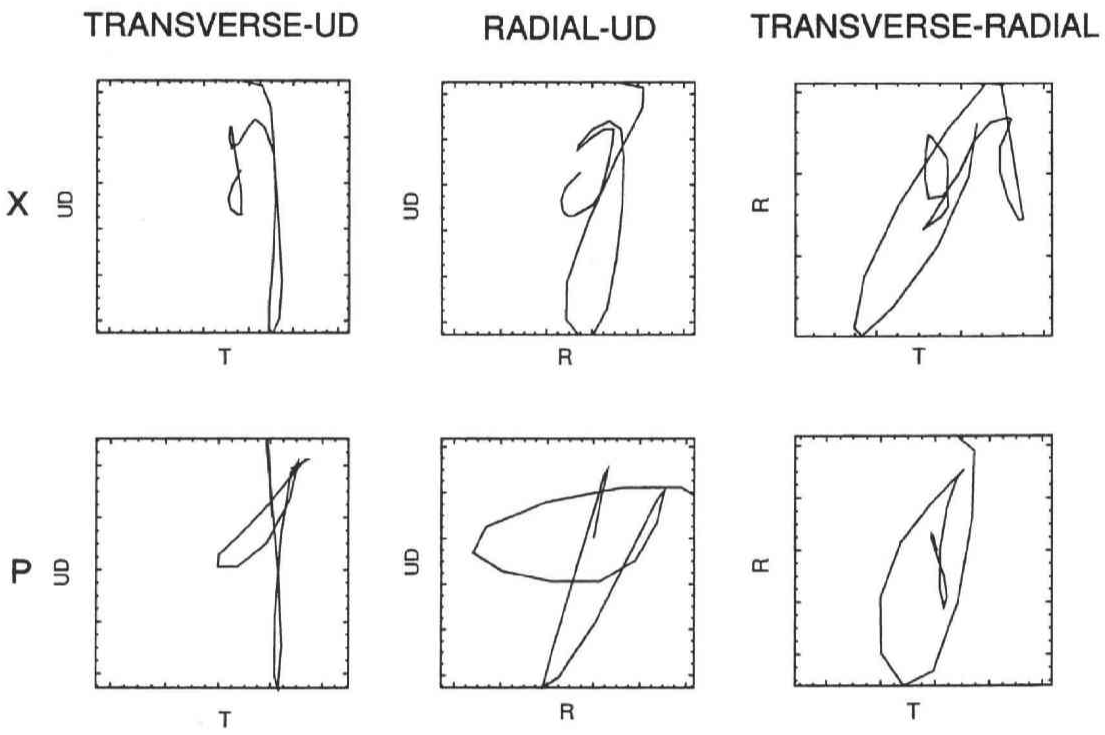

Figure 3.4: Particle motion of the SP phase. Upper figures show the particle motions of the SP-wave, while lower figures show the particle motions of the first P-wave, respectively.

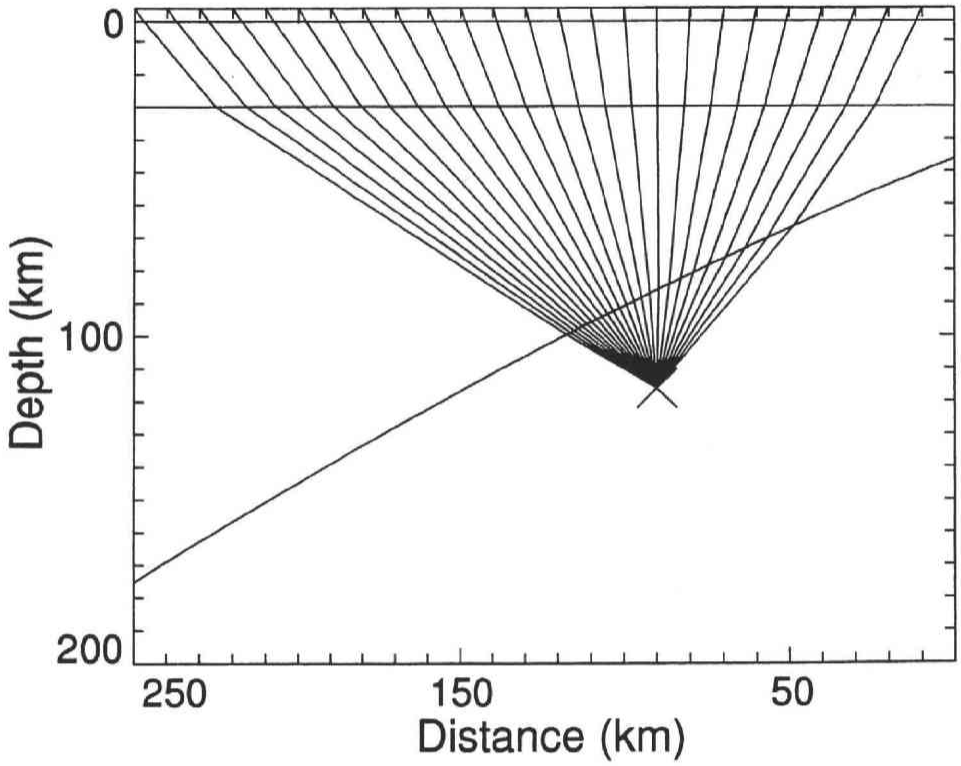

Figure 3.5: Ray diagrams and travel times of first P, S, and SP phases calculated with SEIS83 program. (a) Ray diagram of first P and S phase.

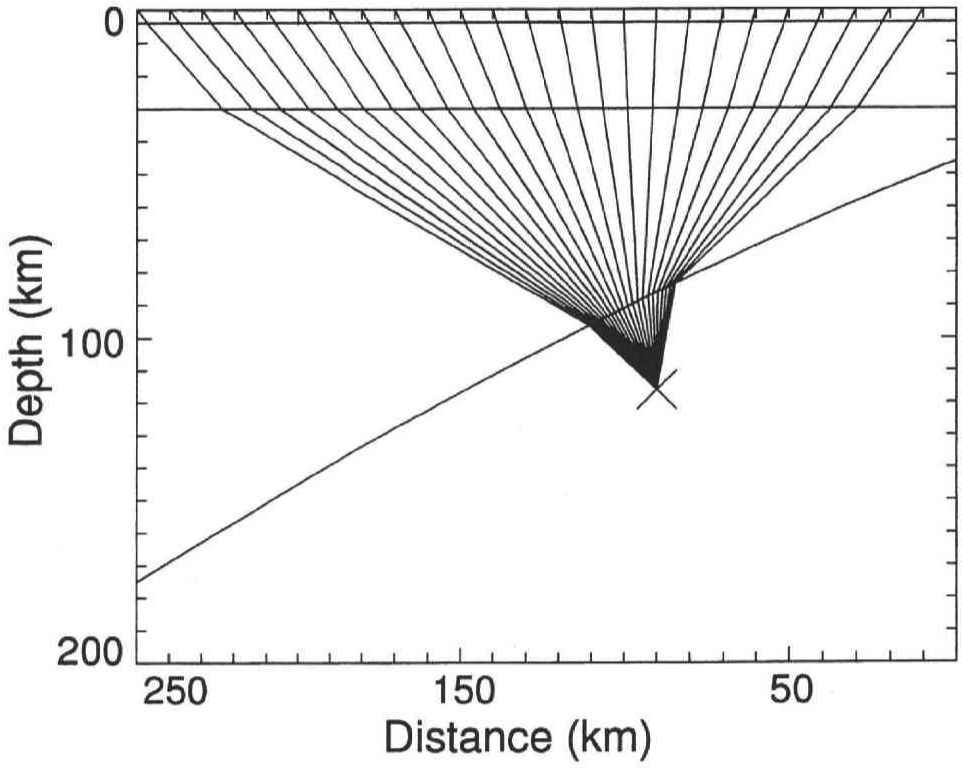

Figure 3.5: Ray diagrams and travel times of first P, S, and SP phases. (b) Ray diagram of SP phase.

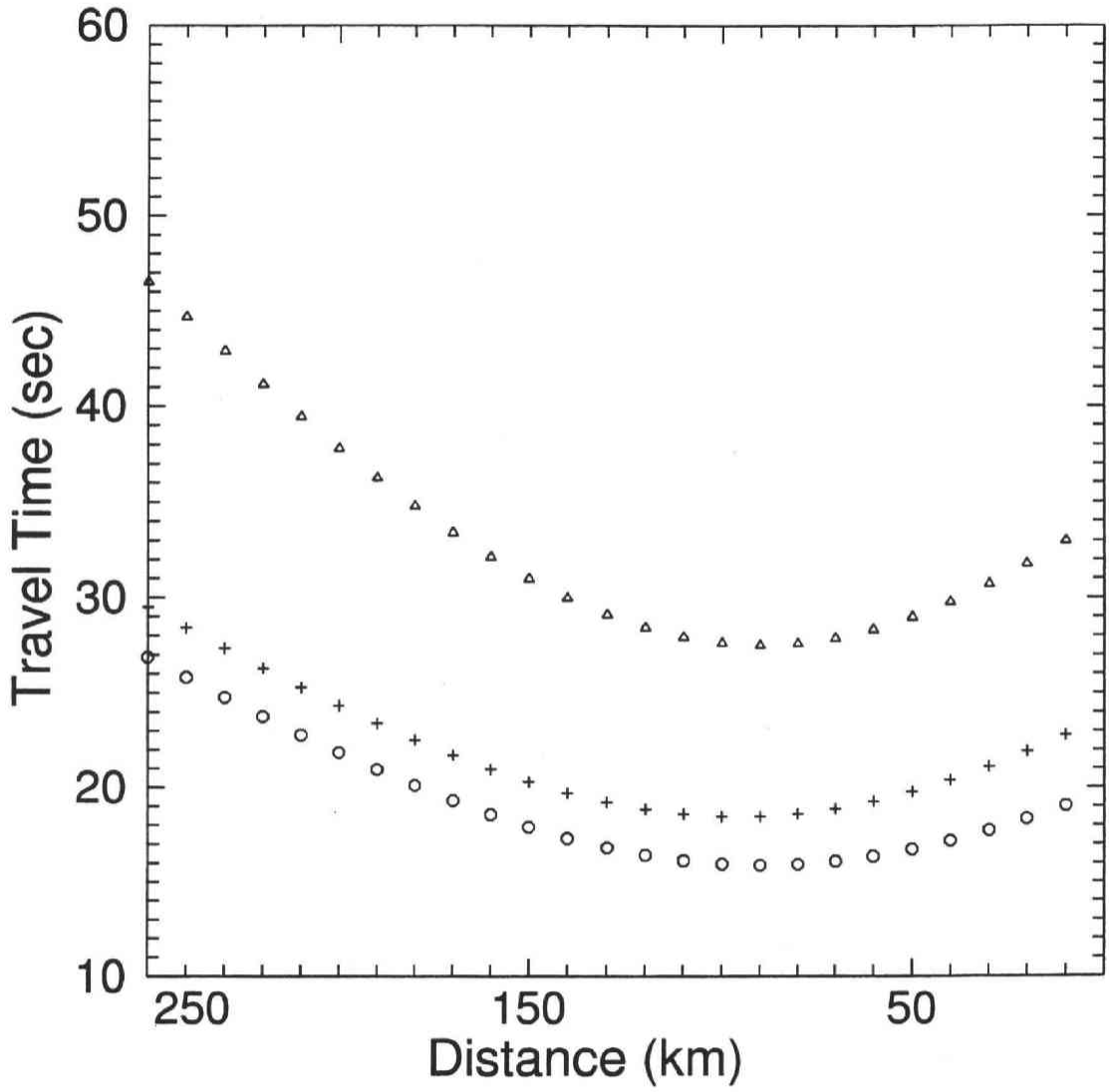

Figure 3.5: Ray diagrams and travel times of first P, S, and SP phases. (c) Theoretical travel time of each phase. Open circles, triangles, and pluses show the the arrival times of first P phase, S phase, and SP phase, respectively.

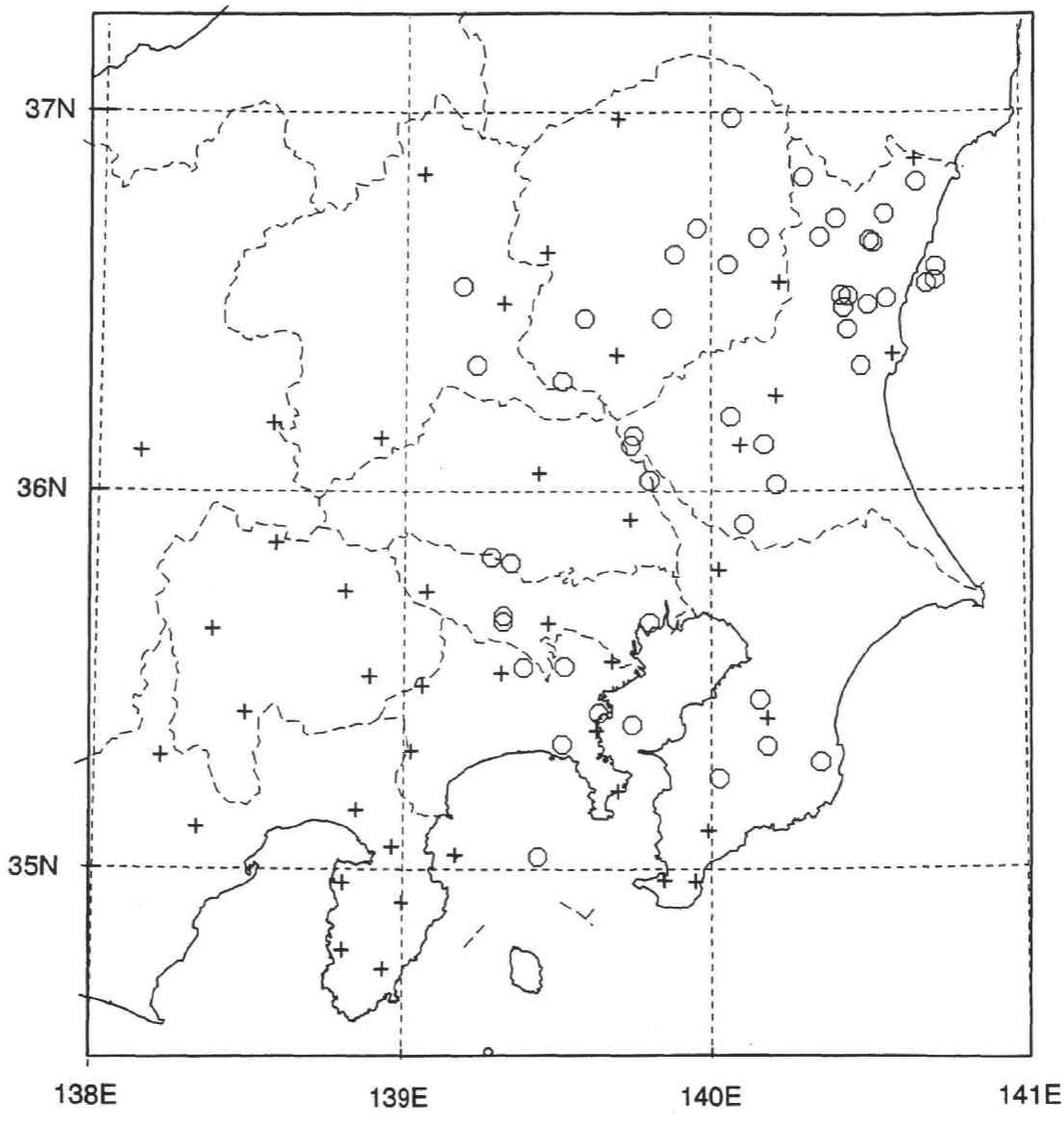

Figure 3.6: Locations of earthquakes used in this study. Open circles denote epicenters and crosses show the seismic stations. 49 earthquakes and 44 stations are plotted.

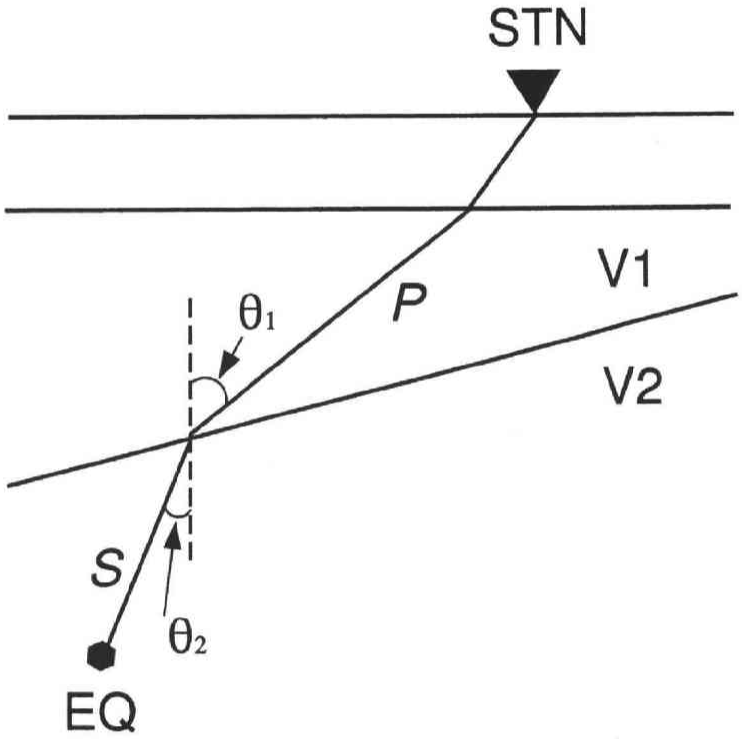

Figure 3.7: Ray path for SP wave projected on the vertical section. EQ represents the hypocenter and STN denotes the seismic station.

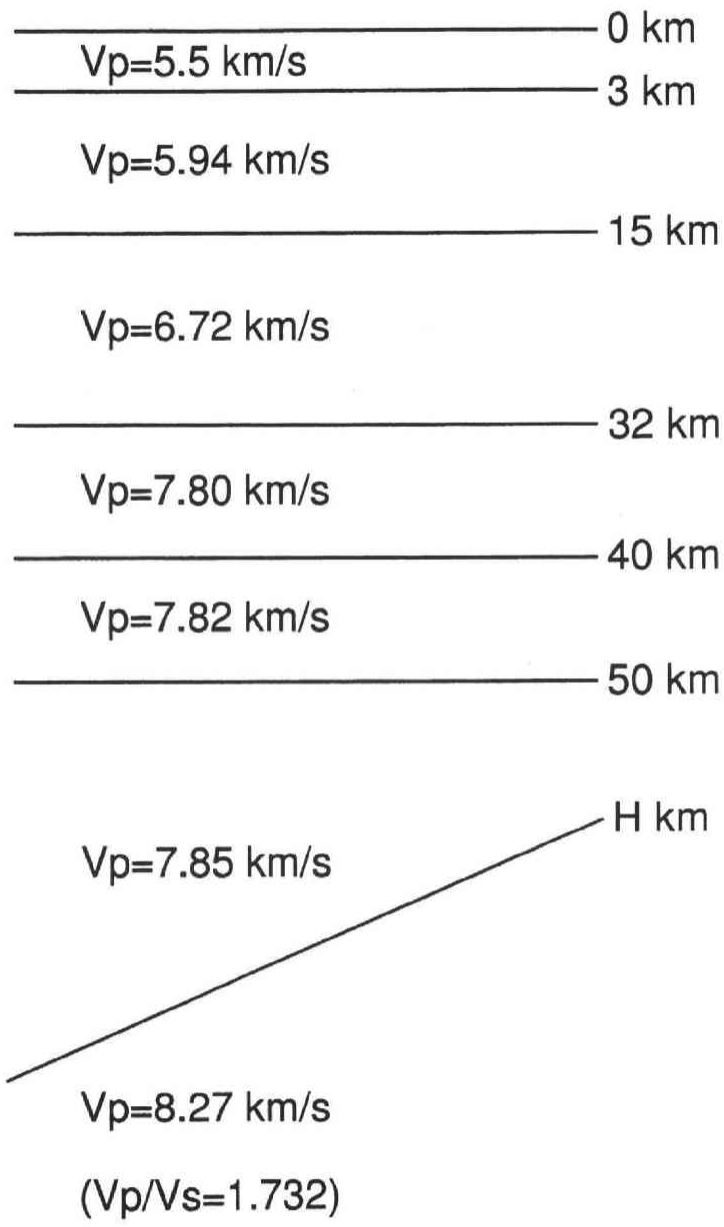

Figure 3.8: Velocity structure used for the travel time calculation. S wave velocity is calculated by assuming $V_P/V_S = 1.73$

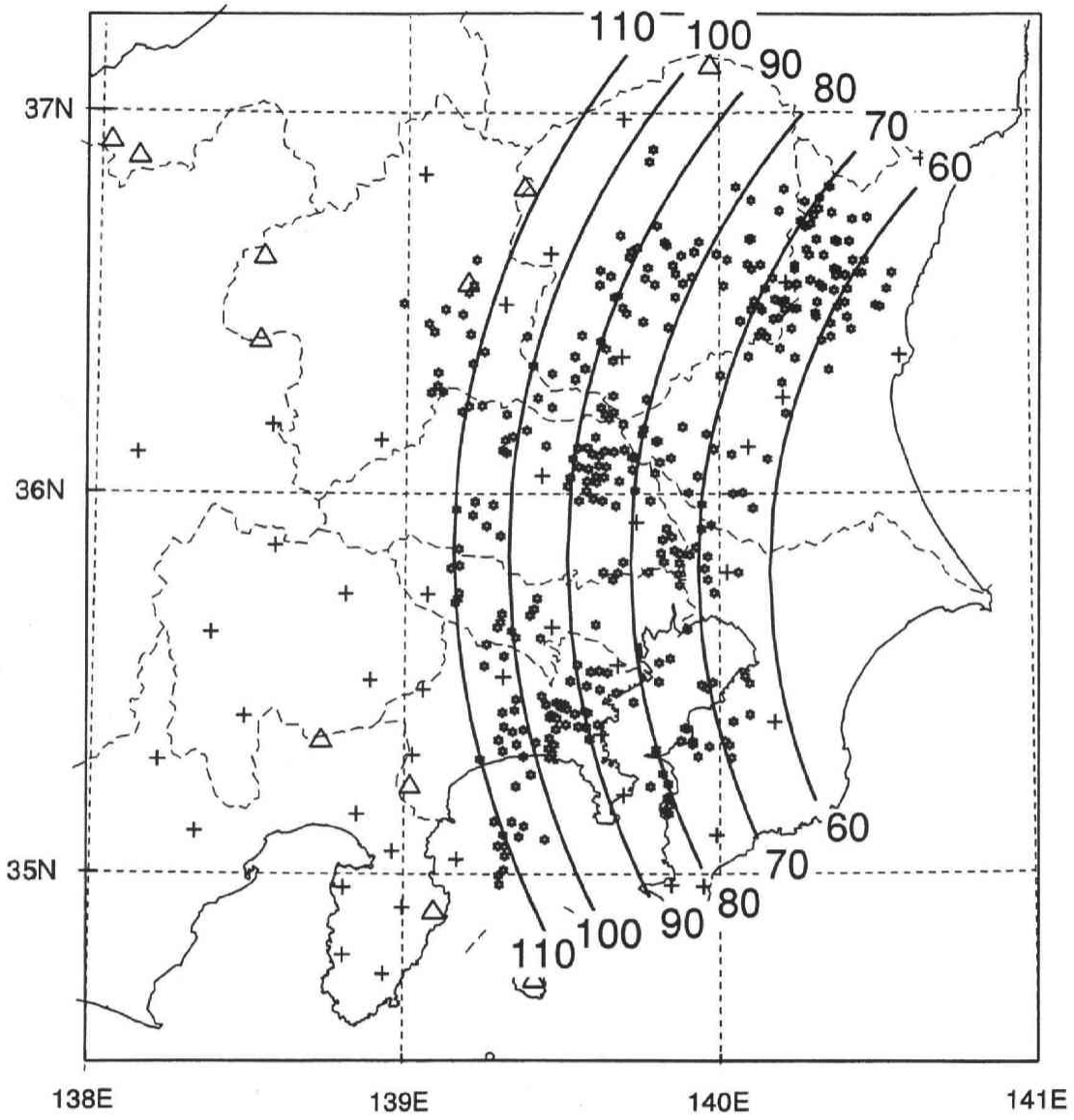

Figure 3.9: Contour map of the conversion interface obtained in this study. Numerals denote the depth to the interface in unit of km. Stars show the conversion points on the interface and open triangles denote active volcanoes.

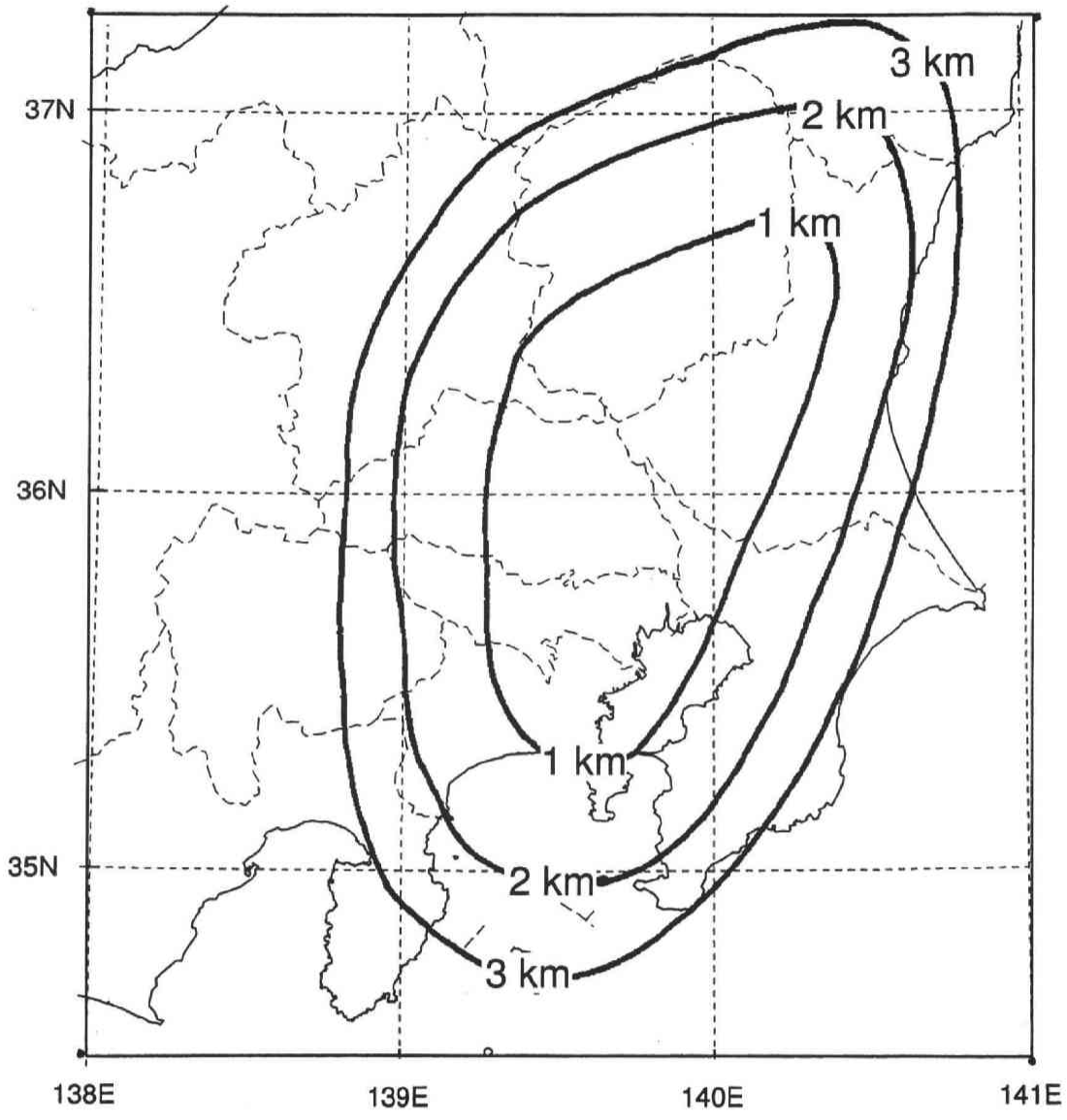

Figure 3.10: Estimation error of the depth to the conversion interface in unit of km.

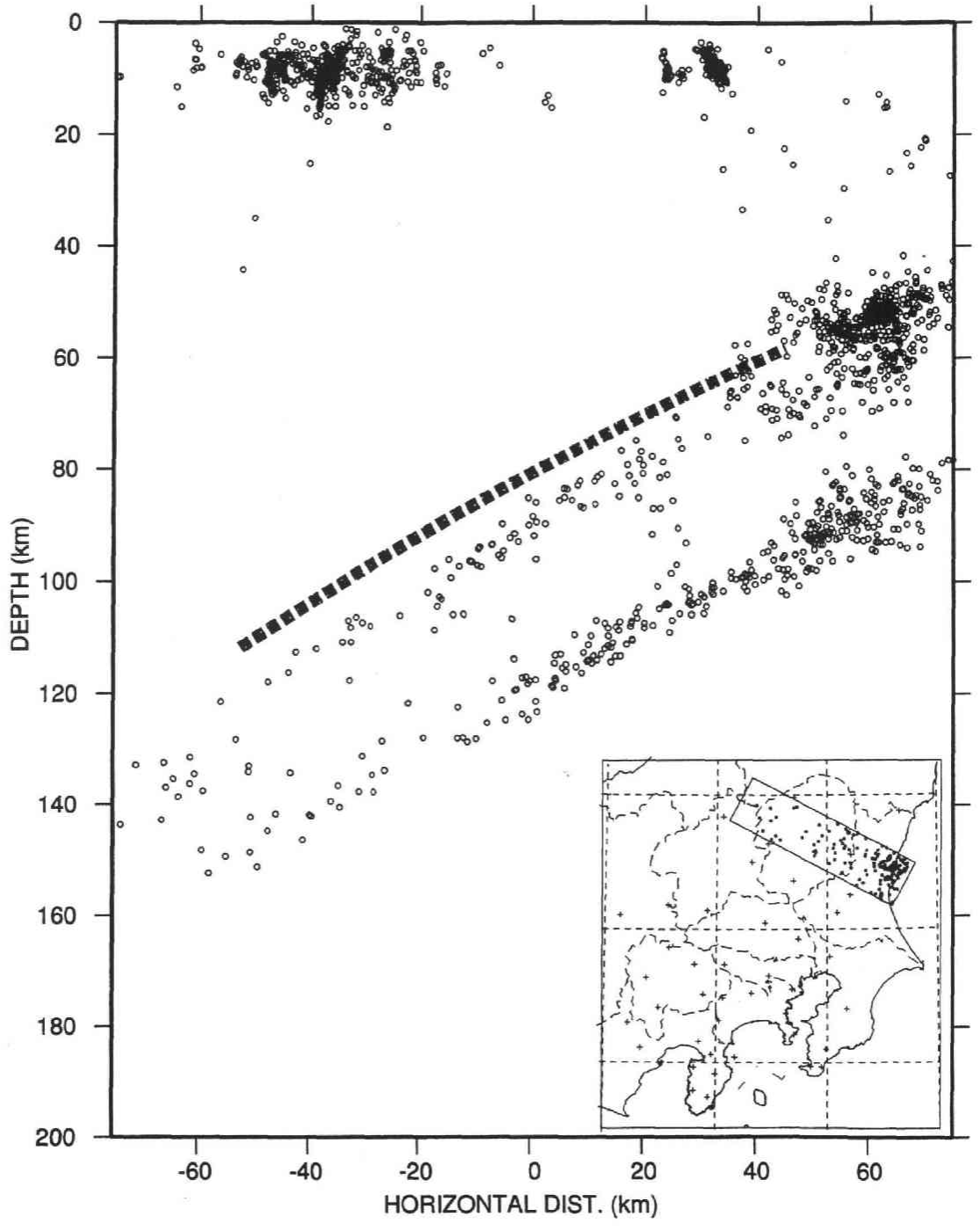

Figure 3.11: Cross sectional view of the conversion interface. The thick grey line represents the conversion interface. Circles denote the events that occurred in the shaded area shown in the inset map. (a) northern Kanto area.

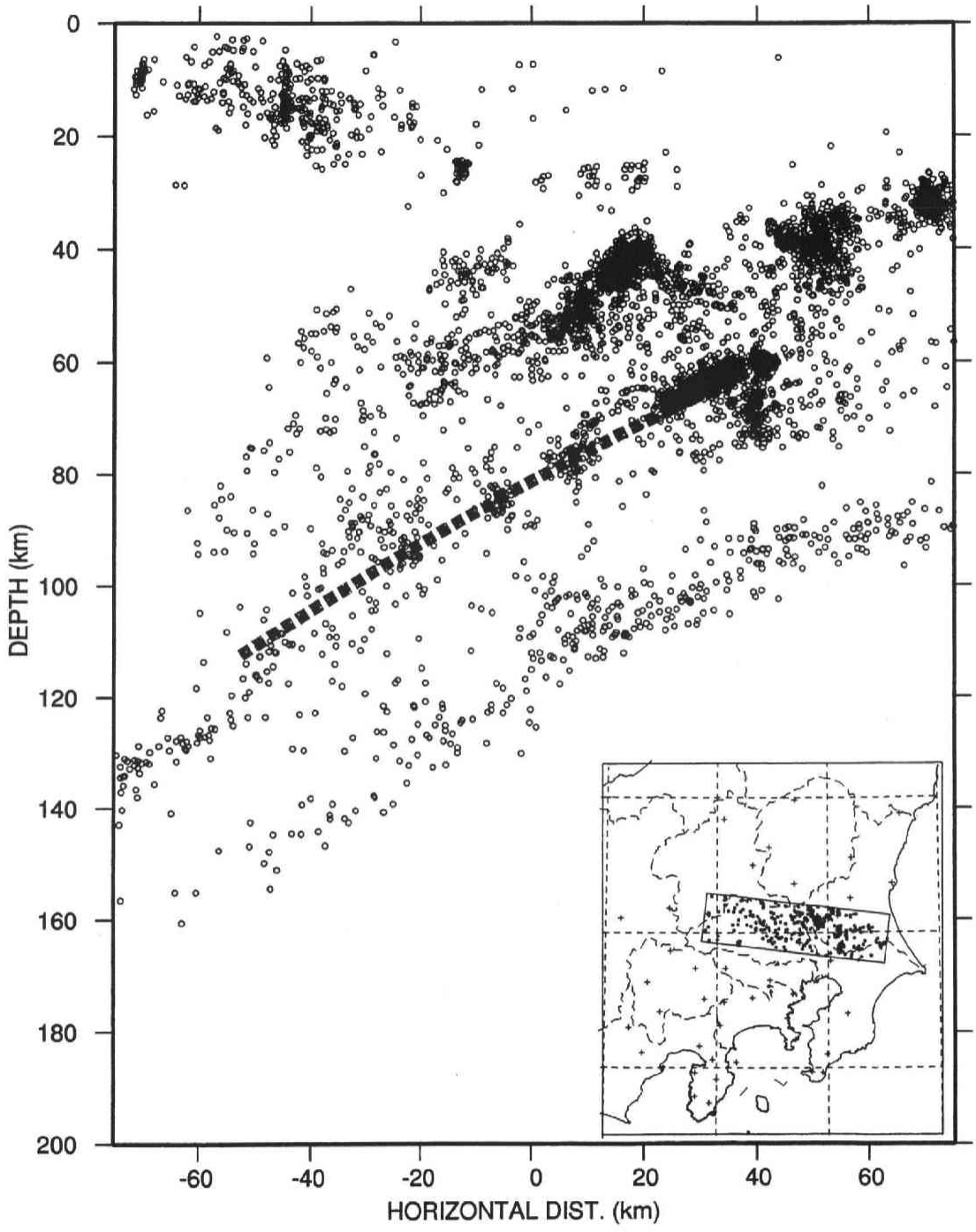

Figure 3.11: (continued). Cross sectional view of the conversion interface. (b) central Kanto area.

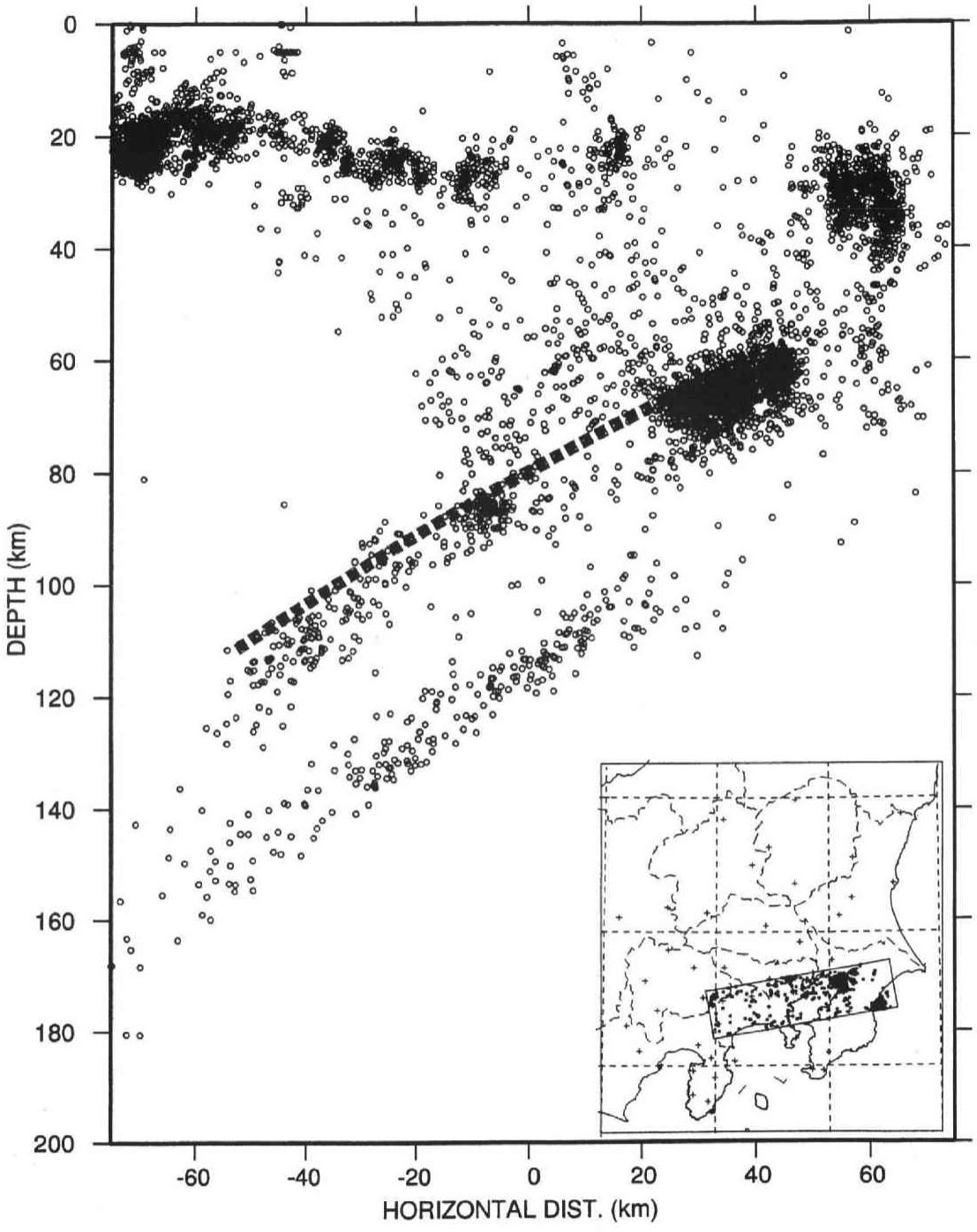

Figure 3.11: (continued). Cross sectional view of the conversion interface. (c) southern Kanto area.

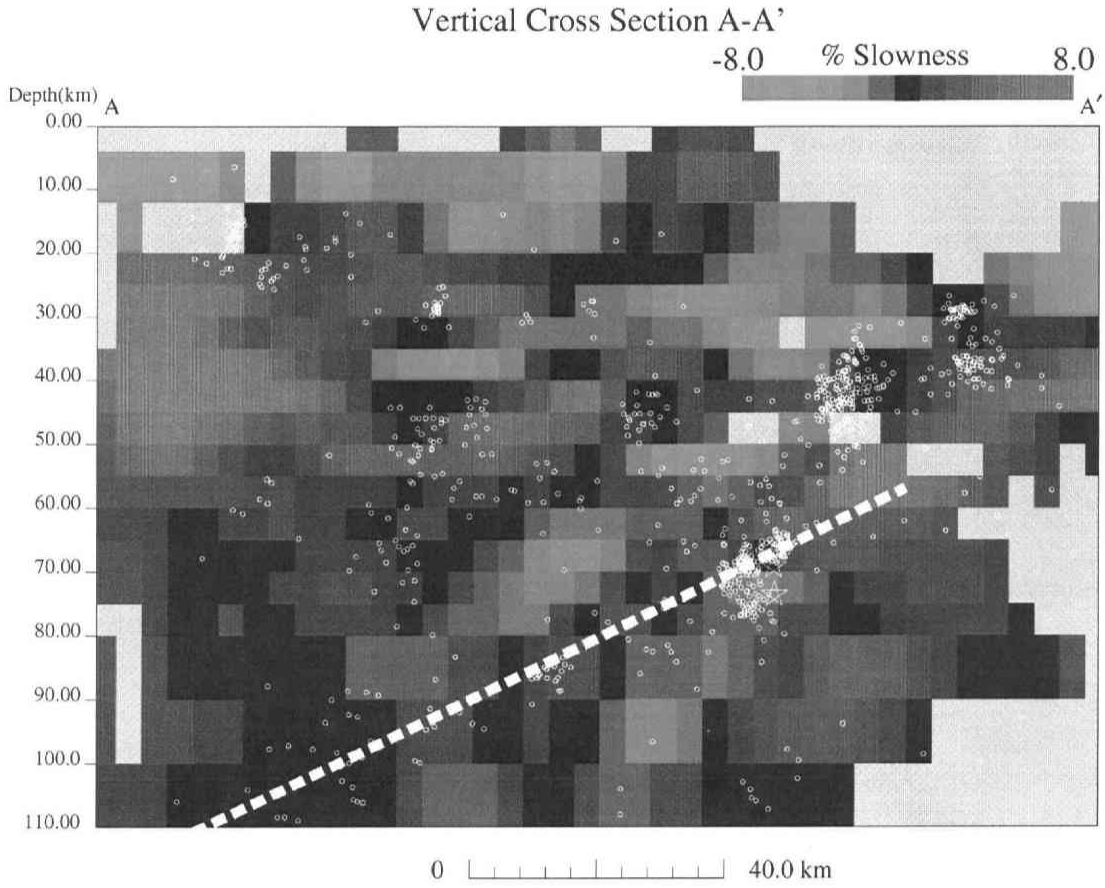

Figure 3.12: Vertical cross sectional view of the conversion interface plotted on the P-wave velocity anomalies. Map view of cross section locations is shown in Figure 2.5

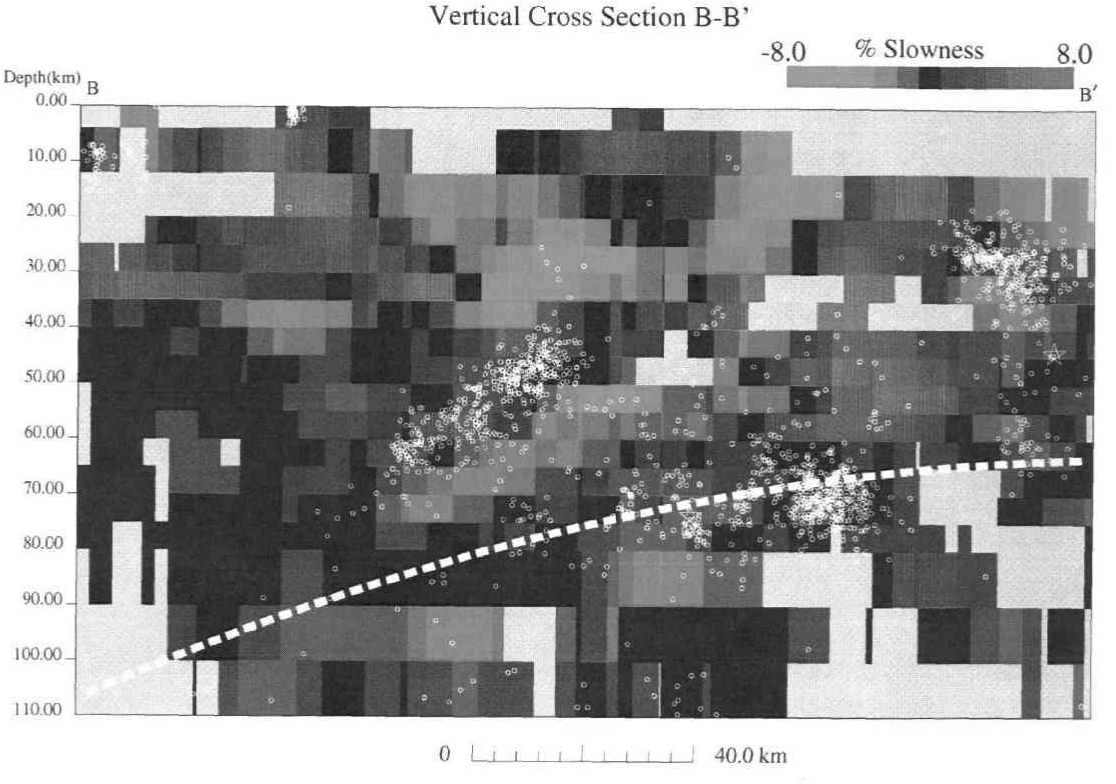

Figure 3.12: (continued). Vertical cross sectional view of the conversion interface plotted on the P-wave velocity anomalies.

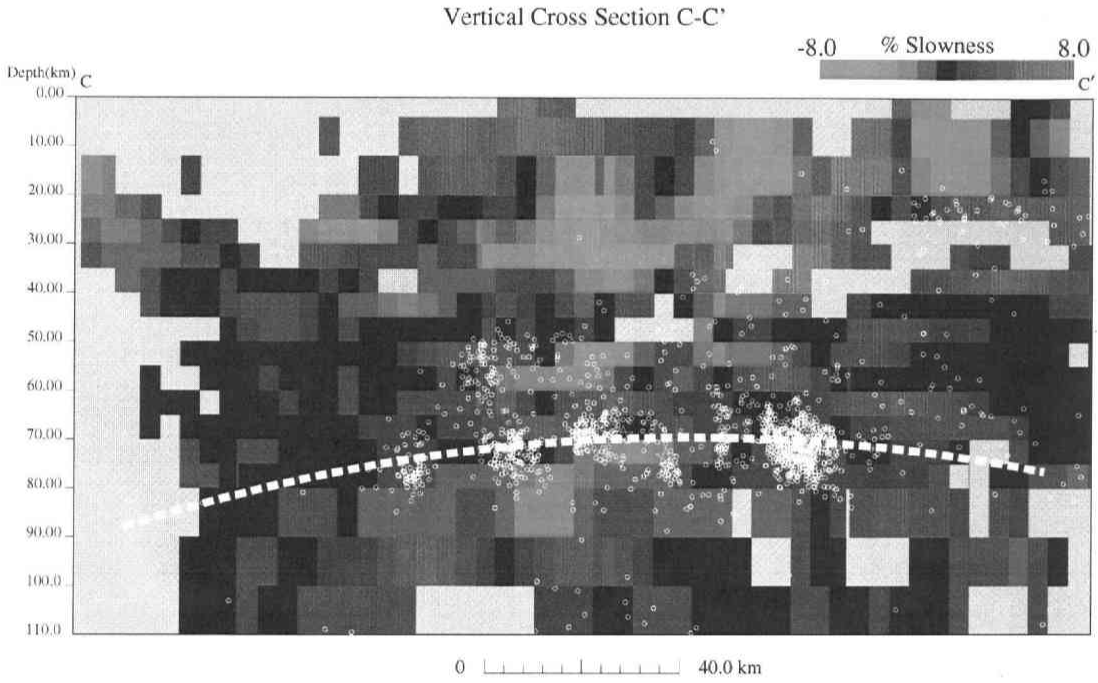

Figure 3.12: (continued). Vertical cross sectional view of the conversion interface plotted on the P-wave velocity anomalies.

Chapter 4

Seismic Velocity Structure near the Plate Boundary and Earthquake Occurrence

4.1 Focal Mechanisms of Earthquakes Associated with the Subduction Process of the Pacific Plate in the Northeastern Japan Arc.

In the previous chapters, we demonstrated the existence of the low velocity layer at the top of the subducting PAC plate, in which low angle thrust fault type earthquakes occur. We also clarified that the conversion interface that generates conspicuous SP wave is located near the low velocity layer. In this section, we discuss the relation among the low velocity layer, the conversion interface, hypocenter distribution, and focal mechanisms.

Focal mechanisms of earthquakes related to the subducting process of PAC beneath the northeastern Japan arc in the Tohoku region can be classified roughly into three types: (1) low angle thrust fault type earthquakes; (2) down dip compression type (DC); and (3) down dip extension type (DE). Low angle thrust fault type events are distributed down to a depth of about 60 km (e.g. Seno and Pongsawat, 1981; Umino and Hasegawa, 1982). The landward boundary of this

type events is nearly identical to the Aseismic Front (Yoshii, 1975; Kawakatsu and Seno, 1983). In the depth range from 50 km to 200 km, clear double-planed structure of deep seismic zone is observed. The upper plane is characterized by down dip compression (DC) type focal mechanisms and the lower plane is by down dip extension (DE) type focal mechanisms (e.g. Umino and Hasegawa, 1975; Hasegawa et al. 1978a). In the region from 36 °N to 39 °N, the double seismic zone extends seaward beyond the aseismic front and overlaps with the main thrust zone. It is called 'triple seismic zone' (Seno and Pongsawat, 1981; Kawakatsu and Seno, 1983). In the triple seismic zone, the main thrust zone and the DC zone is vertically separated by about 10 km.

Taking into account these features observed in Tohoku, we will see the cross sections in the Kanto region in more detail.

4.2 Relationship among the Conversion Interface, Hypocenter Distribution, and Focal Mechanisms near the Upper Boundary of the Pacific Plate.

In order to discuss the relation among the conversion interface, hypocenter distribution, and focal mechanisms, we will present eight vertical cross sections showing hypocenters, namely from C1 through C8 regions from north to south. Hypocenters projected along a 20 km swath are also plotted. In this section, we will focus our interpretation on seismic activities related to the subduction process of the PAC plate beneath the PHS plate.

C1 region. Cross sectional view is shown in Figure 4.1(a). The conversion interface is located about 10 km above the upper plane

of the double planed seismic zone in the depth range from 60 km to 110 km. Hypocenter distribution in the most seaward area consists of three seismic zones, which is probably attributable to 'triple seismic zone'. Figure 4.1(b) shows the typical focal mechanisms in each cluster noted in Figure 4.1(a). Focal mechanisms of some large earthquakes in each cluster, which are routinely determined by NIED, are shown. It is clear that events in A cluster are mostly low angle thrust fault type. On the other hand, DC and DE type events are dominant in B and C clusters, respectively. The conversion interface runs through the low angle thrust events zone.

C2 region. Figure 4.2(a) shows the cross sectional view. In the most seaward area, there is an earthquake cluster (cluster A in Figure 4.2(a)) about 10 km above the upper plane of the double planed seismic zone. Cluster A mainly consists of low angle thrust fault type earthquakes and group B and C consist of DC and DE type events, respectively. Typical focal mechanisms are shown in Figure 4.2(b). Thus this region also forms 'triple seismic zone'. There are other clusters such as D and E cluster. D is located in the northernmost part of the Tsukuba-Chiba seismic belt (Hurukawa and Imoto, 1990) with low angle thrust fault type earthquakes. Cluster E dominantly exhibits NS extensional normal fault type. This agrees with the result of Ukawa and Imoto (1982) who pointed out that NS extensional stress field appears in the upper plane of the double seismic zone beneath the Kanto. The conversion interface passes through the low-angle thrust events zone similarly to the C1 region.

C3 region. Cross section is shown in Figure 4.3(a). Focal mechanisms are shown in Figure 4.3(b). Cluster A is a part of the Tsukuba-Chiba seismic belt of low angle thrust fault earthquakes. There exist

other clusters above them, but we will not give our attention to them here because they are the earthquakes related to the subduction process of the PHS plate beneath the EUR plate. Clusters B and C, that are located seaward of cluster A, mainly show DC and DE type stress state, respectively. Cluster D, on the other hand, shows NS compressional reverse fault type, which also agrees with Ukawa and Imoto (1982)'s interpretation for the lower plane events beneath Kanto. In this region, the conversion interface is located at the bottom of the low angle thrust events zone (cluster A).

C4 region. Figure 4.4(a) shows the cross section. Cluster A is a part of the Tsukuba-Chiba seismic belt of low angle thrust events. Typical focal mechanism solutions are shown in Figure 4.4(b). The separation between the thrust zone and the upper plane of the double seismic zone is not clear, or in other words 'triple seismic zone' is hardly recognized at here. On the other hand, low angle thrust events occur at deeper depths such as in clusters B, C, and D. Cluster C and D also include events of other focal mechanism type such as DE and NS extensional types. The conversion interface is roughly located at the bottom of cluster A, and it penetrates other three clusters.

C5 region. Cross sectional view of C5 region is shown in Figure 4.5(a) and typical focal mechanisms are shown in Figure 4.5(b). The Tsukuba-Chiba seismic belt appears in the depth range from 60 km to 70 km here, which consists of two earthquake clusters, A and B. Cluster A shows a complicated stress field, having not only low angle thrust fault type but also EW extensional normal fault type, which was discussed in Hurukawa and Imoto (1990) ('F. Chiba' region in section 4 of Hurukawa and Imoto (1990)). The Ibaraki-Chiba border earthquake of October, 4, 1985 and their aftershocks took place in

cluster B. The Ibaraki-Chiba border earthquake is interpreted as an intra PAC plate earthquake and it does not show low angle thrust fault type focal mechanism. However, most events in the upper part of the cluster B show low angle thrust type. Cluster C shows NS extensional normal fault type and some low angle thrust fault type. Cluster D shows mainly DE type. The conversion interface is located at the upper boundary of the thrust events clusters, A and B.

C6 region. Cross sectional view is shown in Figure 4.6(a). Focal mechanisms of two clusters are presented in Figure 4.6(b). The Tsukuba-Chiba seismic belt is most active in this region. Focal mechanisms in this cluster show various types in contrast to the other clusters of the Tsukuba-Chiba seismic belt ('F. Chiba' in section 4 of Hurukawa and Imoto, 1990). However, it is also dominantly composed of thrust type earthquakes (cluster A).

On March 18, 1988, a moderate earthquake took place in this region at a depth of 90.5 km. The focal parameters determined by NIED is as follows: latitude = 35.668 °N; longitude = 139.626 °E; focal depth = 90.5 km. It is located in the cluster B, which dominantly exhibits NS extensional stress field. Focal mechanism of the event obtained by NIED is shown in Figure 4.7(a). It also shows NS extensional normal fault type. Okada and Kasahara (1990) remarked based on the aftershock distribution of the event that it was a simple thrust event associated with the subduction of the PAC plate. They owed the inconsistency to the complex tectonic setting of this area suggested by Kasahara (1985). The conversion interface is located at the upper limit of the cluster events with thrust faulting.

C7 region. Figures 4.8(a) and 4.8(b) show the cross sectional view and typical focal mechanisms in this region. The southern end of the

Tsukuba-Chiba seismic belt appears at depths of about 60 km and the conversion interface passes through the upper boundary of the earthquake cluster A. Cluster A is composed of various types of focal mechanisms, but thrust type is dominant.

C8 region. Cross section is shown in Figure 4.9. In this region, separation between the upper seismic plane and the conversion interface is not clear. The earthquake cluster located at depths of about 90 km is composed of an earthquake of magnitude 5.9 (JMA) that occurred on February 2, 1992, and its aftershocks. The focal parameters determined by NIED are as follows: latitude = 35.221 °N; longitude = 139.738 °E; focal depth = 85.3 km. The focal mechanism is shown in Figure 4.7 (b). It is a typical DC type event.

4.3 Comparison to the Case in Tohoku.

The geometry of the conversion interface and the seismic zone near the top of the PAC plate beneath the Kanto are summarized as follows: (1) Oceanic crust that exhibits low velocity anomaly exists at the top of the subducting PAC plate; (2) Low angle thrust fault type earthquakes occur in the low velocity layer; (3) The conversion interface well coincides with the location of the low velocity layer. However, it is not clear whether the conversion interface located at the upper boundary or lower boundary of the low velocity layer; and (4) Thus the conversion interface is located in the low velocity layer, which forms a zone of thrust fault type earthquakes. In the northern Kanto region (C1, C2 area), there exist three layered seismic zones; zones of thrust fault type, down-dip compression type, and down-dip extension type. The conversion interface is located at the zone of thrust fault earthquakes.

On the other hand, the situation in the Tohoku district (e.g. Ma-

tsuzawa et al., 1986) is summarized as follows: (1) The conversion interface that generates SP wave is located just above the upper plane of the double seismic zone; (2) The conversion interface is the upper boundary of the subducting PAC plate; (3) Low velocity layer is located below the conversion interface; (4) Thus the upper plane of the double seismic zone, that consists of down-dip compression type events, is formed in the low velocity layer.

Goto and Hamaguchi (1979, 1980) proposed that the double seismic zone could be explained by thermal stresses caused by the temperature difference between the asthenosphere and the slab. According to their calculation, the zone of down-dip compressional stress extends farther seaward beneath the main thrust zone, if the upper boundary of the descending slab is held fixed in the depth range of 0 - 100 km in space. Seno and Pongsawat (1981) reported that geometry of the triple seismic zone beneath the Tohoku district is partially explained using Goto and Hamaguchi (1980)'s idea.

Matsuzawa et al. (1990) did not mention the separation between the conversion interface and the upper plane of the double seismic zone. On the other hand, the separation is clear in the northern Kanto area. If we can apply Goto and Hamaguchi (1980)'s idea to the tectonics in the Kanto region, it is probable to consider that the zone beneath the main thrust zone should have the down dip compressional stress field. In the Kanto region, deeper penetration of the main thrust zone is observed, while it is not observed in the Tohoku district. Thus it is likely that the down dip compressional stress field extends landward with keeping separation beneath the main thrust zone in the Kanto district. Therefore we can recognize the separation between the conversion interface and the upper plane of the double seismic zone, which is composed of not only main thrust events, but also of

down-dip compressional type earthquakes.

4.4 What is the Conversion Interface ?

The location of the conversion interface estimated from the SP wave analysis well coincides with the low velocity crust at the top of the subducting PAC plate in the Kanto district. Since the converted wave is generated at a velocity boundary, the conversion interface should be either at the upper boundary or lower boundary of the low velocity zone. However it is difficult to distinguish the boundary from our result, though in some case, it seems to be coincide with the lower boundary of the low velocity layer (C3 and C4 regions).

Nakanishi (1980) pointed out that there exists a 'transition zone' at the top of the PHS plate in southwestern Japan. However his result has no sharp velocity change at the interface between the transition zone and underlying lithosphere. Matsuzawa et al. (1990) also suggested that the bottom part of the low velocity layer in the Tohoku region has gradual velocity change and does not generate conversion waves.

In the Kanto region, the thermal condition around the subducting PAC plate may be different from that in Tohoku or Chugoku regions because the PHS plate is also subducting above the PAC plate. Therefore it is likely that sharp velocity jump at the Moho discontinuity of the subducting PAC plate still remains in this depth range. Thus it is probable that both of the upper and lower boundary of the crust have sharp velocity contrasts. The former is the plate boundary itself, and the latter is the Moho discontinuity of the subducting oceanic plate.

In this case, SP converted waves can be generated from both boundaries, and the SP waves from the lower boundary have early travel times. Therefore, the conversion interface obtained in this study may correspond to the Moho discontinuity of the subducting PAC plate

rather than the UBP itself. We can say that we determined a deeper location of velocity jump in the vicinity of the plate boundary. On the other hand, since Obara and Sato (1988), Obara (1989) used SxS reflected waves to locate the UBP, they determined a shallower location of velocity jump. Perhaps the real plate boundary exists between the shallower and deeper velocity discontinuity.

4.5 Focal Region of Low-angle Thrust Earthquakes.

Thrust type earthquakes are occurring in the subducting crust that exhibits low velocity anomaly and has the conversion interface discussed above. Since these thrust type events have low angle slip vector in westward direction, they are regarded as the events occurring at the plate boundary (e.g. Kasahara, 1985). Hashimoto (1981) simulated the observed stress state in southwestern Japan using a three dimensional finite element method (FEM). The plate model in his simulation consists of the subducting PHS, the overriding continental plates, and a weak zone between them. He showed that the low velocity layer (weak zone) gives low angle thrust type stress field in it.

Hurukawa and Imoto (1990) studied the focal mechanisms of the thrust type earthquakes in the Kanto region precisely. They revealed that Hashimoto (1981)'s result is also appreciable in the thrust event zone beneath Kanto area, that thrust events are occurring in the layer, not on a thin interface. If the conversion interface obtained in this study is the subducted Moho discontinuity, it is probable that the thrust earthquakes occur in the whole crust of the subducting slab, between the Moho and the UBP.

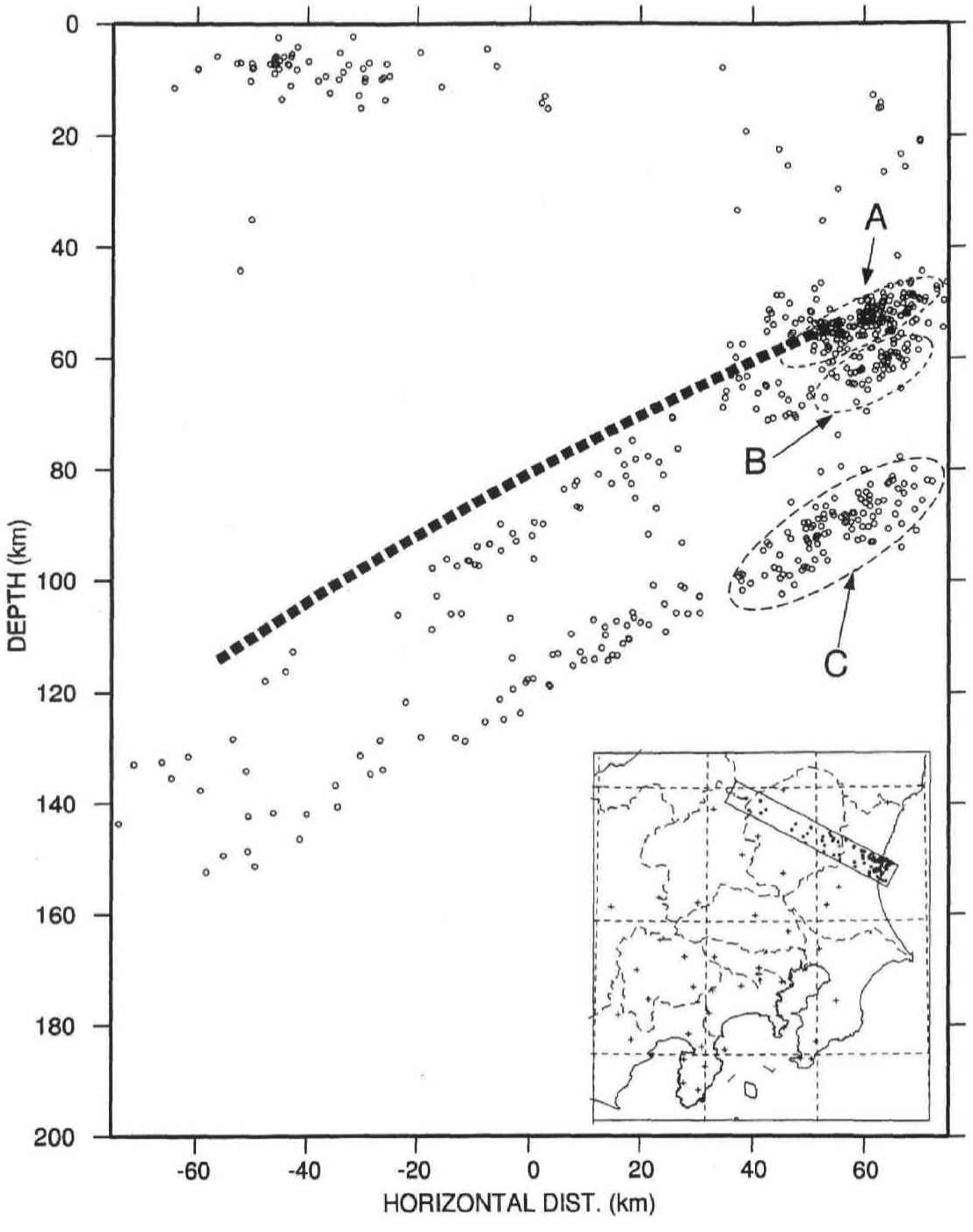

Figure 4.1: (a) Cross sectional view of the conversion interface and seismicity in C1 region. Thick grey line shows the conversion interface. Circles denote hypocenter of events that occurred in the shaded area in the inset map.

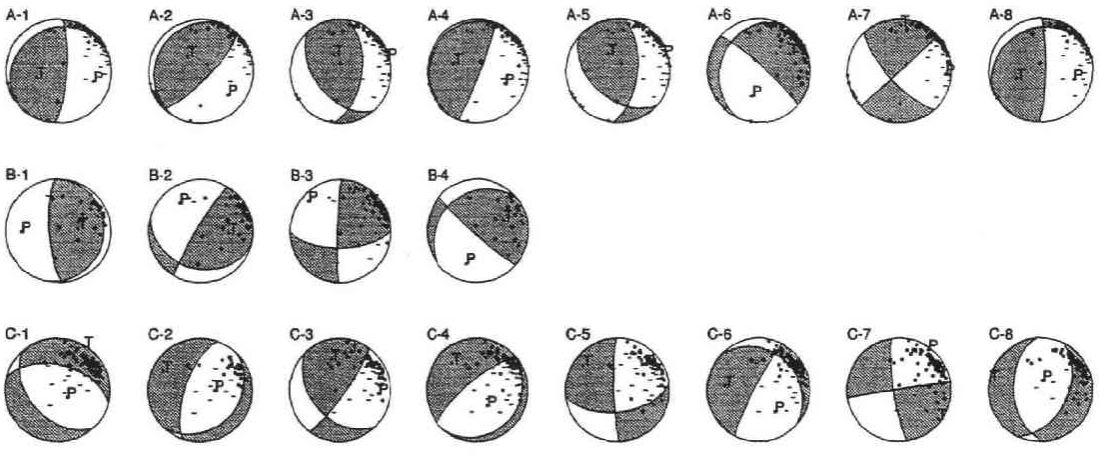

Figure 4.1: (b) Typical focal mechanisms in C1 region. Upper, middle, and lower rows show focal mechanisms of clusters A, B, and C, respectively. The shaded area represent the compressional area projected on the lower focal hemisphere. Focal parameters of the events are shown in Table 4.1.

No.	Origin Time (JST)						Latitude °N	Longitude °E	Depth km	Magnitude
A-1	1986	09	20	12	04	58.45	36.451	140.644	49.8	5.2
A-2	1986	10	25	21	58	16.13	36.431	140.655	46.6	4.3
A-3	1990	01	01	18	03	13.78	36.455	140.581	52.6	4.5
A-4	1990	05	03	16	45	44.23	36.459	140.633	49.9	5.5
A-5	1990	10	06	23	33	01.97	36.441	140.619	50.8	5.2
A-6	1992	05	11	19	07	53.51	36.497	140.514	56.4	5.8
A-7	1992	09	14	11	46	53.98	36.429	140.667	49.1	4.3
A-8	1992	11	06	07	35	51.34	36.435	140.574	53.1	4.3
B-1	1986	08	29	06	40	50.37	36.412	140.602	63.2	2.9
B-2	1987	03	20	02	39	27.65	36.293	140.604	58.6	3.1
B-3	1988	07	16	13	09	53.76	36.335	140.594	60.2	3.6
B-4	1994	02	15	19	18	47.61	36.436	140.567	62.3	2.9
C-1	1986	11	29	22	30	22.97	36.486	140.424	102.4	4.2
C-2	1987	03	31	02	20	27.14	36.331	140.480	90.8	3.2
C-3	1988	02	09	16	35	42.87	36.357	140.482	89.6	3.9
C-4	1990	10	24	20	27	11.70	36.363	140.525	92.4	4.5
C-5	1990	12	09	12	40	53.39	36.349	140.604	94.0	4.7
C-6	1992	05	16	11	54	21.57	36.422	140.658	82.6	4.2
C-7	1992	07	25	06	37	56.59	36.442	140.595	82.7	3.7
C-8	1993	03	03	12	15	22.29	36.396	140.499	79.5	3.4

Table 4.1: List of origin times, locations, and magnitudes of the earthquakes in C1 region shown in Figure 4.1(b)

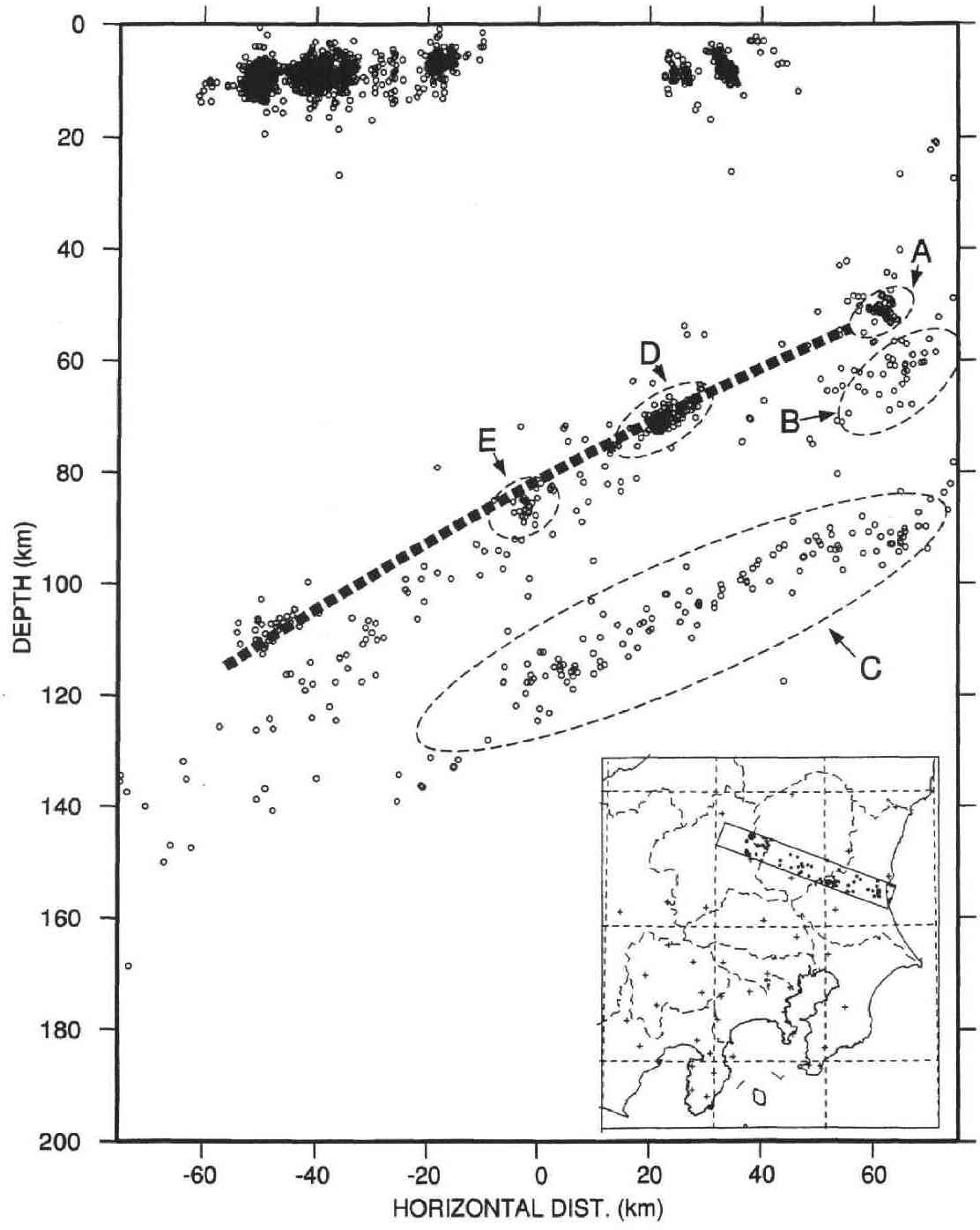

Figure 4.2: (a) Cross sectional view in C2 region.

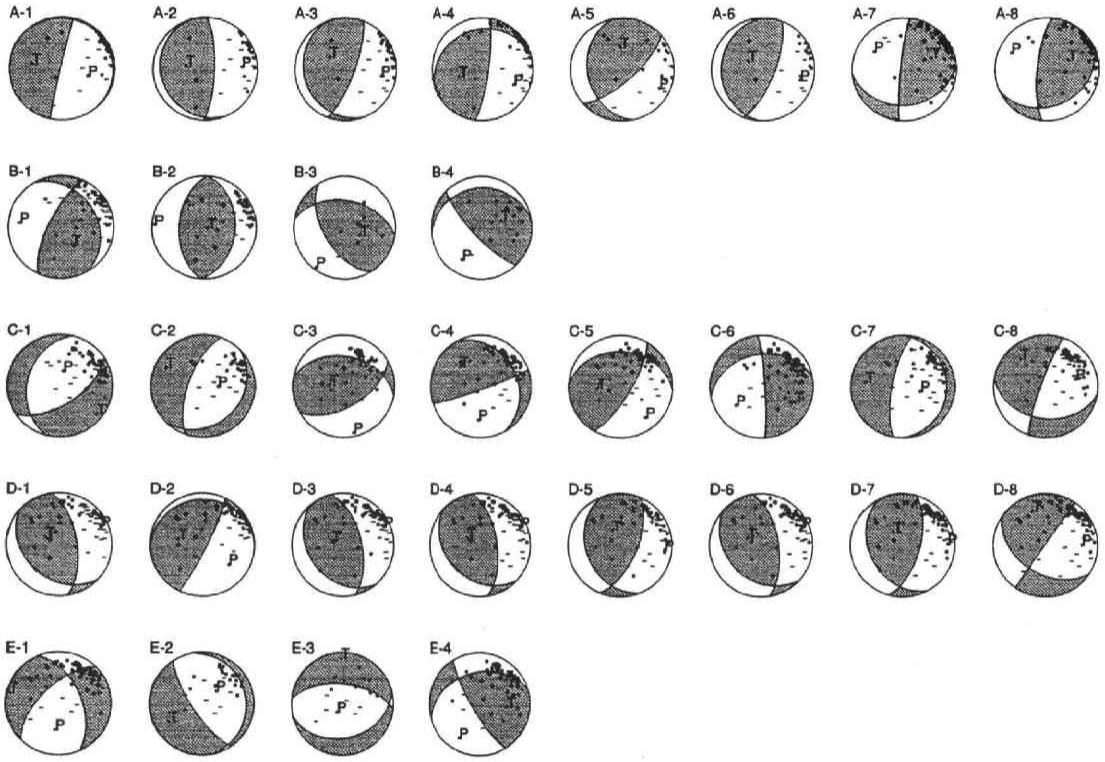

Figure 4.2: (b) Typical focal mechanisms in C2 region. First, second, third, fourth, and fifth rows represent the focal mechanisms of clusters A, B, C, D, and E, respectively. Focal parameters of the events are shown in Table 4.2.

No.	Origin Time (JST)						Latitude °N	Longitude °E	Depth km	Magnitude
A-1	1986	10	24	06	21	26.53	36.261	140.497	50.0	2.7
A-2	1989	04	21	18	39	15.46	36.240	140.463	48.6	2.7
A-3	1989	06	19	17	04	26.61	36.247	140.475	51.5	2.9
A-4	1989	12	23	08	14	17.03	36.262	140.493	47.5	3.5
A-5	1991	01	16	14	04	49.76	36.255	140.493	49.5	3.0
A-6	1989	12	23	23	56	07.30	36.244	140.483	52.6	2.7
A-7	1991	06	19	17	05	42.38	36.258	140.434	55.1	4.2
A-8	1993	07	19	16	54	56.24	36.222	140.486	52.8	3.5
B-1	1986	07	10	11	10	46.10	36.245	140.493	65.6	4.8
B-2	1986	08	01	11	59	00.46	36.218	140.448	66.2	3.3
B-3	1986	10	09	16	20	12.78	36.306	140.512	69.0	2.4
B-4	1988	05	14	01	32	03.74	36.341	140.417	70.8	2.8
C-1	1986	08	08	00	10	25.89	36.290	140.474	89.6	3.2
C-2	1987	03	31	02	20	27.14	36.331	140.480	90.8	3.2
C-3	1990	05	01	07	39	33.77	36.443	139.755	114.9	3.4
C-4	1990	07	17	02	57	30.12	36.418	140.133	97.0	3.3
C-5	1990	07	29	22	42	24.44	36.457	139.839	112.2	3.3
C-6	1992	05	12	17	11	58.18	36.325	140.266	99.7	3.7
C-7	1993	01	01	08	49	46.57	36.343	140.323	88.9	3.3
C-8	1994	01	01	22	53	27.19	36.486	140.018	107.4	3.4
D-1	1986	06	16	05	48	03.71	36.320	140.022	70.8	3.6
D-2	1986	12	22	12	33	22.60	36.364	140.080	67.4	3.5
D-3	1988	08	27	06	40	29.35	36.315	140.025	69.8	3.7
D-4	1990	05	24	17	11	45.32	36.323	140.035	71.4	3.7
D-5	1990	09	12	14	37	40.68	36.328	140.046	69.2	3.5
D-6	1992	09	14	01	01	41.84	36.320	140.024	71.1	3.6
D-7	1993	01	21	13	22	38.77	36.336	140.035	70.3	3.7
D-8	1993	06	23	06	33	26.33	36.326	140.084	67.7	3.8
E-1	1987	09	30	03	11	43.46	36.465	139.783	85.3	3.8
E-2	1987	10	11	15	01	17.94	36.429	139.789	85.1	2.7
E-3	1987	10	17	00	24	48.94	36.426	139.793	85.3	2.6
E-4	1994	06	06	19	10	42.07	36.445	139.796	84.5	3.0

Table 4.2: List of origin times, locations, and magnitudes of the earthquakes in C2 region shown in Figure 4.2(b)

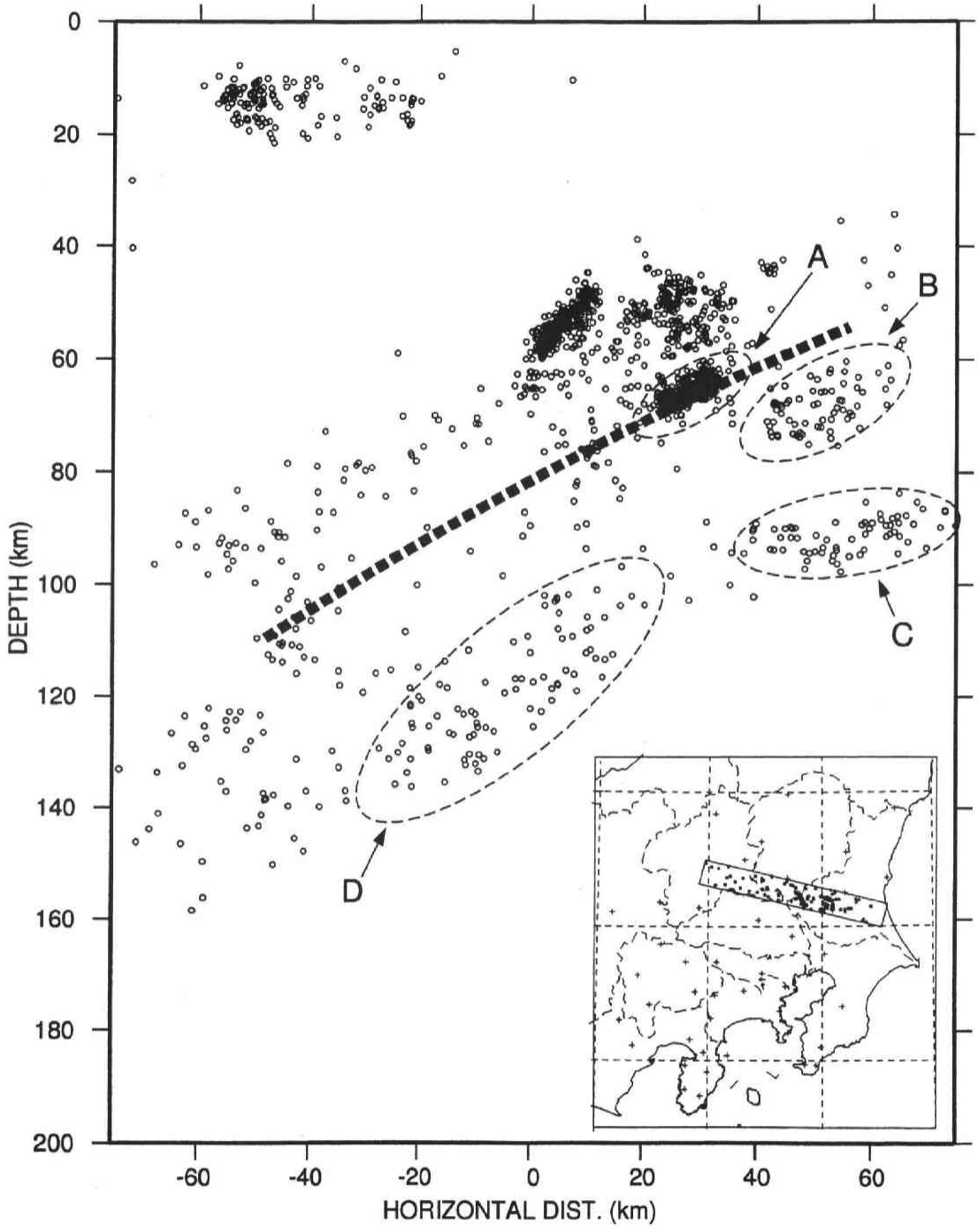

Figure 4.3: (a) Cross sectional view in C3 region.

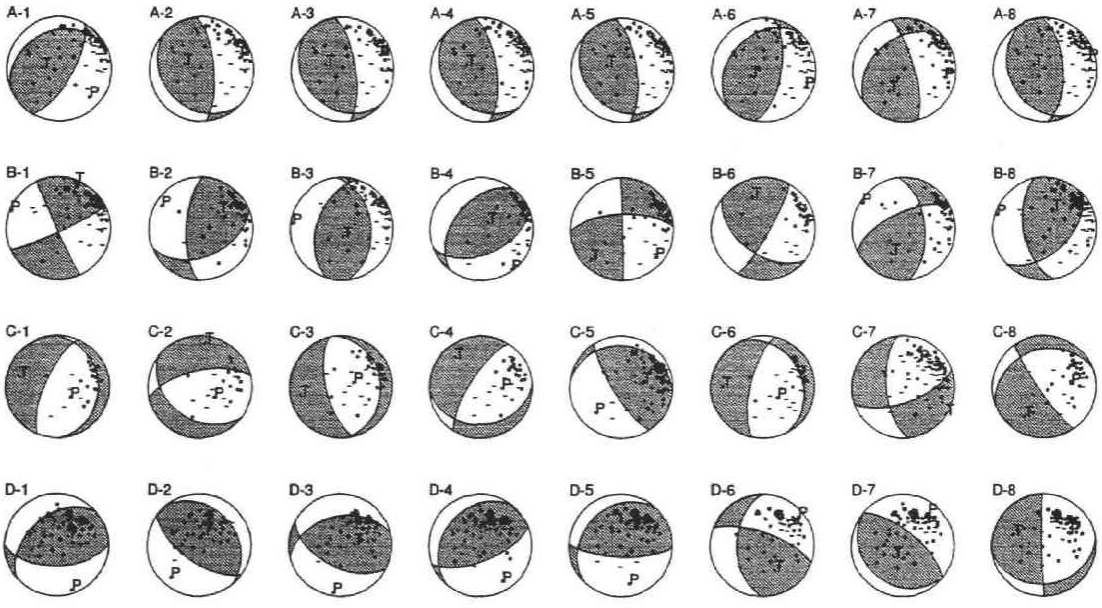

Figure 4.3: (b) Typical focal mechanisms in C3 region. Four rows represent the focal mechanisms of clusters A, B, C, and D, respectively. Focal parameters of the events are shown in Table 4.3.

No.	Origin Time (JST)						Latitude °N	Longitude °E	Depth km	Magnitude
A-1	1987	02	25	08	52	44.76	36.109	140.016	64.7	3.7
A-2	1988	06	02	08	09	37.37	36.149	140.091	64.2	3.7
A-3	1989	01	23	19	51	34.24	36.153	140.088	66.0	3.7
A-4	1989	05	09	02	51	11.77	36.148	140.097	65.3	4.7
A-5	1991	02	04	15	09	50.63	36.145	140.099	64.7	3.9
A-6	1991	07	15	07	55	39.08	36.131	139.998	70.4	4.0
A-7	1992	03	13	09	17	09.03	36.141	140.093	66.0	3.8
A-8	1993	09	10	19	43	41.79	36.155	140.101	68.9	4.4
B-1	1986	05	11	17	47	30.24	36.124	140.205	67.8	4.1
B-2	1988	09	25	22	48	32.71	36.133	140.259	66.9	3.4
B-3	1989	03	10	14	14	12.13	36.197	140.330	65.6	4.1
B-4	1990	10	04	21	17	09.35	36.168	140.332	61.7	2.8
B-5	1991	10	09	12	49	57.99	36.133	140.238	67.2	3.2
B-6	1993	02	01	05	05	45.06	36.106	140.231	70.7	2.8
B-7	1993	06	27	18	13	36.86	36.182	140.318	65.7	2.9
B-8	1993	11	01	21	22	29.21	36.109	140.208	73.3	4.8
C-1	1987	09	25	06	56	40.72	36.065	140.430	90.5	2.9
C-2	1988	01	25	04	36	49.34	36.068	140.423	89.3	2.9
C-3	1988	07	12	22	46	44.85	36.138	140.309	93.3	2.9
C-4	1988	09	26	02	23	09.89	36.148	140.439	89.3	3.1
C-5	1989	09	21	06	01	12.94	36.040	140.364	85.2	3.7
C-6	1989	11	16	23	15	33.34	36.057	140.382	88.9	2.9
C-7	1991	09	07	23	19	20.10	36.124	140.168	102.1	4.7
C-8	1992	03	30	00	12	45.82	36.179	140.306	94.0	3.0
D-1	1986	04	01	09	38	34.59	36.202	139.550	123.5	3.8
D-2	1987	01	21	19	24	03.49	36.292	139.515	133.6	3.3
D-3	1988	09	05	00	09	44.36	36.312	139.722	119.3	3.3
D-4	1989	01	12	01	02	36.93	36.281	139.474	131.2	3.6
D-5	1990	03	24	20	18	24.74	36.337	139.689	117.4	3.7
D-6	1990	10	29	08	57	25.74	36.188	139.730	109.1	3.4
D-7	1993	05	11	02	58	15.78	36.278	139.516	118.4	3.8
D-8	1994	01	08	08	04	50.23	36.320	139.669	125.4	3.6

Table 4.3: List of origin times, locations, and magnitudes of the earthquakes in C3 region shown in Figure 4.3(b).

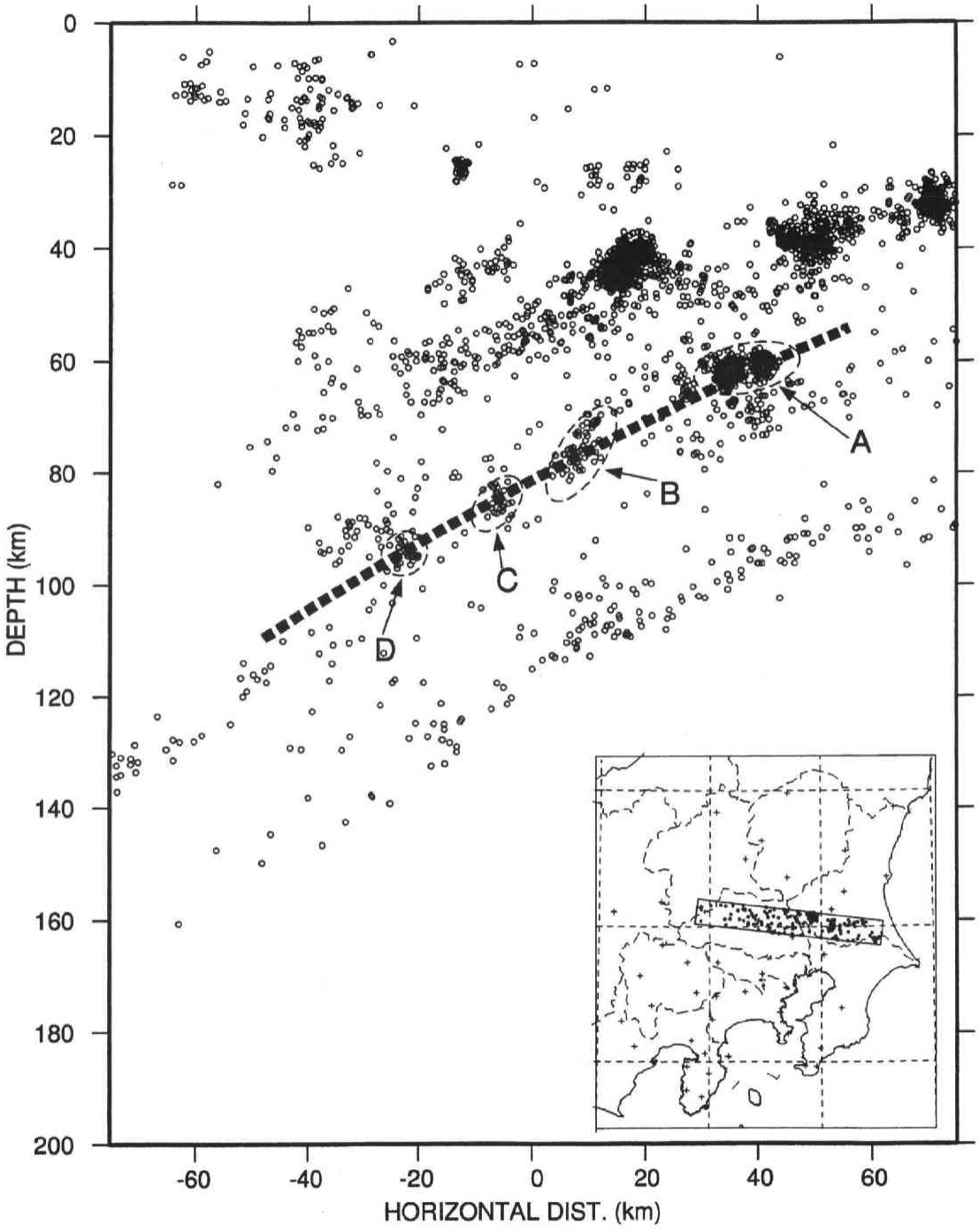

Figure 4.4: (a) Cross sectional view in C4 region.

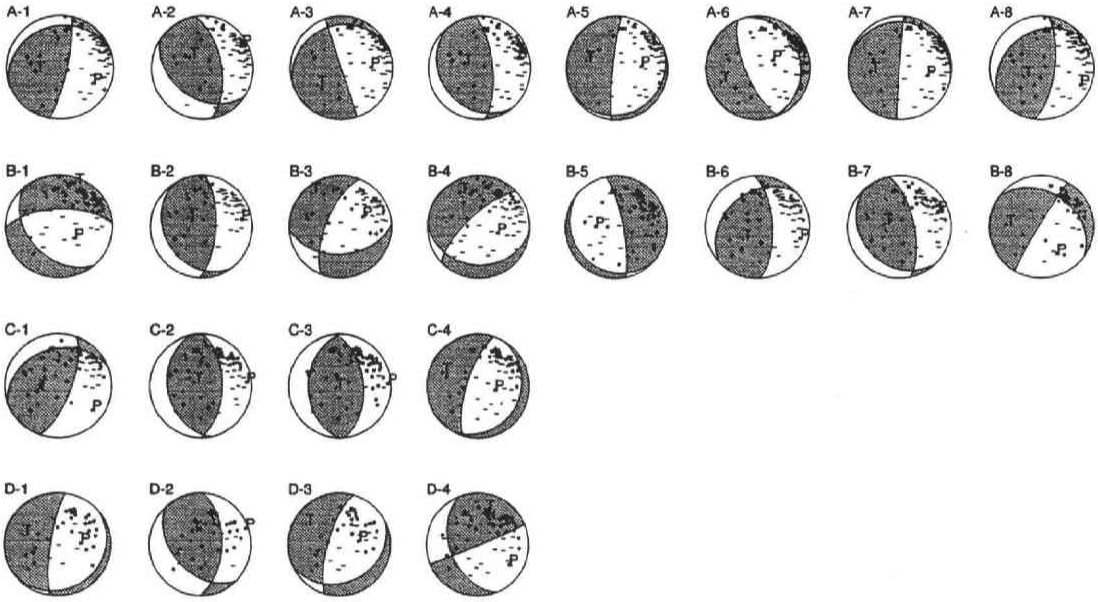

Figure 4.4: (b) Typical focal mechanisms in C4 region. Four rows represent the focal mechanisms of clusters A, B, C, and D, respectively. Focal parameters of the events are shown in Table 4.4.

No.	Origin Time (JST)						Latitude °N	Longitude °E	Depth km	Magnitude
A-1	1987	09	03	21	22	06.36	35.905	140.131	63.5	4.4
A-2	1988	07	15	03	17	47.51	35.905	140.146	66.2	4.4
A-3	1989	04	23	14	13	54.61	36.006	140.171	62.4	4.3
A-4	1989	11	25	16	02	50.44	35.969	140.090	67.5	4.7
A-5	1990	07	04	03	32	15.19	36.033	140.112	67.0	5.1
A-6	1991	02	11	17	07	47.79	35.983	140.063	67.5	4.6
A-7	1991	11	29	00	27	46.89	35.972	140.169	62.9	4.4
A-8	1994	02	16	12	38	41.83	35.968	140.079	69.8	4.6
B-1	1986	08	23	13	13	59.24	36.091	139.811	79.5	4.1
B-2	1987	02	22	05	39	02.48	36.053	139.771	80.1	4.5
B-3	1987	03	10	14	49	01.62	35.994	139.748	76.8	3.7
B-4	1987	06	04	07	56	18.44	35.948	139.736	80.5	4.4
B-5	1989	07	10	01	45	32.90	35.938	139.817	77.9	3.3
B-6	1990	10	26	02	29	21.55	36.048	139.784	81.3	4.1
B-7	1993	09	09	10	50	18.63	36.040	139.778	79.4	3.8
B-8	1993	11	17	07	26	33.26	36.097	139.798	76.7	3.0
C-1	1986	11	28	01	10	33.42	36.127	139.660	86.4	3.5
C-2	1990	08	14	04	28	20.22	36.113	139.674	89.9	3.6
C-3	1993	02	13	15	31	59.16	36.119	139.665	86.6	3.5
C-4	1993	07	27	09	51	23.20	36.096	139.679	87.5	3.4
D-1	1986	04	07	06	54	32.66	36.033	139.465	94.7	3.1
D-2	1987	06	16	21	20	47.26	36.011	139.467	96.3	2.9
D-3	1988	01	10	04	29	54.02	35.977	139.441	94.0	3.0
D-4	1989	06	26	22	56	56.43	36.022	139.423	97.4	3.3

Table 4.4: List of origin times, locations, and magnitudes of the earthquakes in C4 region shown in Figure 4.4(b).

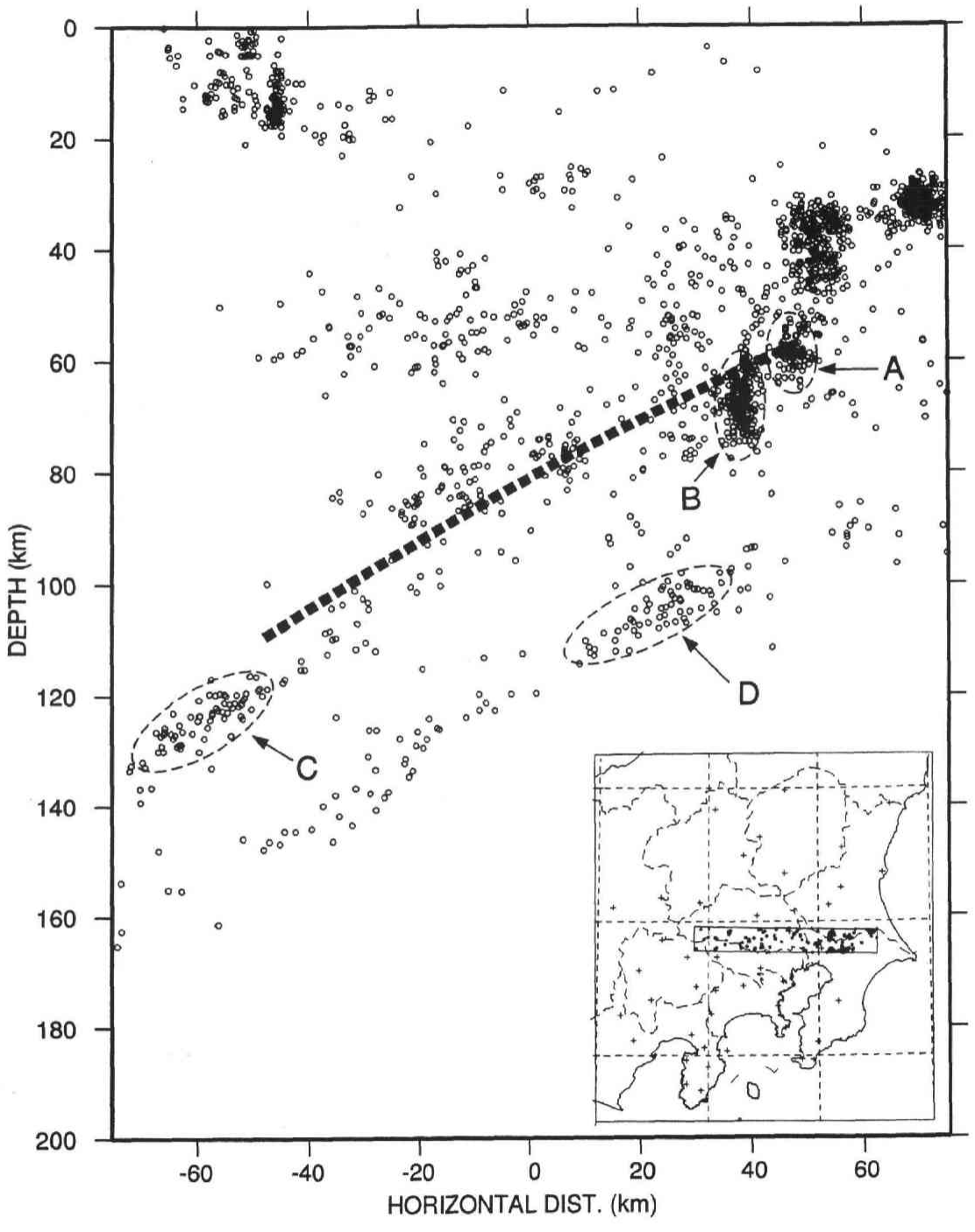

Figure 4.5: (a) Cross sectional view in C5 region.

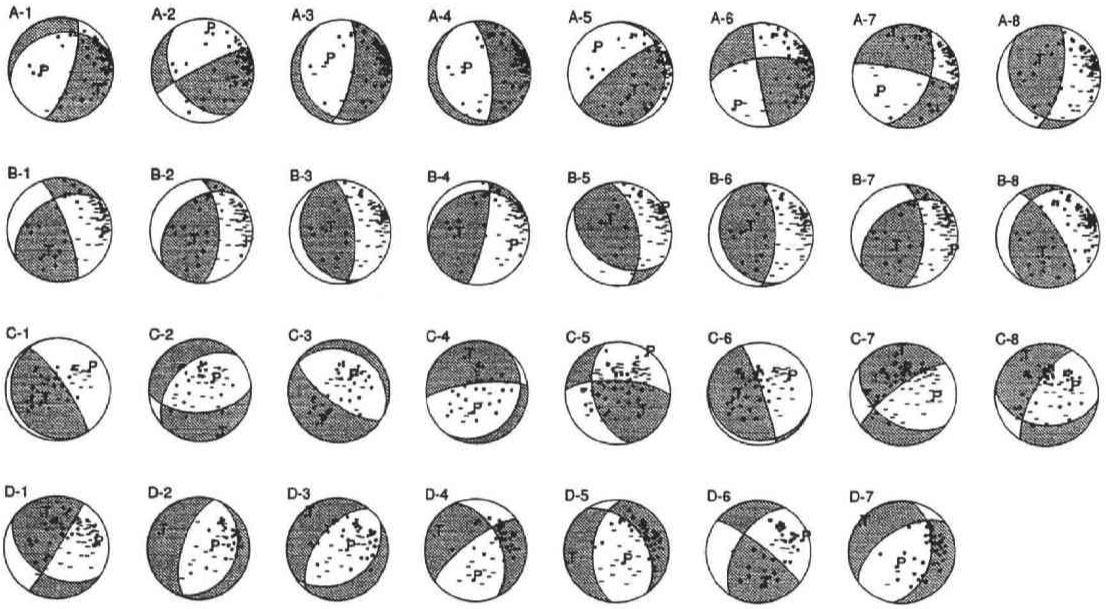

Figure 4.5: (b) Typical focal mechanisms in C5 region. Four rows represent the focal mechanisms of clusters A, B, C, and D, respectively. Focal parameters of the events are shown in Table 4.5.

No.	Origin Time (JST)						Latitude °N	Longitude °E	Depth km	Magnitude
A-1	1986	07	03	13	13	08.61	35.765	140.196	61.0	3.2
A-2	1987	05	23	18	26	46.13	35.814	140.210	58.6	3.3
A-3	1987	05	29	18	29	40.46	35.797	140.209	58.4	3.7
A-4	1987	05	29	21	38	24.25	35.798	140.216	58.7	3.4
A-5	1987	06	21	10	39	10.78	35.782	140.226	57.3	3.4
A-6	1987	07	18	21	03	38.22	35.882	140.238	58.6	3.9
A-7	1990	09	02	04	49	39.20	35.836	140.215	55.9	4.1
A-8	1993	05	10	04	58	52.26	35.770	140.238	64.9	3.9
B-1	1987	01	14	04	56	27.15	35.768	140.108	67.5	4.3
B-2	1987	04	17	16	33	41.11	35.771	140.112	70.5	5.0
B-3	1987	07	09	20	44	42.37	35.776	140.137	68.7	4.3
B-4	1987	09	03	21	22	06.36	35.905	140.131	63.5	4.4
B-5	1988	07	15	03	17	47.51	35.905	140.146	66.2	4.4
B-6	1989	03	26	15	47	46.17	35.764	140.110	71.1	4.4
B-7	1991	09	29	13	13	59.89	35.773	140.114	70.3	4.9
B-8	1991	09	29	14	00	01.77	35.767	140.118	69.1	4.5
C-1	1986	12	14	22	10	37.73	35.820	138.932	132.9	2.9
C-2	1988	10	08	03	04	03.27	35.947	139.003	129.4	3.0
C-3	1988	11	10	05	51	45.53	35.886	139.000	128.8	3.1
C-4	1989	09	16	16	12	39.64	35.820	139.038	120.7	2.9
C-5	1990	04	15	07	51	16.96	35.867	138.958	130.0	4.2
C-6	1991	08	14	20	38	29.78	35.942	138.929	131.9	3.1
C-7	1993	03	14	19	30	32.16	35.883	139.063	116.9	3.9
C-8	1994	03	20	06	13	01.44	35.803	139.071	122.1	3.0
D-1	1986	07	27	15	13	49.76	35.898	139.833	112.8	4.2
D-2	1986	08	23	06	01	07.78	35.834	139.934	102.8	2.9
D-3	1987	08	15	20	37	02.63	35.889	139.834	111.7	3.0
D-4	1988	08	10	10	32	46.25	35.830	139.981	101.5	3.0
D-5	1989	03	20	12	11	14.26	35.913	140.105	97.5	3.5
D-6	1989	10	18	08	47	08.62	35.836	139.908	106.8	3.1
D-7	1993	05	11	11	21	41.19	35.775	140.099	98.2	3.1

Table 4.5: List of origin times, locations, and magnitudes of the earthquakes in C5 region shown in Figure 4.5(b).

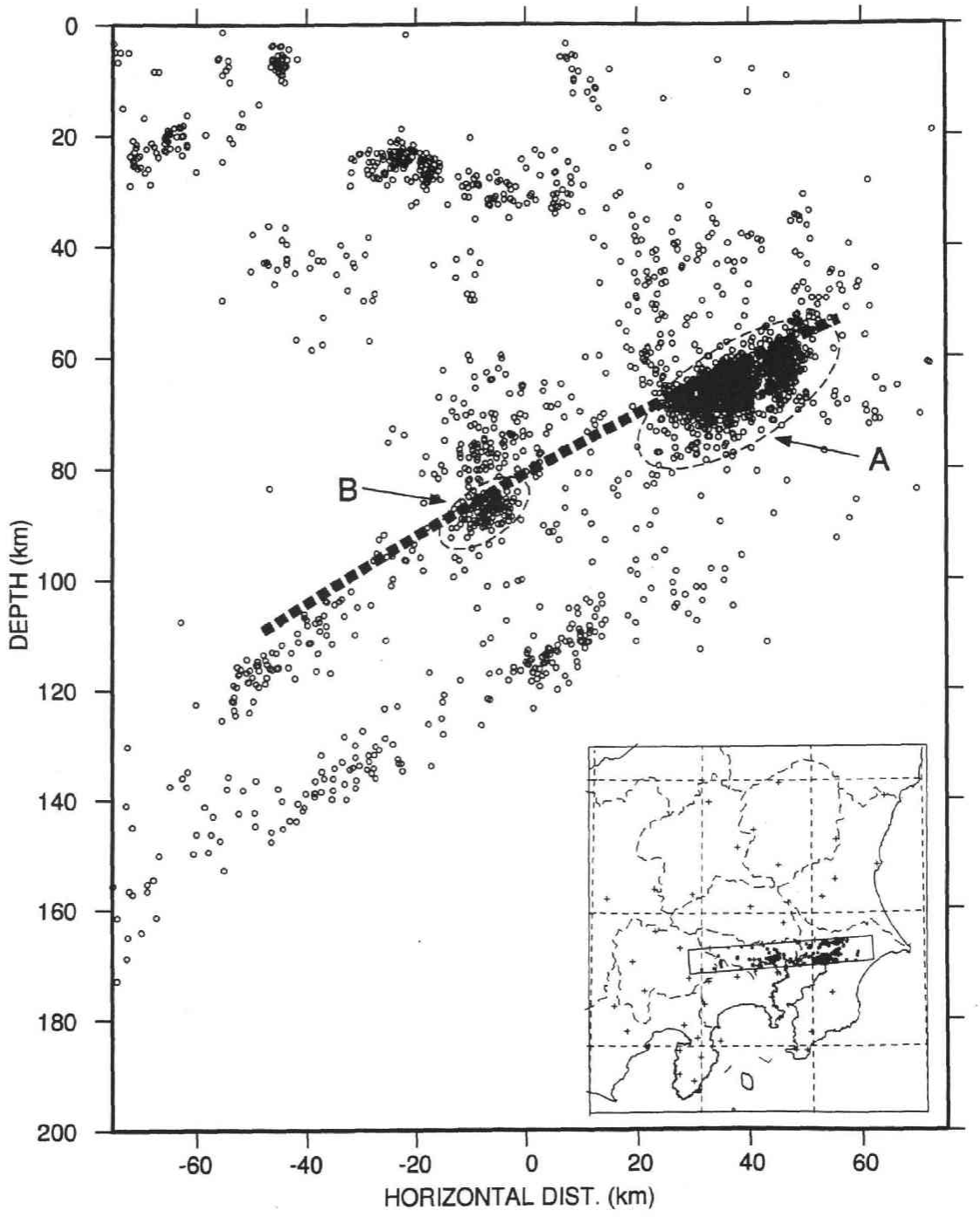

Figure 4.6: (a) Cross sectional view in C6 region.

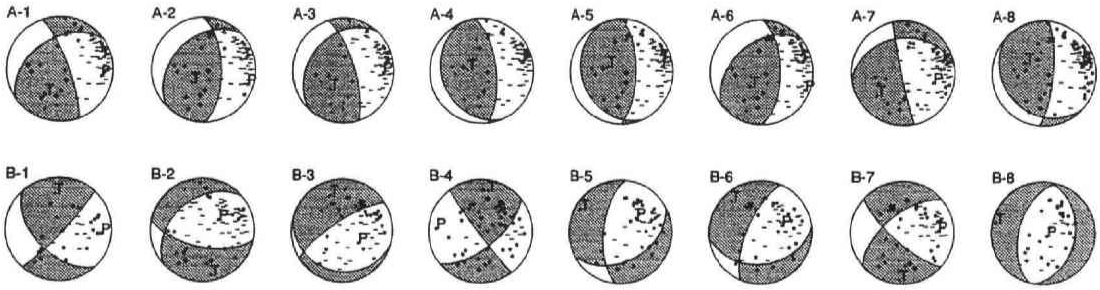

Figure 4.6: (b) Typical focal mechanisms in C6 region. Upper and lower rows show the typical focal mechanisms of cluster A and B, respectively. Focal parameters of the events are shown in Table 4.6.

No.	Origin Time (JST)						Latitude °N	Longitude °E	Depth km	Magnitude
A-1	1987	01	14	04	56	27.15	35.768	140.108	67.5	4.3
A-2	1987	04	17	16	33	41.11	35.771	140.112	70.5	5.0
A-3	1987	06	16	00	30	54.13	35.624	140.202	69.8	4.7
A-4	1987	07	09	20	44	42.37	35.776	140.137	68.7	4.3
A-5	1989	03	26	15	47	46.17	35.764	140.110	71.1	4.4
A-6	1991	09	29	13	13	59.89	35.773	140.114	70.3	4.9
A-7	1993	07	23	16	33	57.25	35.619	140.113	76.1	4.3
A-8	1994	07	20	13	31	57.44	35.770	140.120	72.2	4.3
B-1	1986	12	23	01	02	08.23	35.617	139.567	92.3	2.7
B-2	1988	04	12	23	59	20.60	35.662	139.622	89.7	3.9
B-3	1988	07	22	19	04	18.45	35.665	139.609	90.3	3.2
B-4	1989	02	18	19	11	21.52	35.650	139.646	91.1	3.3
B-5	1989	09	29	15	47	34.96	35.756	139.587	92.3	2.9
B-6	1990	02	04	11	08	44.59	35.754	139.555	90.6	3.2
B-7	1990	06	05	15	54	17.01	35.657	139.582	89.9	3.2
B-8	1991	06	04	10	27	37.85	35.750	139.658	93.0	2.9

Table 4.6: List of origin times, locations, and magnitudes of the earthquakes in C6 region shown in Figure 4.6(b).

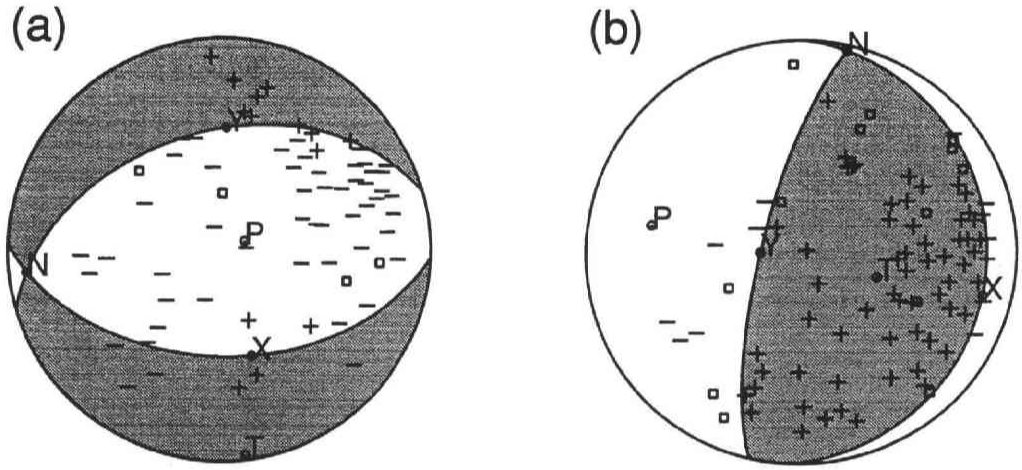

Figure 4.7: Focal mechanisms of two moderate earthquakes. (a) Earthquake in the eastern Tokyo region on March 18, 1988. (b) Earthquake in the southern Tokyo Bay region on February 2, 1992.

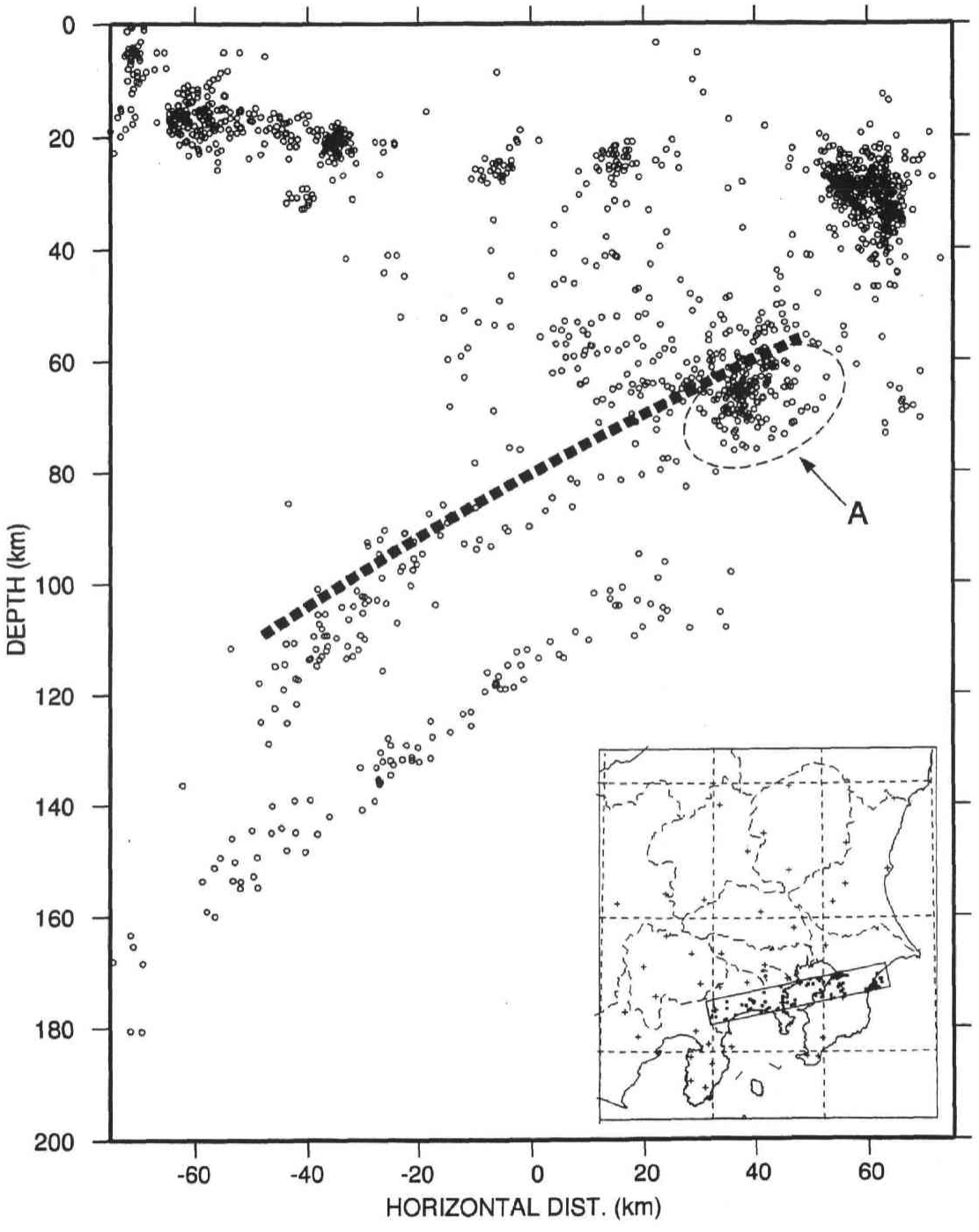

Figure 4.8: (a) Cross sectional view in C7 region.

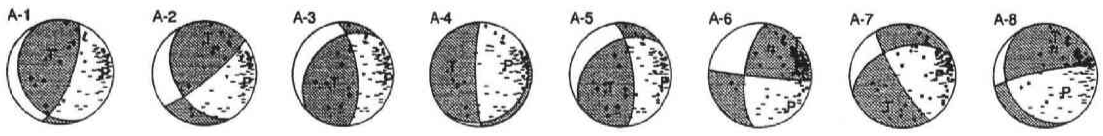

Figure 4.8: (b) Typical focal mechanisms in C7 region. They are typical focal mechanisms of cluster A. Focal parameters of the events are shown in Table 4.7.

No.	Origin Time (JST)						Latitude °N	Longitude °E	Depth km	Magnitude
A-1	1988	04	01	07	22	43.08	35.566	140.169	70.4	4.6
A-2	1988	12	16	02	50	50.24	35.489	140.160	73.0	4.2
A-3	1989	09	05	13	07	05.04	35.552	140.147	72.6	4.8
A-4	1989	09	16	17	03	06.46	35.585	140.160	75.7	4.5
A-5	1991	03	15	09	01	36.55	35.541	140.126	75.0	4.6
A-6	1992	10	23	13	11	24.71	35.561	140.178	70.8	4.3
A-7	1994	07	13	00	51	10.63	35.560	140.159	68.7	4.0
A-8	1994	09	04	10	19	10.93	35.582	140.137	76.2	4.4

Table 4.7: List of origin times, locations, and magnitudes of the earthquakes in C7 region shown in Figure 4.8(b).

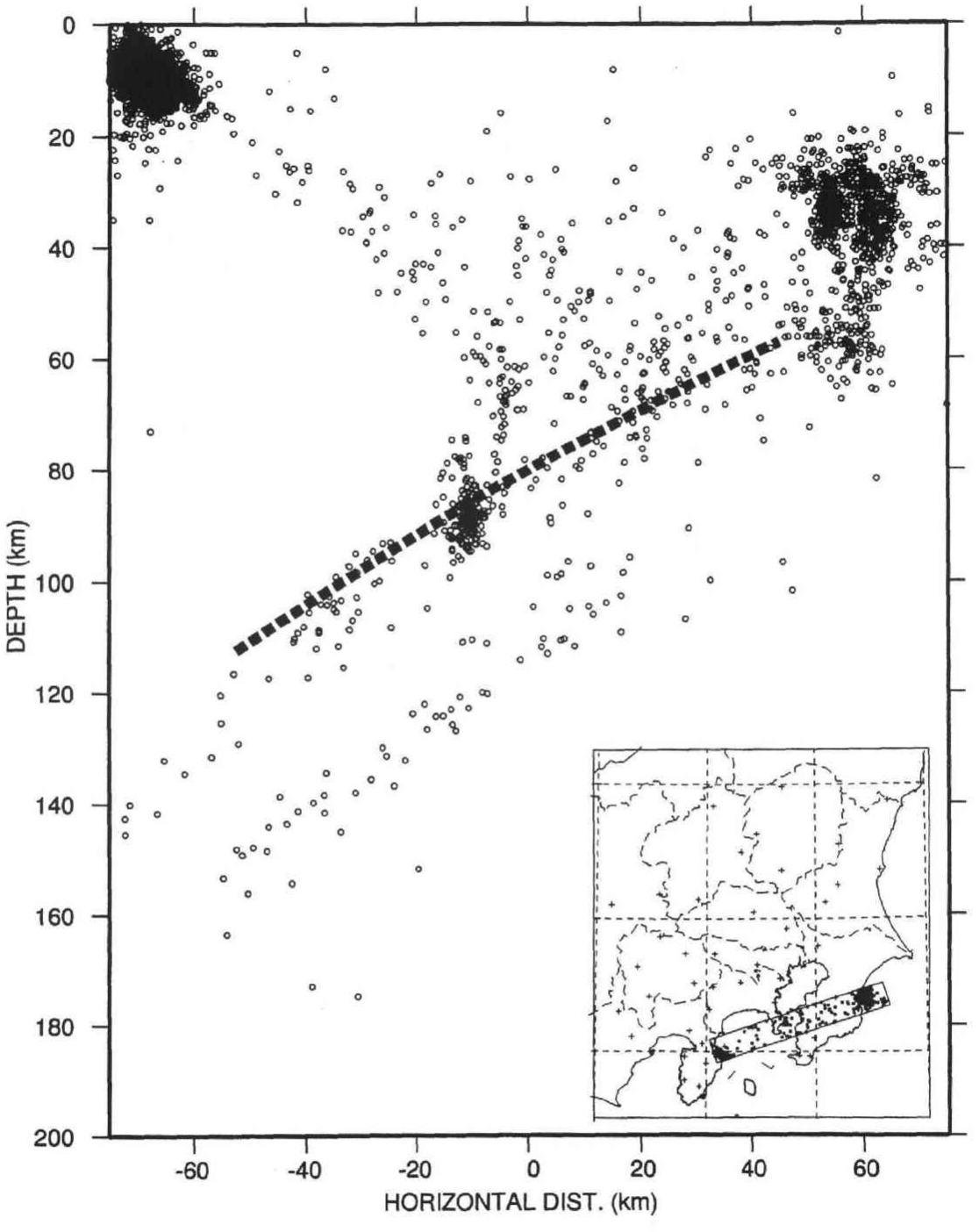

Figure 4.9: Cross sectional view in C8 region.

Chapter 5

Conclusion

In this study, a fine structure of the subducting Philippine Sea and Pacific plates beneath the Kanto district is revealed from a high resolution seismic tomography analysis and a travel time analysis of SP converted waves.

In chapter 2, a high resolution seismic tomography technique is applied to the regional seismic data obtained by a dense seismic network in the Kanto area operated by NIED, in order to delineate the slowness perturbation of the target area. The dataset is composed of 40,763 high quality first P-wave arrival times from 3,038 local earthquakes recorded at 41 seismic stations. The target area is divided into 47×57×18 blocks measuring 4 km per side and 4 - 10 km thicknesses in depth. A tomographic inversion method developed by Lees and Crosson (1989) is applied to obtain slowness perturbations in the target area. Since hypocenters are not relocated in the inversion procedure, the method of Hurukawa and Ohmi (1993) is used to get accurately determined initial hypocenters.

The result of the inversion shows generally small estimation errors, less than 2.4 % variation in all regions. Subducted oceanic crusts that attaches at the top of both the Philippine Sea and the Pacific plates are detected as thin low velocity layers. Their thicknesses are 5 - 10 km for both plates and the velocities are about 12 % and 3 % lower

than the surrounding mantle for the Philippine Sea and the Pacific plates, respectively. Relatively high velocity thick layers, which are the mantle portions of the subducted slabs, underlie the low velocity layers. The low velocity layers are detectable down to a depth of $\sim$ 60 km for the Philippine Sea plate and $\sim$ 90 km for the Pacific plate.

Low-angle thrust fault type earthquakes, such as the southwestern Ibaraki swarm that are interpreted as interplate earthquakes between the Eurasia and the Philippine Sea plates, occur in the low velocity layer attached on the Philippine Sea plate. Similar fault type earthquakes occur in the low velocity layer on the Pacific plate. Examples of them are the swarm activity of the Tsukuba - Chiba seismic belt and the southern Ibaraki earthquake of 1983 that are interplate earthquakes between the Philippine Sea and the Pacific plate.

On the other hand, events regarded as intraplate earthquakes are located in the high velocity portions. Examples of these events are the Ibaraki-Chiba border earthquake of 1985, which is interpreted as an intra Pacific plate earthquake, and the east off Chiba earthquake of 1987, which is an intra Philippine Sea plate event.

The low velocity layer on the top of the Philippine Sea plate is recognized down to a depth of 65 - 70 km in some regions in the northwest Kanto area. The gabbro-eclogite transition may not occur at this depth, though it is expected in this depth range from previous studies.

Low velocity bodies are detected in the mantle wedge portion beneath active volcanoes in the northwest Kanto area, which are probably associated with the deep structure of the volcanoes. The Philippine Sea plate has a complicated shape in the southern Kanto area, which is possibly caused by the buoyancy of the young plate.

In chapter 3, we studied a detailed structure of the Pacific plate

by using conspicuous SP converted waves that are generated near the upper boundary of the Pacific plate. These SP waves are observed for earthquakes occurring in the lower plane of the double seismic zone of the subducted Pacific plate. They are identified to be S-to-P converted waves (SP waves) near the upper plate boundary, because the travel time difference between the first P-wave arrival and the SP phase is in the range from 3 to 6 s and no significant correlation is found between the travel time difference and the focal depth or the epicentral distance. The location of the conversion interface is estimated by inverting the observed T_{SP-P} times. We assumed that the interface is expressed by a power series. The interface is located above the upper seismic plane of the double seismic zone. It generally coincides with the results of previous studies on the upper boundary of the subducting Pacific slab with slight differences in the northern Kanto area. Comparing the obtained result with that of the three dimensional tomographic inversion, we showed that the conversion interface is located in the low velocity layer that attaches at the top of the Pacific plate.

In chapter 4, we compare the results of the tomographic inversion and the SP converted wave analysis with hypocenter distribution and focal mechanisms and discuss the relation between the low velocity layers at the top of the Pacific plate and the conversion interface. We made several vertical cross sections showing the SP conversion interface together with hypocenter distributions in the target area for the comparison.

In northern Kanto, most seaward area forms 'triple seismic zone', where the double seismic zone extends seaward beyond the aseismic front and overlaps with the main thrust zone. In this region, the location of the conversion interface of SP waves coincides with that of

the main thrust zone which is about 10 km shallower than the upper plane of the double seismic zone.

In the northern part of central Kanto, low-angle thrust fault type earthquakes occur at deeper depths than in the northern Kanto region. There is no clear separation between the conversion interface and the upper seismic plane. The conversion interface is located at the bottom of the earthquake cluster zone with low-angle thrust faulting.

In the southern part of central Kanto and southern Kanto, the separation between the upper seismic plane and the conversion interface is not clear. The conversion interface is located at the the upper boundary of the earthquake cluster of thrust fault type events.

Since the converted wave is generated only at a velocity boundary, the conversion interface should be located either at the shallower boundary or deeper boundary of the low velocity layer. Previous studies conducted in the Tohoku district attributed the conversion interface to the shallower boundary of the low velocity layer. On the other hand, in the central Kanto district, the conversion interface seems to be located at the deeper boundary of the low velocity layer. This shows that the sharp velocity jump at the Moho discontinuity, which is the deeper boundary of the subducting Pacific plate, still remains in this depth range in the Kanto district. The thermal condition around the subducting Pacific plate in the Kanto district may be different from that in the Tohoku district because of the existence of the subducting Philippine Sea plate above the Pacific plate. This may cause the difference from Tohoku and both of the shallower and deeper boundaries of the crust that attaches on the top of the Pacific plate may act as conversion interfaces. The observed travel times of the SP converted waves show that the conversion interface derived in this study corresponds to the Moho discontinuity of the subducing Pacific plate in

the central Kanto area. The distribution of low-angle thrust fault type earthquakes indicates that these earthquakes occur in the whole crust portion of the subducting slab, between the Moho discontinuity and the upper boundary of the Pacific plate.

References

Ashiya, K., Asano, S., Yoshii, T., Ishida, M., and Nishiki, T., 1987. Simultaneous determination of the three-dimensional crustal structure and hypocenters beneath the Kanto-Tokai district, Japan. *Tectonophys*, 140:13-27.

Červený, V. and Pšenčík, I., 1984. SEIS83 - Numerical modeling of seismic wave fields in 2-D laterally varying layered structures by the ray method, in Documentation of Earthquake Algorithms, E. R. Engdahl (ed.), World Data Center (A), Boulder.

Comte, D., Roecker, S. W., and Suárez, G., 1994. Velocity structure in northern Chile: evidence of subducted oceanic crust in the Nazca plate. *Geophys. J. Int.*, 117:625-639.

Crosson, R. S., 1976. Crustal structure modeling of earthquake data. 1. Simultaneous least squares estimation of hypocenter and velocity parameters. *J. Geophys. Res.*, 81:3036-3046.

Efron, B., 1982. The jackknife, the bootstrap and other resampling plans. *Soc. Ind. Appl. Math.*, Philadelphia, PA, 92 pp.

Fukao, Y., Hori, S., and Ukawa, M., 1983. A seismological constraint on the depth of basalt-eclogite transition in a subducting oceanic crust. *Nature*, 303:413-415.

Furumura, T. and Moriya, T., 1990. Three-dimensional Q structure in around the Hidaka mountains, Hokkaido, Japan. *J. Seismol. Soc. Jpn., Ser. 2*, 43:121-132. (In Japanese with English abstract).

Geological Survey of Japan, 1992. *Geological Atlas of Japan (second edition)*, Asakura Publishing, Tokyo, 26 pp.

Goto, K., and Hamaguchi, H., 1979. A double-planed structure of the intermediate seismic zone - Thermal stress within the descending lithospheric slab (2). *Programme Abstr., Seismol. Soc. Jpn.*, 1:20 (In Japanese).

Goto, K., and Hamaguchi, H., 1980. Distribution of thermal stress within the descending lithospheric slab. *Programme Abstr., Seismol. Soc. Jpn.*, 2:48 (In Japanese).

Hamada, K., Ohtake, M., Okada, Y., Matsumura, S., Yamamizu, F., Sato, H., Imoto, M., Tatsukawa, M., Ohkubo, T., Yamamoto, E., Ishida, M., Kasahara, K., Katsuyama Y., and Takahashi, H., 1982. Kanto-Tokai Observation network of crustal activities - National Research Center for Disaster Prevention. *J. Seismol. Soc. Jpn.*, 35:401-426 (In Japanese with English abstract).

Hasemi, A. H., Ishii, H. and Takagi, A., 1984. Fine structure beneath the Tohoku district, northeastern Japan arc, as derived by an inversion of P-wave arrival times from local earthquakes. *Tectonophys.*, 101:245-265.

Hasegawa, A., Umino, N., and Takagi, A., 1978a. Double-planed structure of the deep seismic zone in the Northeastern Japan Arc. *Tectonophys.*, 47:43-58.

Hasegawa, A., Umino, N., and Takagi, A., 1978b. Double-planed deep seismic zone and upper-mantle structure in the Northeastern Japan Arc. *Geophys. J. R. astr. Soc.*, 54:281-296.

Hashida, T. and Shimazaki, K., 1985. Seismic tomography: 3-D image of upper mantle attenuation beneath the Kanto district, Japan. *Earth Planet. Sci. Lett.*, 75:403-409.

Hashimoto, M., 1981. Three-dimensional stress distribution in southwestern Japan as expected from the configuration of the subducting Philippine Sea plate (Part 2). *J. Seismol. Soc. Jpn.*, 34:197-211.

Hino, R., Nishizawa, A., Horiuchi, S., Hasegawa, A., Kanazawa, T., Iwasaki, T., Shiobara, H., and Shimamura, H., 1992. Crustal structure of the Izu-Bonin arc deduced from seismic profiling using ocean bottom seismographs. *Abstracts, 1992 Japan Earth and Planetary Science Joint Meeting*, 321 (in Japanese).

Hirahara, K., 1981. Three-dimensional seismic structure beneath southwest Japan: the subducting Philippine Sea plate. *Tectonophys.*, 79:1-41.

Hirahara, K., Ikami, A., Ishida, M., and Mikumo, T., 1989. Three-dimensional P-wave velocity structure beneath central Japan: low-velocity bodies in the wedge portion of the upper mantle above high-velocity subducting plates. *Tectonophys.*, 163:63-73.

Hirahara, K. and Hasemi, A., 1993. Tomography of subduction zones using local and regional earthquakes and teleseisms. In: Iyer, H. M. and Hirahara, K. (Editors), *Seismic Tomography. Theory and Practice*, Chapman and Hall, pp. 519-562.

Hori, S., 1986. The earthquake mechanism of the M 6.1 event occurred near the border of Chiba and Ibaraki prefectures, central Japan, on October 4, 1985 and its tectonic implication. *J. Seismol. Soc. Jpn., Ser. 2*, 39:457-468. (In Japanese with English abstract).

Hori, S., 1988. Later phases in the seismogram of intermediate earthquake observed in the Kanto district. *Programme Abstr., Seismol. Soc. Jpn.*, 2:86 (in Japanese).

Hori, S., 1990. Seismic waves guided by untransformed oceanic crust subducting into the mantle: the case of the Kanto district, central Japan. *Tectonophys.*, 176:355-376.

Hori, S., Inoue, H., Fukao, Y., and Ukawa, M., 1985. Seismic detection of the untransformed 'basaltic' oceanic crust subducting into the mantle. *Geophys. J. R. astr. Soc.*, 83:169-197.

Horie, A. and Aki, K., 1982. Three-dimensional velocity structure beneath the Kanto district, Japan. *J. Phys. Earth*, 30:255-281.

Horiuchi, S., Ishii, H., and Takagi, A., 1982. Two-dimensional depth structure of the crust beneath the Tohoku district, the northeastern Japan arc. part 1. Method and conrad discontinuity. *J. Phys. Earth*, 30:47-69.

Humphreys, E. and Clayton, R. W., 1988. Adaptation of back projection tomography to seismic travel time problems., *J. Geophys. Res.*, 93, 1073-1085.

Hurukawa, N., 1983. Pn velocity and Moho-offset at the west of Lake Biwa in the Kinki district, Japan. *J. Phys. Earth*, 31:33-46.

Hurukawa, N. and Hirahara, K., 1980. Structure of the Philippine Sea plate subducting beneath the Kii peninsula. *J. Seismol. Soc. Jpn., Ser. 2*, 33:303-316. (In Japanese with English abstract).

Hurukawa, N. and Imoto, M., 1990. Fine structure of an underground boundary between the Philippine Sea and Pacific plates beneath the Kanto district, Japan. *J. Seismol. Soc. Jpn., Ser. 2*, 43:413-429. (In Japanese with English abstract).

Hurukawa, N. and Imoto, M., 1992. Subducting oceanic crusts of the Philippine Sea and Pacific plates and weak-zone-normal compression in the Kanto district, Japan. *Geophys. J. Int.*, 109:639-652.

Hurukawa, N. and Imoto, M., 1993. A non double-couple earthquake in a subducting oceanic crust of the Philippine Sea plate. *J. Phys. Earth*, 41:257-269.

Hurukawa, N. and Ohmi, S., 1993. A hypocenter-determination method using station corrections as a function of hypocenter coordinates. *J. Seismol. Soc. Jpn., Ser. 2*, 46:285-295. (In Japanese with English abstract).

Iidaka, T., Nakamura, I., and Mizoue, M., 1989. The upper boundary of the Pacific plate beneath the Kanto region estimated from PS converted waves, *Bull. Earthq. Res. Inst. Univ. Tokyo*, 64:37-50

Ishibashi, K., 1987. Geometry of the Philippine Sea plate subducted at the northern Sagami trough - Izu region. *Programme Abstr., Seismol. Soc. Jpn.*, 1:96 (In

Japanese).

Ishibashi, K., 1988a. 'Kanagawa-ken-seibu earthquake' and earthquake prediction (1). *Science Journal Kagaku*, 58:537-547 (In Japanese).

Ishibashi, K., 1988b. 'Kanagawa-ken-seibu earthquake' and earthquake prediction (2). *Science Journal Kagaku*, 58:771-780 (In Japanese).

Ishida, M., 1984. The spatial distribution of earthquake hypocenters and the three-dimensional velocity structure in the Kanto-Tokai district, Japan. *J. Phys. Earth*, 32:399-422.

Ishida, M., 1992. Geometry and relative motion of the Philippine Sea plate and Pacific plate beneath the Kanto-Tokai district, Japan. *J. Geophys. Res.*, 97:489-513.

Ishida, M. and Hasemi, A., 1984. The three-dimensional P-wave velocity structure in the Kanto-Tokai district, Japan. *Res. Notes Natl. Res. Cent. Disaster Prev.*, 58:1-11 (In Japanese), National Research Center for Disaster Prevention, Tsukuba, Japan.

Ishida, M., 1986. The configuration of the Philippine Sea and the Pacific plates as estimated from the high-resolution microearthquake hypocenters in the Kanto-Tokai district, Japan. *Rep. Natl. Res. Cent. Disaster Prev.*, 36:1-19 (In Japanese with English abstract).

Ishida, M. and Hasemi, A. H., 1988. Three-dimensional fine velocity structure and hypocentral distribution of earthquakes beneath the Kanto-Tokai district, Japan. *J. Geophys. Res.*, 93:2076-2094.

Iwasaki, T., Shiobara, H., Nishizawa, A., Kanazawa, T., Suyehiro, K., Hirata, N., Urabe, T., and Shimamura, H., 1989. A detailed subduction structure in the Kuril trench deduced from ocean bottom seismographic refraction studies. *Tectonophys.*, 165:315-336.

Iwasaki, T., Hirata, N., Kanazawa, T., Melles, J., Suyehiro, K., Urabe, T., Möller, L., Makris, J., and Shimamura, H., 1990. Crustal and upper mantle structure

in the Ryukyu Island arc deduced from deep seismic sounding. *Geophys. J. Int.*, 102:631-651.

Kasahara, K., 1985. Patterns of crustal activity associated with the convergence of three plates in the Kanto-Tokai area, central Japan. *Rep. Natl. Res. Cent. Disaster Prev.*, 35:33-137 (In Japanese with English abstract), National Research Center for Disaster Prevention, Tsukuba, Japan.

Kawakatsu, H. and Seno, T., 1983. Triple seismic zone and the regional variation of seismicity along the northern Honshu arc. *J. Geophys. Res.*, 88:4215-4230.

Kono, Y. and Furuse, N., 1989. *Gravity anomaly map in and around the Japanese islands*, University of Tokyo Press, Tokyo, Japan, 76 pp.

Kudo, T. and Kono, Y., 1993. Shaded relief gravity anomaly maps over the Japanese islands. (1) Making the shaded relief maps. *J. Seismol. Soc. Jpn., Ser. 2*, 46:237-243. (In Japanese with English abstract).

Kudo, T. and Kono, Y., 1994. Shaded relief gravity anomaly maps over the Japanese islands. (2) Comparison of the shaded relief maps with geological, geophysical features in and around the Fossa Magna, central Japan. *J. Seismol. Soc. Jpn., Ser. 2*, 46:371-379. (In Japanese with English abstract).

Lees, J. M. and Crosson, R. S., 1989. Tomographic inversion for three-dimensional velocity structure at Mount St. Helens using earthquake data. *J. Geophys. Res.*, 94, 5716-5728.

Lees, J. M. and Ukawa, M., 1992. The south Fossa Magna, Japan, revealed by high-resolution P- and S-wave travel time tomography. *Tectonophys.*, 207:377-396.

Maki, T., 1984. Focal mechanisms and spatial distribution of intermediate-depth earthquakes beneath the Kanto district and vicinity with relation to the double seismic planes. *Bull. Earthq. Res. Inst.*, 59:1-51.

Matsumoto, S. and Hasegawa, A., 1989. Two-dimensional coda Q structure beneath Tohoku, NE Japan. *Geophys. J. Int.*, 99:101-108.

Matsuzawa, T., Umino, N., Hasegawa, A. and Takagi, A., 1986. Upper mantle velocity structure estimated from PS-converted wave beneath the north-eastern Japan arc. *Geophys. J. R. astr. Soc*, 86:767-787.

Matsuzawa, T., Kono, T., Hasegawa, A. and Takagi, A., 1990. Subducting plate boundary beneath the northeastern Japan arc estimated from SP converted waves. *Tectonophys.*, 181:123-133.

McKenzie, D. P. and Morgan, W. J., 1969. Evolution of triple junctions. *Nature*, 224:125-133.

Mikumo, T., 1966. A study on crustal structure in Japan by the use of seismic and gravity data, *Bull. Earthq. Res. Inst.*, 44:965-1007.

Miyamachi, H. and Moriya, T., 1984. Velocity structure beneath the Hidaka mountains in Hokkaido, Japan. *J. Phys. Earth*, 32:13-42.

Miyamachi, H., Kasahara, M., Suzuki, S., Tanaka, K., and Hasegawa, A., 1994. Seismic velocity structure in the crust and upper mantle beneath northern Japan. *J. Phys. Earth*, 42:269-301.

Nakanishi, I., 1980. Precursors to ScS phases and dipping interface in the upper mantle beneath southwestern Japan. *Tectonophys.*, 69:1-35.

Obara, K., Hasegawa, A. and Takagi, A., 1986. Three-dimensional P and S wave velocity structure beneath the northeastern Japan arc. *J. Seismol. Soc. Jpn. Ser. 2*, 39:201-215 (In Japanese with English abstract).

Obara, K. and Sato, H, 1988. Existence of an S wave reflector near the upper plane of the double seismic zone beneath the southern Kanto district, Japan. *J. Geophys. Res.*, 93:15037-15045.

Obara, K, 1989. Regional extent of the S wave reflector beneath the Kanto district, Japan. *Geophys. Res. Lett.*, 16:839-842.

Ohmi, S. and Hori, S., 1994. Location of the upper boundary of the Pacific plate derived from SP converted waves, *Programme Abstr., Seismol. Soc. Jpn.*, 2:379 (In Japanese).

Okada, Hm., 1971. Forerunners of ScS waves from nearby deep earthquakes and upper mantle structure in Hokkaido. *J. Seismol. Soc. Jpn. Ser. 2*, 24:228-239 (In Japanese with English abstract).

Okada, Y. and Kasahara, K., 1990. Earthquake of 1987, off Chiba, central Japan and possible triggering of eastern Tokyo earthquake of 1988. *Tectonophys.*, 172:351-364.

Oliver, J. and Isacks, B., 1967. Deep earthquakes zones, anomalous structures in the upper mantle, and the lithosphere. *J. Geophys. Res.*, 72:4259-4275.

Paige, C. C. and Saunders, M. A., 1982. LSQR: An algorithm for sparse linear equations and sparse least squares. *ACM Trans. Math. Software*, 8:43-71.

Roecker, S. W., 1982. Velocity structure of the Pamir-Hindu Kush region: possible evidence of subducted crust. *J. Geophys. Res.*, 87:945-959.

Sekiguchi, S. 1991. Three-dimensional Q structure beneath the Kanto-Tokai district, Japan. *Tectonophys.*, 195:83-104.

Sekiguchi, S., 1992. Amplitude distribution of seismic waves for laterally heterogeneous structures including a subducting slab. *Geophys. J. Int.*, 111:448-464.

Seno, T. and Pongsawat, B., 1981. A triple-planed structure of seismicity and earthquake mechanisms at the subduction zone off Miyagi Prefecture, northern Honshu, Japan. *Earth Planet. Sci. Lett.*, 55:25-36.

Sugimura, A. and Uyeda, S., 1973. *Island Arcs; Japan and its Environs*, Elsevier, New York.

Takanami, T., 1982. Three-dimensional seismic structure of the crust and upper mantle beneath the orogenic belts in southern Hokkaido, Japan. *J. Phys. Earth*, 30:87-103.

Tanaka, T., 1987. *Seismic Structure of the Crust and the Upper Mantle Beneath the Shikoku and the Chugoku Region, Japan*, Masters Thesis, Okayama University.

Tsumura, N., Hasegawa, A., and Horiuchi, S., 1996. Simultaneous estimation of attenuation structure, source parameters, and site response spectra using small earthquakes recorded at many stations. *Phys. Earth Planet. Int.*, 93:105-121.

Ukawa, M. and Imoto, M., 1982. Focal mechanisms of the double planed seismic zone beneath the Kanto district. *Programme Abstr., Seismol. Soc. Jpn.*,2:33 (In Japanese).

Ukawa, M., Ishida, M., Matsumura, S., and Kasahara, K., 1984. Hypocenter determination method of the Kanto-Tokai observational network for microearthquakes. *Res. Notes Natl. Res. Cent. Disaster Prev.*, 53:1-88 (In Japanese with English abstract), National Research Center for Disaster Prevention, Tsukuba, Japan.

Ukawa, M., Ishida, M., Matsumura, S., and Kasahara, K., 1984. Hypocenter determination method of the Kanto-Tokai observational network for microearthquakes, *Res. Notes, Nat'l Res. Center Disaster Prev.*, 53:1-88 (In Japanese with English abstract).

Umino, N. and Hasegawa, A. 1975. On the two-layered structure of deep seismic plane in Northeastern Japan Arc. *J. Seismol. Soc. Jpn. Ser. 2*, 27:125-139 (In Japanese with English abstract).

Umino, N. and Hasegawa, A. 1982. A detailed structure of the deep seismic zone and earthquake mechanism in the northeastern Japan arc. *J. Seismol. Soc. Jpn. Ser. 2*, 35:237-257 (In Japanese with English abstract).

Umino, N. and Hasegawa, A. 1984. Three-dimensional Qs structure in the northeastern Japan arc. *J. Seismol. Soc. Jpn., Ser. 2*, 37:217-228 (In Japanese with English abstract).

Utsu, T., 1967. Anomalies in seismic wave velocity and attenuation associated with a deep earthquake region, 1. *J. Fac. Sci., Hokkaido Univ., Ser. 7*, 3:1-25.

Utsu, T., 1971. Seismological evidence for anomalous structure of island arcs with special reference to the Japanese region. *Rev. Geophys.*, 9:839-890.

Yoshii, T., 1975. Proposal of the "Aseismic Front". *J. Seismol. Soc. Jpn., Ser. 2*, 28:365-367 (In Japanese).

Zhao, D., Hasegawa, A., and Horiuchi, S., 1992. Tomographic imaging of P and S wave velocity structure beneath northeastern Japan. *J. Geophys. Res.*, 97:19909-19928.

Zhao, D. and Hasegawa, A., 1993. P-wave tomographic imaging of the crust and upper mantle beneath the Japan Islands, *J. Geophys. Res.*, 98:4333-4353.